Master of Science in
Cultural Heritage Materials & Technologies

Department of History, Archaeology
& Cultural Resources Management
University of the Peloponnese

UNIVERSITY OF THE PELOPONNESE

AREZINA SAKKA
(R.N. 1012201502009)

DIPLOMA THESIS:

"STUDY OF THE SPATIAL DIFFERENTIATION OF ANTIQUITIES' EXPOSURE TO AEROSOLS IN GREECE, USING SPACE – BORNE REMOTE SENSING"

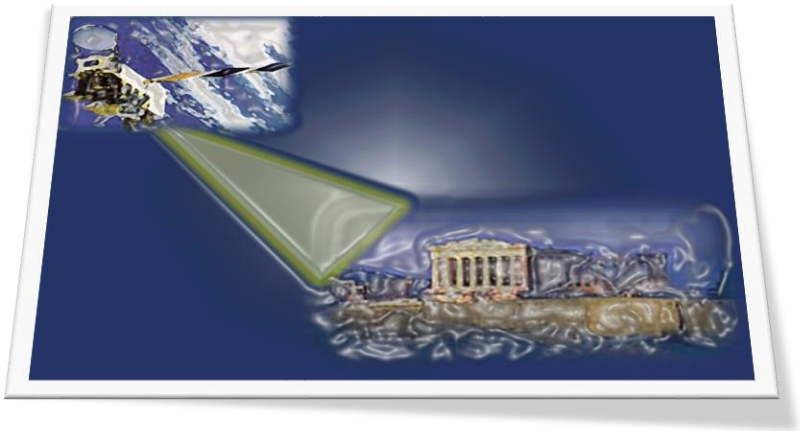

SUPERVISING COMMITTEE:
- Dr. Gerasopoulos Evangelos
- Dr. Keramitsoglou Iphigenia

EXAMINATION COMMITTEE:
- Associate Professor Zacharias Nikos
- Dr. Gerasopoulos Evangelos
- Dr. Keramitsoglou Iphigenia

KALAMATA, JANUARY 2017

ACKNOWLEDGEMENTS

I would like to express my gratitude and thank warmly Doctor Gerasopoulos Evangelos, research director of the Institute for Environmental Research and Sustainable Development, who did me the honor to accept to work with me in preparing my diploma thesis, for his unstinting help and guidance in the implementation of my work, for the hosting at the National Observatory of Athens and for his consistence towards the assigned tasks. Most of all, I would like to acknowledge him for the excellent cooperation and for his significant contribution to the development of my knowledge.

I would also like to thank Doctor Keramitsoglou Iphigenia, senior researcher at the Institute for Astronomy, Astrophysics, Space Applications and Remote Sensing, for the search and inspiration of this innovative elaborated topic, which was made in collaboration with Doctor Gerasopoulos Evangelos.

I would like to thank Doctor Zacharias Nikos, Associate Professor at the University of Peloponnese, in the Department of History, Archaeology and Cultural Resources Management, for the enthusiasm and his support towards the specific topic.

Moreover, I would like to thank all my CultTech classmates for their moral support arising from our common experiences. Especially, a big thank you to my fellow classmate, Dimitris Mitsos, for his valuable help in technological issues.

Finally, I would like to express my gratitude to my beloved parents, who supported me, morally and financially, throughout my postgraduate studies and for the patience they have shown in this important period of my life.

…dedicated to my classmates…

TABLE OF CONTENTS

LIST OF FIGURES

LIST OF TABLES

LIST OF DIAGRAMS

TABLE OF GRAPHS

TABLE OF CHARTS

ABSTRACT

In the present thesis, twenty-one archaeological sites in Greece were selected to be studied using space borne remote sensing, with respect to their exposure to air pollution and the potential impact on the structural materials of the monuments.

Fourteen years (2002 – 2016) of observations of Aerosol Optical Depth (AOD) were retrieved via two satellite remote sensing instruments, MODIS and CALIPSO.

The average levels of aerosols are greater in the north and north-eastern parts of Greece, while slightly lower levels of pollution are observed in southern areas.

The presence of polluted dust and mineral dust is intense in the northern regions. Heading to the west, elevated levels of smoke are observed. In central and south Greece, mineral dust is observed and in the east, apart from dust, clean marine aerosols are frequently encountered as well (seaside areas). In the southern part of the country polluted dust, dust and polluted continental aerosols along with clean marine are noted.

The presence of aerosols reveals a summer maximum for the northern regions and a spring maximum for the southern and western parts. The eastern side shows a moderately stable rate the whole year. A negative trend of aerosol optical depth is observed during the last ten years for all sites. The higher reduction is observed at the north and the lowest at the east parts of Greece.

The above spatiotemporal characteristics of aerosols over Greece, determine the different exposure that monuments may be subjected in terms of location and season.

INTRODUCTION

The aim of the thesis is to study the spatial and temporal variability of aerosols over Greece and the potential effect on the materials of exposed cultural heritage monuments.

Actually, aerosol impacts on cultural heritage materials have not been studied in depth, and this has been an additional motivation for the selection of this specific topic, and especially the use of remote sensing.

The intensity and the type of aerosols and whether it is the same above the selected areas, the geographical differentiation of both intensity and type, their seasonality and trends during the last fifteen years, were among the questions that this thesis attempted to examine and answer, paving the ground for relevant, follow up analysis in the future.

Monitoring air pollution from space and documenting the paths through which antiquities are affected by air pollution, is critical for the preservation and maintenance of cultural heritage sites. The retrieval of Aerosol Optical Depth observations from space, could be one way, one additional useful instrument, for better understanding the background and level of potential chemical weathering mechanisms of materials, leading to more suitable selection of conservation strategies.

For easier understanding of the topic, the methodological approach, as it is shown in Chart 1, was designed in such a way as to present a smoothly transition among the sections, starting with the theoretical part, which presents the needed information and knowledge on technical acquisition and processing of data derived from the used space platforms.

In the following chapters the effect of various atmospheric factors, particularly particulate air pollution (aerosols), on cultural heritage monuments and the deterioration patterns of the materials due to air pollution are presented. Follows the description of remote sensing methods and data, used in the present work, with emphasis on their

use in archaeology and in monitoring air pollution over archaeological sites.

The basic part of the thesis consists of the technical approach (methodology) and the results. The methodology followed, is presented in detail, describing all the steps, the instruments and the techniques for data acquisition and retrieval that were used. The results are demonstrated elaborately, accompanied by tables and diagrams in order to be better comprehended.

Finally, the conclusions reached are presented, in attempt to answer the questions initially raised in the current study.

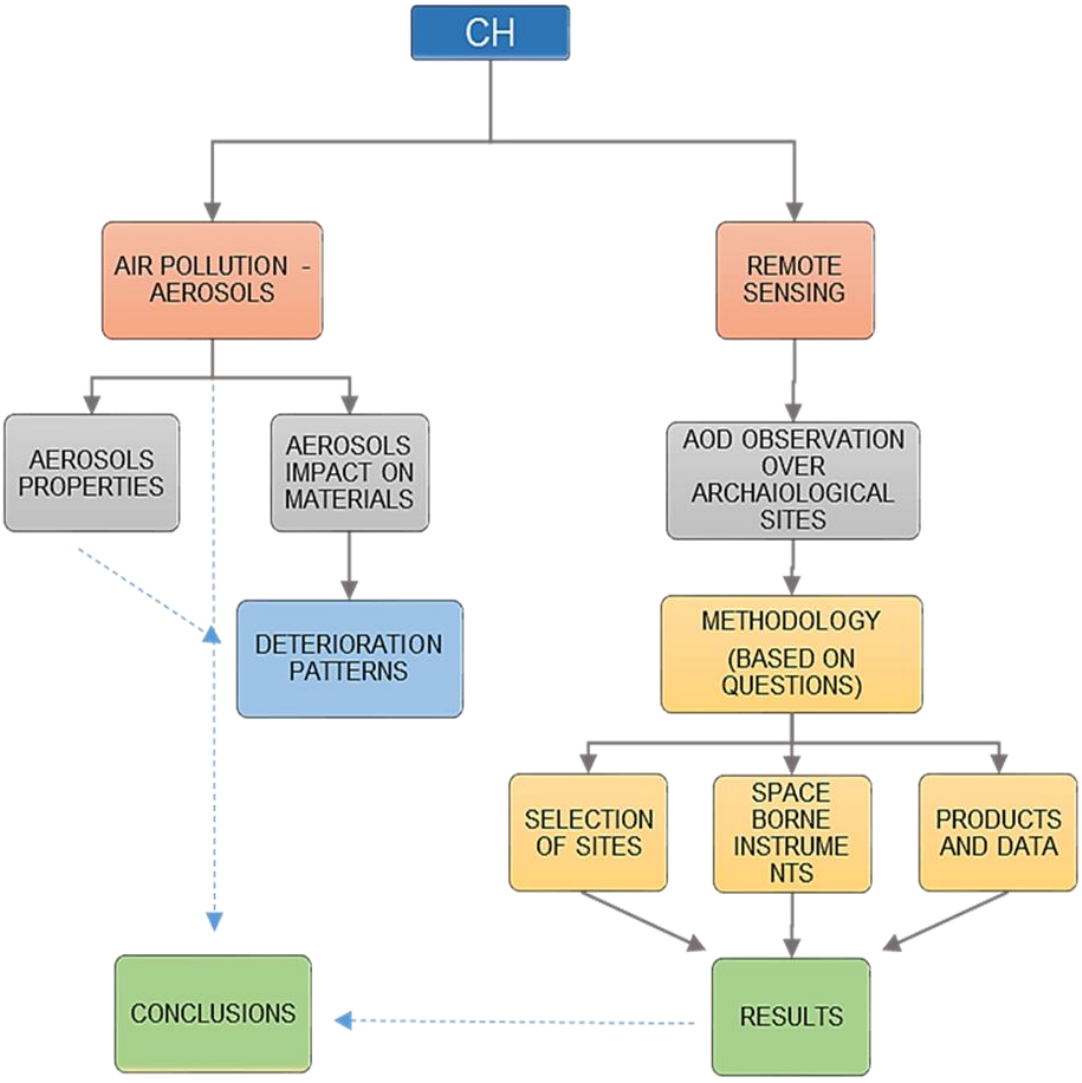

Chart 1 Methodological diagram of the topic

1. CULTURAL HERITAGE AND THE ENVIRONMENT

Cultural Heritage (CH) is the value that people have given to items and places through their association with them, passed from generation to generation from antiquity till present. As a human activity, cultural heritage has created tangible artistic representations of these values, such as buildings and monuments.

Cultural heritage monuments and sites are constantly exposed to a multitude of environmental factors. The environment in which monuments are, plays an important role on their long-term preservation.

1.1. ENVIRONMENTAL FACTORS INFLUENCING CULTURAL HERITAGE MATERIALS

Building materials weather progressively in the natural environment and some factors may accelerate this procedure (air pollution). Materials degrade in polluted as well as in unpolluted conditions (remote areas) (Watt, et al., 2009).

The process of deterioration of materials by external environmental factors is a composite interaction of climatic, biological and chemical processes resulting from the impact of contaminants and natural elements of the surrounding setting (Moncmanova, 2007). The principal environmental factors which influence cultural heritage materials are: ***Moisture***, ***Temperature***, ***Solar radiation***, ***Precipitation***, ***Chemical*** *and* ***Biochemical attack*** *and* ***Air pollution*** (Labropoulos, 2003). The present thesis focuses on the exposure of CH related materials to air pollution and specifically aerosols.

1.2. AEROSOLS

Aerosols can be found over every ecosystem on the earth. They come into earth's atmosphere and despite their tiny size, they have major impacts on climate, human health, ecosystems and materials (Voiland, 2010). They are defined as particles, in solid or liquid form, in suspension in the atmosphere. The amount and properties of aerosols are variable in space and time. The most significant

characteristics of an aerosol population are the ***size*** distribution, ***chemical composition***, and the ***shape*** of the particles (Boucher, 2015).

Their diameters range from few nanometers to few micrometers. Their composition and shape depend on their origin and atmospheric processing. Aerosols from about 0.05 to 10 micrometers are particles which interact directly with sunlight and create most of aerosol mass (Chin, 2009).

Airborne particles in the atmosphere (dust, smoke, pollution) can block sunlight by absorbing or scattering light. The amount of these particles and an atmospheric column is quantified by an optical measure, the ***Aerosol Optical Depth***[1] (AOD). It is a dimensionless quantity that measures, usually vertically, the extinction of solar beam by dust and haze (how much direct sunlight is prevented by aerosols particles) (NOOA, 2005).

1.2.1. TYPES AND SOURCES OF AEROSOLS

There are a lot of possible classifications of aerosols based on their origin, properties, formation processes etc. (Penner, et al., 2001;

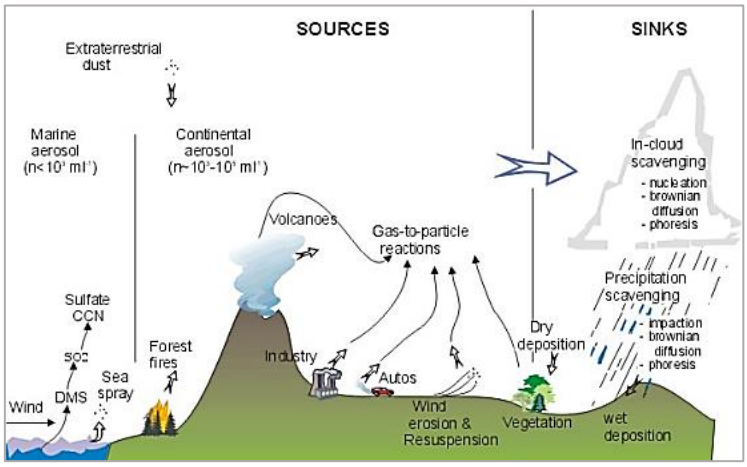

Figure 1 Schematic of sources and sinks of atmospheric aerosols (Farrell & Cleugh, 2003)

[1] AOD is also known as AOT (Aerosol Optical Thickness) (Chin, 2009).

Seinfeld & Pandis, 2016; Kulkani, et al., 2011). In table 1, various categories of aerosols taxonomies are collectively presented.

It must be noted that none of the above categories are totally representative, because of the complexity of aerosols' nature and interaction with atmospheric elements.

Table 1 Collective table of possible classification of aerosols

TYPES AND SOURCES OF AEROSOLS			
	Sources	***Emissions***	***Type***
Properties	Primary[2]		
	Secondary[3]		
Origin	Natural	• Ocean • Soils • Vegetation • Fires • volcanoes	Sea salt spray, desert/mineral dust, volcanic ash, soil dust, SO_2, H_2S, biogenic
	Anthropogenic	• Combustion of fossil fuels • Biofuels • Industrial activities • Transportation • Heating	Carbonaceous soot, black carbon, organic carbon, VOCs, Nitrogen oxides, Sulfur oxides
Environment	• Urban • Continental • Desertic • Marine • Volcanic		

1.2.2. CHEMICAL COMPOSITION OF AEROSOLS

Atmospheric aerosols have very complex chemical compositions (table 2) due to the various sources and transformations. (Seinfeld & Pandis, 2016). They are composed by sulphates, nitrates, ammonium, organic material, crustal species, sea salts, metal oxides and hydrogen ions. Sulphate, ammonium and organic carbon are mainly found in *fine particles*. Crustal and biogenic organic materials are mostly in the *coarse[4] aerosol fraction* (Boucher, 2015; Marley & Gaffney, 2006).

[2] Aerosols directly emitted into the atmosphere.
[3] Aerosols formed in the atmosphere by chemical reactions of gases.
[4] Large particles generated by mechanical processes (wind erosion) (Marley & Gaffney, 2006).

Table 2 Coarse and fine particulate matter

Chemical Composition of Aerosols		
	Sources	***Elements/ Components***
Coarse particles	• Soil • Oceans	Si, Al, Fe, Mg, Ca, Na, K Na, Cl, Mg, Ca, K
Fine particles	Gas to particle conversion and combustion	SO_4, NO_3, NH_4, elemental and organic carbon

1.2.3. THE SPATIAL - TEMPORAL VARIABILITY OF AEROSOLS

Aerosols are continuously present in the atmosphere in quite variable concentrations. This is due to the very large heterogeneity in aerosols sources and their moderately short residence time in the atmosphere (Boucher, 2015). For example, photochemically produced aerosols are found in higher concentrations during summer, however during winter, there can be supplementary sources of organic particles, because of excessive various types of fuels burning for heating purposes (Seinfeld & Pandis, 2016).

Aerosols are transported by winds, so continental[5] aerosol can be seen over oceans and vice versa marine aerosol over land. They also subject to atmospheric sinks. Their spatial and temporal variability depend on the distribution of sources and sinks and how these interact with transport. *Dry deposition* at the Earth's surface *and wet deposition* from precipitation are the two major sinks of aerosols (Boucher, 2015).

1.3. IMPACTS OF AEROSOLS ON CULTURAL HERITAGE MATERIALS

Some substances of a polluted atmosphere, combined with various external environmental factors (humidity, temperature etc.) affect the structural materials of cultural heritage monuments (Skoulikidis, 2000).

Stone, as the principal structural element of monuments, is the main concern of scientists regarding air pollution impacts. Although

[5] Aerosol origin over the continents with industrial, urban, agricultural, forest, and desert sources, with potential for high concentrations of hygroscopic aerosol (AMS, 2015).

aerosols impact on cultural heritage materials has not been studied in depth, there are many studies that demonstrate that the main deterioration pattern of stones due to aerosols action is the *formation of crusts* (table 3) (Vallero, 2008; Di Turo, et al., 2016).

Anthropogenic aerosols usually contain inorganic salts, acids (sulphates, nitrates) and metals. Sulphate ions (as acid particles) attack carbonate stones such as limestone and sandstone and calcareous stones, such as marbles. Salts from coastlines containing chlorides acids and fly ashes, are the most destructive particles. On the other hand, dust particles have no direct impact on stone, but may have harmful mechanical effects through abrasion[6] and soiling[7]. These particles, sometimes, may also carry corrosive chemicals (sulphates, nitrates and chlorides) through "coating" processes, which create an oxidative environment on the surface of the stone (Moncmanova, 2007; Doehne & Price, 2010; (Moropoulou, et al., 2001).

The reactions of materials with air pollutants deposited on their surface can lead to the formation of salt layers (fig. 2 – 4), namely crusts whose composition and form differs depending on the type of the stone, the composition of airborne particles and the climate of the area (Amoroso & Fassina, 1984; Borrelli, 1999; Doehne & Price, 2010).

[6] Gradual loss of material of the surface by the constant exposure to environmental elements.

[7] Surface blackening which reduce the artistic appeal, caused by alterations, deposition and biological colonization (Saiz - Jimenez, 2004).

Table 3 Types of crust according to their composition and environment

Types of Crust		
Black crusts (cities / industrial areas)	• Hard black crust • Loose particulate deposits	Gypsum, recrystallized calcium carbonate and carbon particulate matter (sheltered areas).
Carbonaceous crusts (natural environment)		Salts deposit in the surface from the interior. Integration of elemental and biological particles.
Salt crusts		Soluble salts (presence of high salt levels) formed by wet and dry cycles.

Figure 3 Deposition of aerosols particles on recrystallized calcium carbonate (marble) (YSMA, 2011)

Figure 2 Salt crust formation and recrystallized on limestone (ICOMOS, 2010)

Figure 4a, 4b Hard black crusts on limestone
(ICOMOS, 2010)

2. CULTURAL HERITAGE ASPECTS FROM SPACE

Remote sensing, in science, refers to the acquisition of information about an object without having physical contact with it. Remote sensing includes techniques that use electromagnetic radiation so as to detect and measure a range of phenomena. Satellite remote sensing, aerial photography, geophysical surveys, terrestrial laser scanners, constitute a sample of remote sensing techniques (Hadjimitsis, et al., 2013).

Satellite remote sensing prevails over the other conventional methods because of the frequency and quickness of data acquisition over large areas. However, satellite remote sensing is an expensive technique for mapping small areas and requires specialized training for analysing data, which sometimes are difficult to be interpreted (Cracknell & Hayes, 2007).

2.1. REMOTE SENSING APPLICATIONS

Satellite remote sensing has developed into a common mean of research and prediction of environmental alterations. Satellite observations can provide quick and reliable information by monitoring and measuring in a global scale, natural and anthropogenic events over vast and unreachable areas (Agapiou, et al., 2015).

The technology of remote sensing has been successfully applied in several scientific fields. *Agriculture, climatology, forestry, geology, glaciology, oceanography, cryosphere, pollution monitoring, urban mapping and archaeology*, are some of the disciplines that comprise the list of remote sensing applications (table 4) (Roy, et al., 2010; Lillesand, et al., 2008).

2.2. REMOTE SENSING IN ARCHAEOLOGY

Remote sensing has opened up new horizons for the science of archaeology. Cultural Heritage monuments and sites are constantly endangered by both anthropogenic and natural threats (earthquakes, fires, urbanization, etc.) (Agapiou, et al., 2015; Hadjimitsis, et al., 2013). Remote sensing technologies, as innovative, non-destructive techniques, have shown a great potential as a significant tool for the protection of monuments and sites gathering data and information for vast areas by systematic monitoring (table 5) (Lasaponara & Masini, 2012; Wiseman & El - Baz, 2007).

Table 4 Fields and applications deploying Satellite Remote Sensing

USES OF SATELLITE REMOTE SENSING	
Geosphere	• **Geological mapping** • **Mineral exploration** • **Geoengineering**
Biosphere	• **Agriculture** • **Forestry** • **Land use/ Land cover mapping** • **Urban and regional planning** • **Archaeology**
Hydrosphere	• **Hydrology/ Marine resources** • **Oceanography**
Cryosphere	• **Glaciology**
Atmosphere	• **Weather forecasting/Climatology** • **Air pollution monitoring**

Table 5 Remote Sensing Applications in the field of Archaeology

USE OF REMOTE SENSING IN ARCHAEOLOGY	
Detection and modelling	• **Archaeological sites** • **Individual features**
Marine survey	• **Archaeological sites in marine environments**
Safeguarding from natural and anthropogenic hazards	• **Looting monitoring** • **War damage** • **Extreme weather conditions**
Management and maintenance of sites	• **Documentation of human activities at CH sites** • **Conservation**
Palaeoenvironmental studies	• **Changes of paleoclimate** • **Reconstruction of ancient environments**

2.3. AIR POLLUTION MEASUREMENTS OBSERVATIONS OF INTEREST FOR CULTURAL HERITAGE MONUMENTS

Industrialization and human activities have led to excessive emissions of aerosol particles into the atmosphere. In the following, focus is placed on aerosols and not NO^2/SO^2 whose impacts on materials via acid rain is much better documented (Li, et al., 2009).

Atmospheric particle deposition on surfaces of monuments causes, apart from aesthetic alterations on the surface, a sequence of chemical reactions which as a result, appear as serious damages. Therefore, there is a need for systematic monitoring and mapping of air pollution for areas where important archaeological sites and monuments are found (Agapiou, et al., 2013).

The systematic measurement of air quality is a requirement in most of the heritage conservation plans. However, in relation to other environmental parameters (humidity, temperature, etc.), air pollution is less often monitored (Agbota, et al., 2013).

Satellite remote sensing of air quality has evolved dramatically over the last decade and satellite data can be efficiently used to monitor air pollution and its effects (Themistocleous , et al., 2012).

However, documentation of the way cultural heritage sites are affected by air pollution, as seen from space, is still limited in our days. The identification of polluted cultural heritage sites, the knowledge of aerosols type, their concentration in the atmosphere and their effect on materials undoubtedly can contribute to better understanding the corrosion mechanisms of materials and hence to the most suitable selection of conservation strategies.

Through satellite remote sensing, data which cover long time periods can be evaluated and analyzed so as to study the exposure of cultural heritage materials on ambient air pollution.

Satellite remote sensing is a relatively new application in studying cultural heritage (Themistocleous , et al., 2012). The following table (table 6) summarizes the advantages and the drawbacks of this technique based on the atmospheric aerosols monitoring.

Table 6 Advantages and Disadvantages of Satellite Remote Sensing

ADVANTAGES	*DISADVANTAGES*
• **Fast acquisition of data** • **Non- invasive technique** • **Covers large areas in limited time**	• Spatial and temporal variability of aerosols – uncertainties 15 – 25 % • Retrieval quality • Combination of methods

Monitoring air pollution is not an easy task (radiometric calibration, assumption of aerosol properties, cloud contamination etc.) (Li, et al., 2009). Permits a maximum expanded uncertainty of 15-25% for methods using fixed monitors, depending on the pollutant, while indicative measurements and modelling techniques have broader limits of error of up to 25-50%. Due to their spatial and temporal variability, atmospheric aerosol monitoring is difficult. Retrieval errors caused by these factors can reduce the retrieval quality (Themistocleous , et al., 2012).

3. METHODOLOGY

Twenty-one archaeological sites in Greece (table 7, fig. 5) were chosen to be studied using Space Borne Remote Sensing, with regards to their exposure to air pollution and the potential impact on the structural materials of the monuments.

Two satellite remote sensing instruments were used in order to map air pollution over the points of interest, *MODIS*[8] and *CALIPSO*[9] for retrieving AOD[10] monthly data for the time period 2002 – 2016 (14 years). Data from MODIS were acquired through the *Giovanni* program (http://giovanni.gsfc.nasa.gov/giovanni/), a web application developed by the GES DISC[11] which provides a simple way to visualize and analyze vast amounts of data from satellites. Data from Calipso satellite were available through the *LIVAS project* (http://lidar.space.noa.gr/) which aims to provide a global and extensive aerosol and cloud optical database.

Satellite data acquisition and retrievals were implemented after training at the National Observatory of Athens (NOA), and particular in the Institute for Environmental Research and Sustainable Development (IERSD), located in Penteli-Athens, by NOA's expert staff.

3.1. SELECTION OF ARCHAEOLOGICAL SITES

The selection of Cultural Heritage sites was based on the following criteria:

- Full and dense geographical coverage of Greece in latitude and longitude so as to obtain a representative picture of the prevailing conditions and hence for more valid results.
- Acquisition and study of data for different environmental conditions namely urban, remote and seaside areas.
- Constantly exposed monuments to external environmental conditions.

[8] MODIS – aqua Dark target 550nm
[9] Cloud-Aerosol Lidar and Infrared Pathfinder Satellite Observation
[10] Aerosols Optical Depth (or Thickness)
[11] NASA Goddard Earth Sciences Data and Information Services Center

- Historical and archaeological significance of the monuments.

The studied areas are presented shorted from North to South as follows:

Table 7 Collective table showing the studied archaeological sites

Archaeological sites				
Code	***Archaeological site***	***Location***	***Coordinates***	***Characterization of area***
1MR	Maronia	Thrace	*N 40.88º E 25.52º*	Rural / close to the sea
2AV	Avdira	Thrace	*N 40.91º E 24.96º*	Rural
3FL	Filippoi	E. Macedonia	*N 41.01º E 24.28º*	Rural / close to the city
4WT	White Tower	Central Macedonia	*N 40.62º E 22.95º*	Urban
5VR	Vergina	Central Macedonia	*N 40.48º E 22.31º*	Rural / close to the city
6LS	Ancient Theatre of Larissa	Eastern Thessaly	*N 39.64º E 22.41º*	Urban
7DD	Dodoni	Epirus	*N 39.54º E 20.78º*	Rural
8NC	Nicopolis	Epirus	*N 39.22º E 20.73º*	Rural
9MS	Sanctuary of Messa	Northern Aegean	*N 39.19º E 26.30º*	Seaside
10PL	Palamari	Sporades	*N 38.95º E 24.51º*	Seaside
11DE	Delphi	Central Greece	*N 38.48º E 22.49º*	Rural
12AC	Acropolis	Central Greece	*N 37.97º E 23.72º*	Urban
13MC	Mycenae	NE Peloponnese	*N 37.73º E 22.76º*	Rural
14OL	Olympia	W Peloponnese	*N 37.64º E 21.62º*	Rural
15IR	Ireon	Eastern Aegean	*N 37.66º E 26.88º*	Seaside
16ME	Messene	SW Peloponnese	*N 37.17º E 21.92º*	Rural
17DL	Delos	Cyclades	*N 37.40º E 25.26º*	Seaside
18ST	Ancient Thira	Cyclades	*N 36.35º E 25.39º*	Seaside
19RH	Rhodes	Dodecanese	*N 36.44º E 28.22º*	Seaside
20FS	Falassarna	NW Crete	*N 35.49º E 23.65º*	Seaside
21KN	Knossos	Eastern Crete	*N 35.29º E 25.16º*	Urban

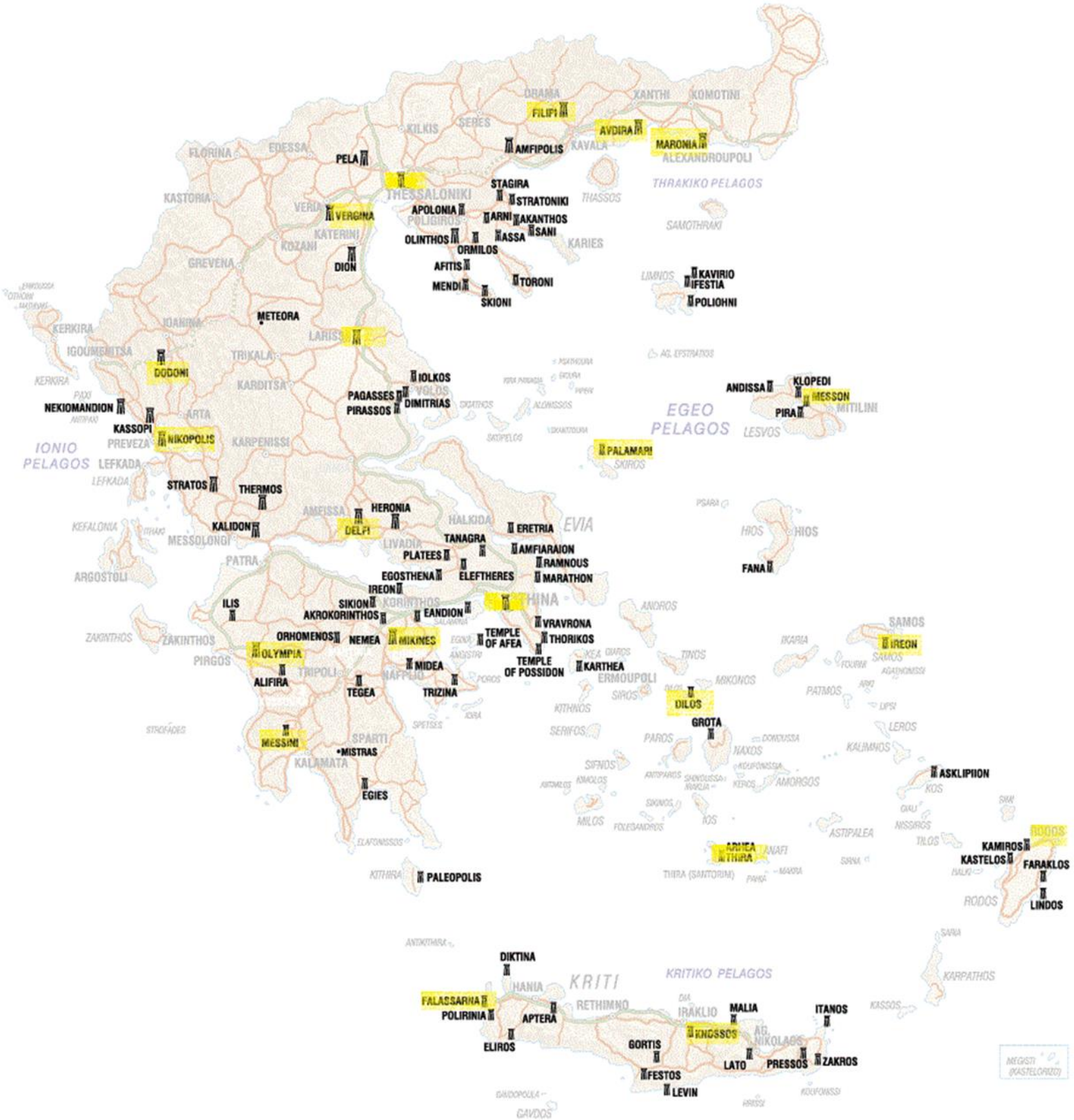

Figure 5 Map of Greece: Archaeological sites of interest (yellow areas) (Productions, 2016).

3.2. SPACE – BORNE REMOTE SENSING INSTRUMENTS

3.2.1. MODIS

MODIS (Moderate Resolution Imaging Spectro - radiometer) is an instrument aboard the Terra and Aqua satellites (fig. 6). Aqua 's orbit around the Earth passes south to north over the equator in the afternoon. Aqua MODIS is viewing the entire Earth's surface every 1 to 2 days (viewing band width of 2.330 km), obtaining data in 36 spectral bands[12] (between 0.405 and 14.385 μm) and acquires data at three spatial resolutions 250m, 500m, and 1000m.

MODIS is suitable for global monitoring of atmospheric properties from space. Also, enables multidisciplinary studies of earth–atmosphere and ocean–atmosphere interactions to be explored (King, et al., 1992).

The data derived from MODIS observations describe characteristics of the land, oceans and the atmosphere that can be used to study the processes and trends on local to global scales (NASA, 2016).

Figure 6 Aspect of MODIS Aqua satellite (NASA, 2016)

3.2.2. CALIPSO

CALIPSO (fig. 7) is a LIDAR mission developed by NASA and it is mostly focused on the investigation of the role of aerosols (direct or indirect forcing) (Lajas, et al., 2007).

[12] Groups of wavelengths

CALIPSO observations are acquired at resolutions 532 nm and 1064 nm and aims to give a new understanding of the role that clouds and atmospheric aerosols play in regulating the Earth's climate and air quality.

The vertical structure and properties of aerosols that are not currently provided by operating observational satellites, can be determined (the altitude of aerosol layers in the atmosphere) by three co-aligned instruments: 1) *3 - channel lidar (CALIOP)*: 532 nm, 2) *Imaging IR radiometer (IIR)* and 3) *Wide-field camera (WFC)* (NOA, 2013).

Figure 7 Aspect of CALIPSO satellite (NASA, 2016)

3.2.3. REMOTE SENSING SATELLITE PRODUCTS AND DATA RETRIEVAL

A gateway to acquire and analyse data from MODIS (Aqua and Terra) satellite is provided via **Giovanni** program. Giovanni[13] offers a friendly web-based environment to explore interactively various remote sensing atmospheric data (Leptoukh, 2007).

The user can easily attain remote sensing information from around the world. Access is provided through a common Web browser on a typical personal computer, so there is no need for further special applications (fig. 8).

[13] Goddard Interactive Online Visualization and Analysis Infrastructure (Leptoukh, 2007)

Procedure of data acquisition:

1. From the web page the user is able to select the spatial area "box" for the desired region via a Java image map by entering the coordinates defining the bounding box (fig. 9, 10).
2. The user also selects the temporal range for the data, one or more parameters from this data set (fig.11), and the desired output type (several plot types) (fig.12).

The user is then able to refine this analysis and download the results (fig.13). Depending on the choice of parameters, the results can be seen online in just few seconds.

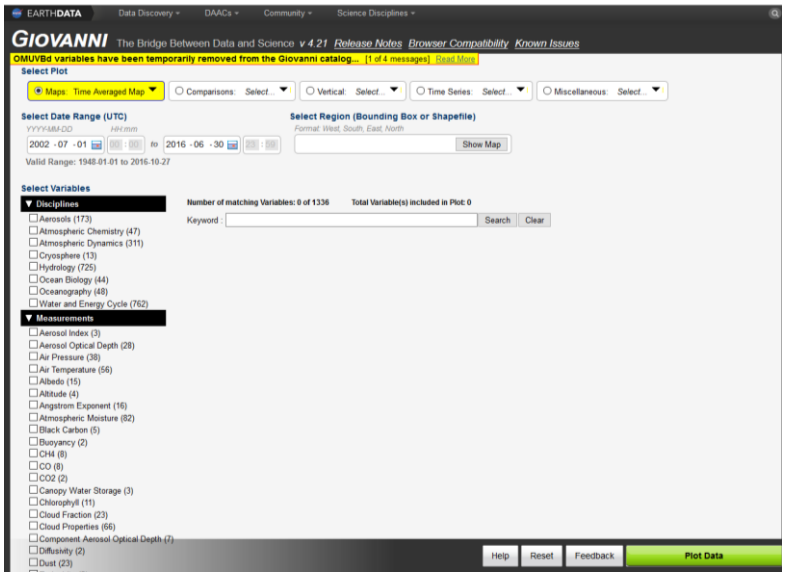

Figure 8 Home page of Giovanni website

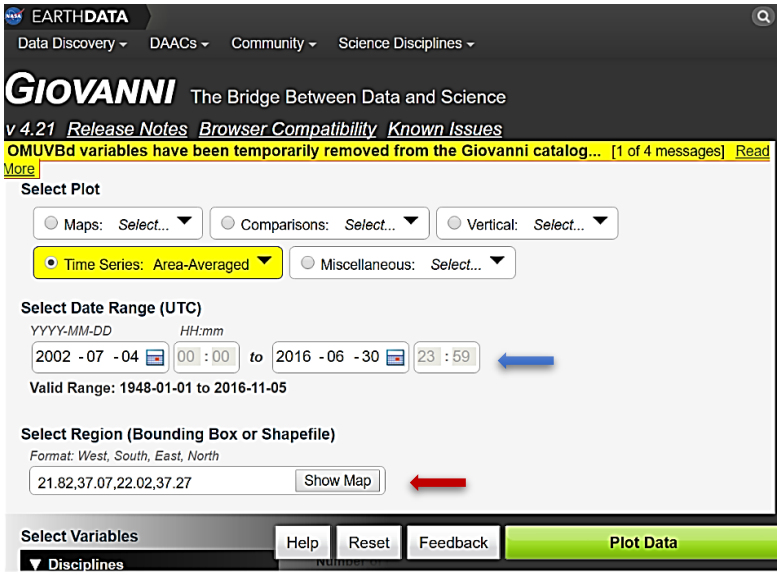

Figure 9 Selection of the date range (blue arrow) and entering of the coordinates (red arrow).

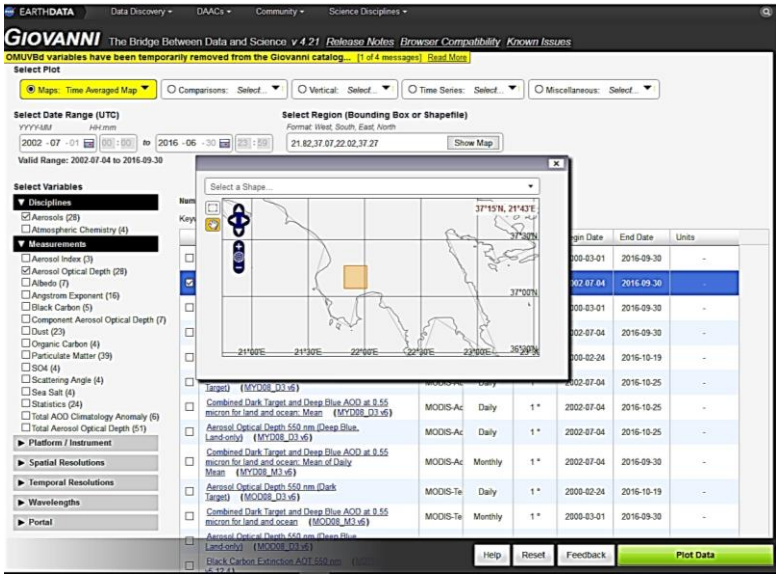

Figure 10 Creation of "bounding box" (orange square) by entering the coordinates and of the image map showing the desired region

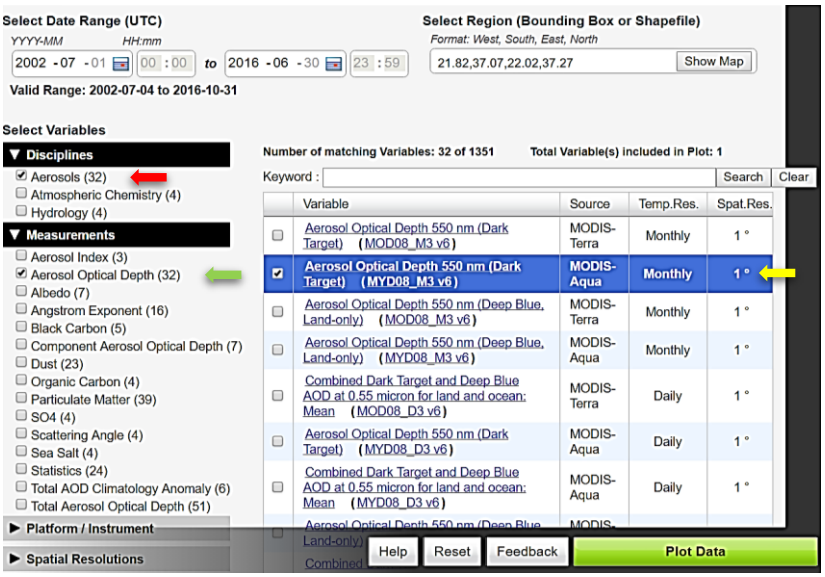

Figure 11 Selection of several variables (disciplines (red arrow), measurements (green arrow), product (yellow arrow))

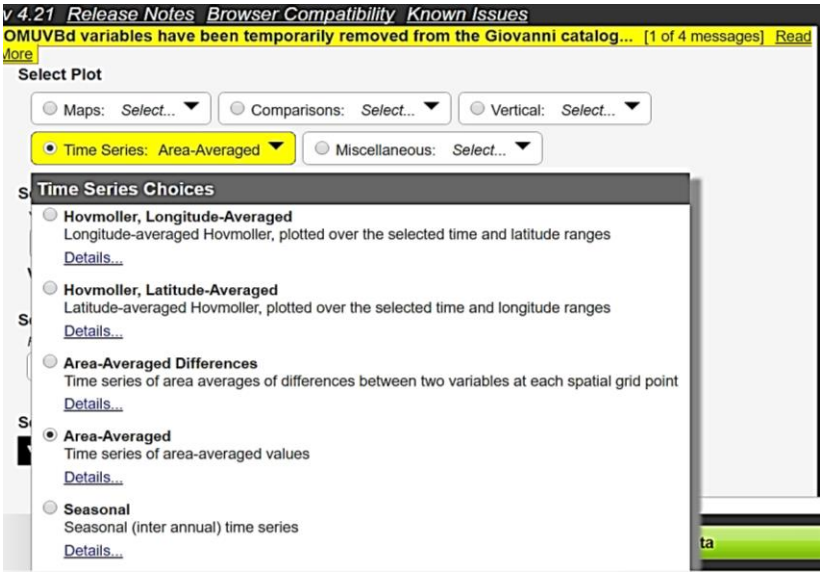

Figure 12 Plot selection

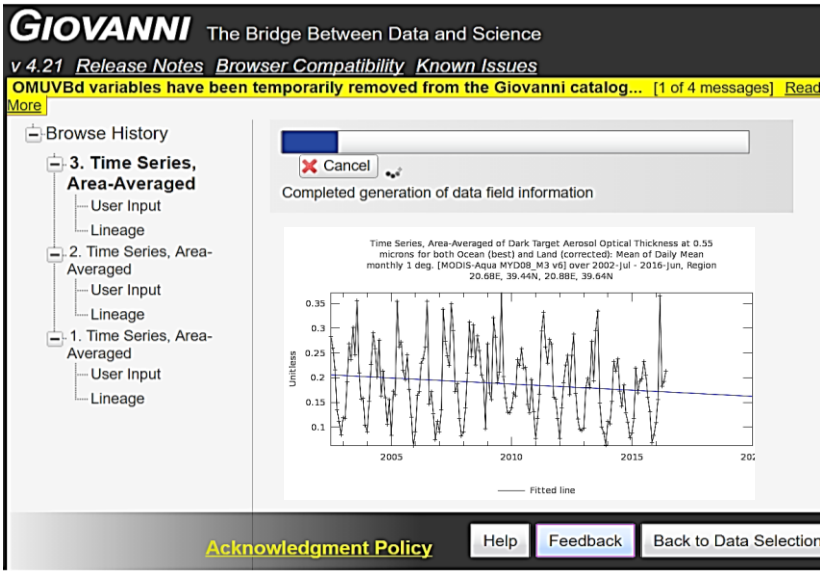

Figure 13 The generation of data and the final plot

CALIPSO specific retrievals are available through the **LIVAS** database. LIVAS[14] for space-based lidar simulation studies is an ESA[15] project coordinated by NOA, aiming to provide a global and extensive aerosol and cloud optical database (fig. 14). LIVAS provides a global 3-dimensional aerosol and cloud optical climatology and a collection of case studies focused on atmospheric episodes related to specific aerosol/cloud types (dust events, smoke, volcanic eruption events etc.).

A global cloud climatology, a climatology for the stratospheric features, as well as a set of selected scenes of extreme atmospheric phenomena (e.g. dust outbreaks, volcanic eruptions, wild fires etc.) are provided based on CALIPSO observations at 532 nm (NOA, 2013).

Procedure of data acquisition:

1. Selection of "Climatology" (fig. 15) page of the web portal LIVAS which contains:
   - *The dynamic World map (grid selector)*
   - *The dynamic Product Selector*

[14] Lidar climatology of Vertical Aerosol Structure
[15] European Space Agency

- *The Chart panel*
- *The Statistics panel*

2. Selection of the desired Grid cell on the dynamic World Map (fig. 16).
3. In the Product selector, the user hovers the menu from left to right. The allowable selections are greyed brighter (fig.17). Then the operator clicks on the desired product.
4. When the user selects a product from the Product Selector, the requested charts for the cell selected on the global map, are displayed (fig. 18). The left panel shows the user-requested parameter and the right panel shows the number of total aerosol samples used by the averaging procedure.
5. The portal provides statistical parameters for each grid cell for the corresponding product selected by the product selector displayed on a table located at the upper-right panel of the page (fig. 18).

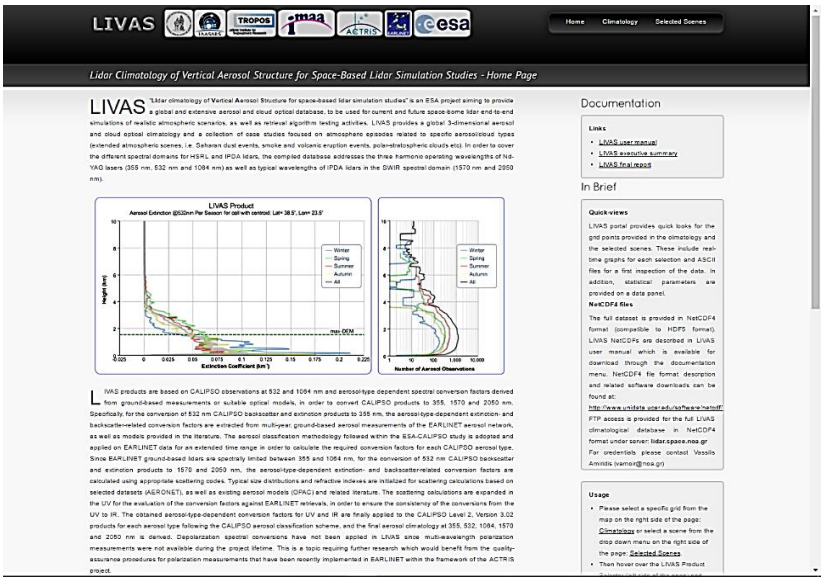

Figure 14 LIVAS web portal home page

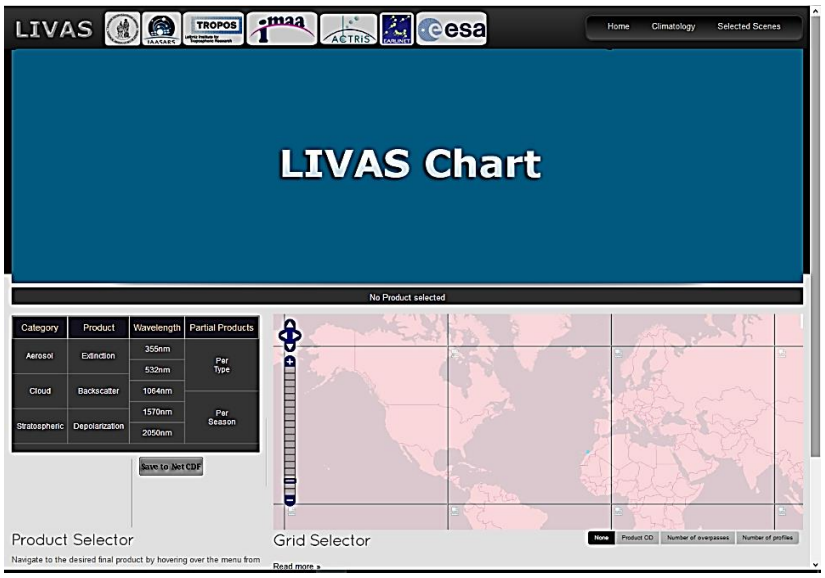

Figure 15 "Climatology" page and its' contents

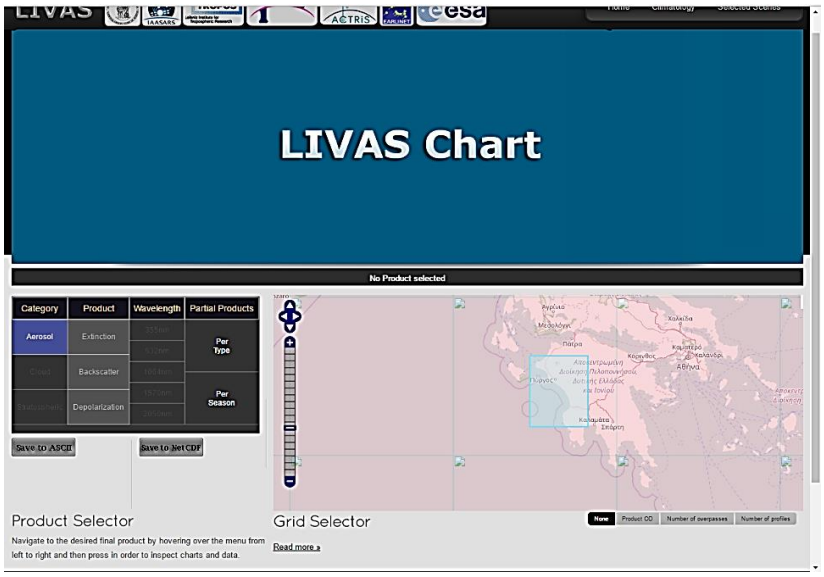

Figure 16 Grid Selector: Selection of the desired Grid cell

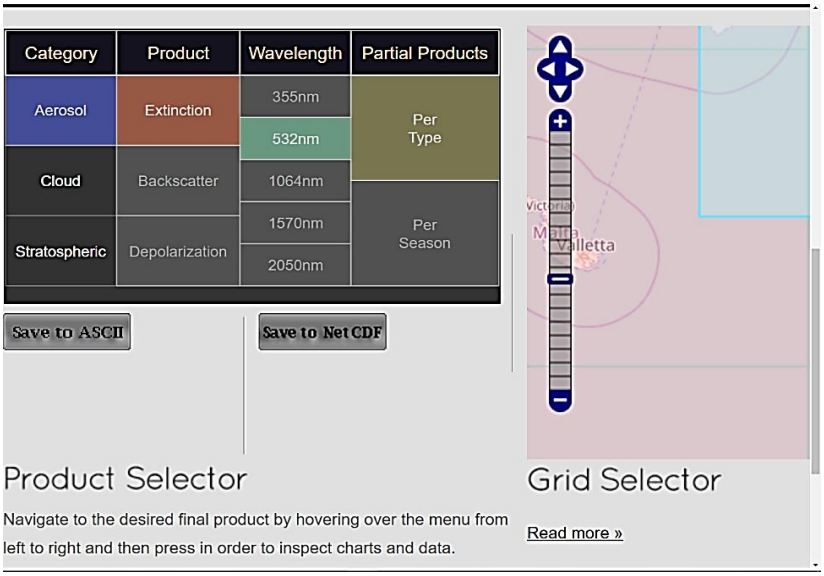

Figure 17 Product Selector: Selection of the desired products (bright colors)

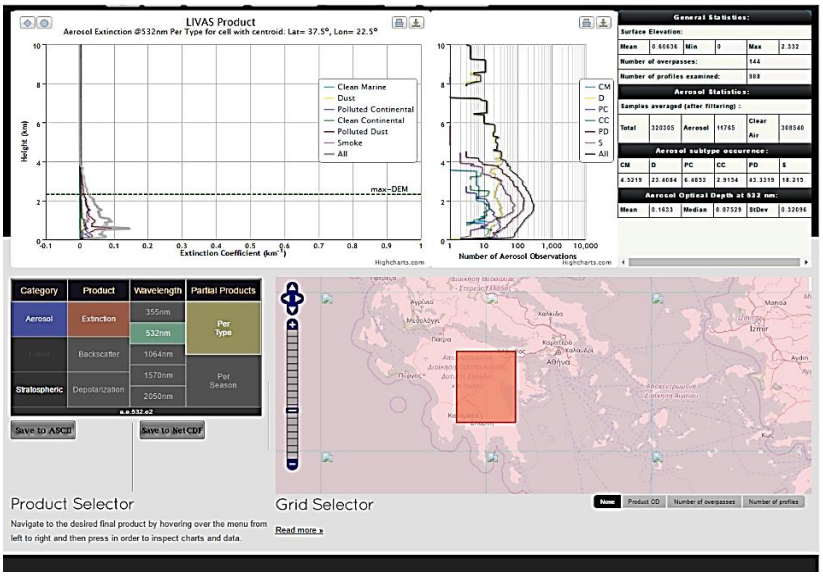

Figure 18 Chart Panel: The charts of the selected grid cell are displayed. The left chart shows the requested parameters. The right panel shows the total number of measurements. The statistic table is also presented (upper-right panel).

3.3. TECHNICAL APPROACH OF THE THESIS

As it has already been mentioned in the previous chapters, aerosols and their impact on cultural heritage materials has not been thoroughly investigated.

Satellite Remote Sensing is an excellent implement to monitor the spatial and temporal variability of aerosols and document the potential effects of air pollution on cultural heritage monuments and sites.

In the present thesis, monthly data of aerosol columnar concentrations were acquired covering a period of 14 years, from 04/04/2002 to 30/06/2016. In order to achieve adequate geographical coverage of Greece (north, south, west and east) considering the diverse climatic conditions, twenty-one (21) archaeological sites/ stations were selected.

The "data analyses" part includes the following stages:

1. Initially, the coordinates of all the studied areas were found and converted into decimal. Then it was decided that a representative width of the rectangular bounding box on the dynamic map in Giovanni web page will be (± 0,1) degrees from the selected site coordinates (fig. 19). For example, given that the coordinates of Ancient Messene are *N 37.17º and E 21.92º,* then for defining the bounding box we used:

W (-)	*S (-)*	*E (+)*	*N (+)*
21.82	37.07	22.02	37.27

The selected variables are Aerosols and the Aerosol Optical Depth (measurement). The product from which the AOD data were retrieved is MODIS – Aqua Dark Target 550 nm (MYD08 M3 v6). Finally, for obtaining the desired plots *Time – Series: Area – Averaged* from "*Select Plot"* were selected. So, were downloaded twenty-one plots of average time series accompanied by their respective raw data, one for each archaeological station.

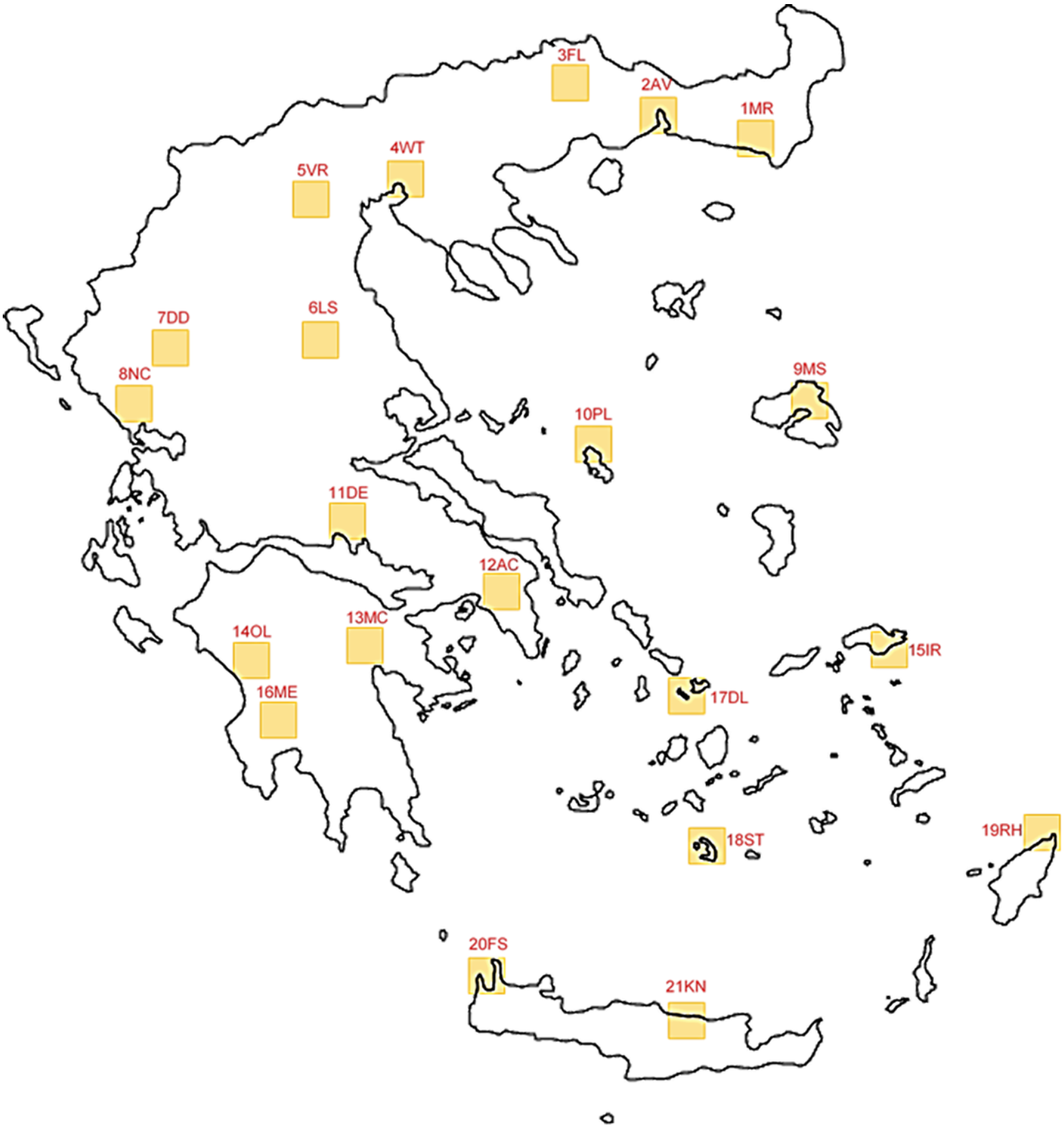

Figure 19 Map of Greece indicating the "bounding boxes". Each measured box/ area has a code name (WorldAtlas, 2016)

2. In the page "Climatology" of LIVAS Database, graphs of the vertical structure of aerosols (type and seasonality) were obtained. According to the area of study, each time (21), the corresponding grid cell was selected. First, in the product selector panel aerosol extinction of 532nm per type was selected for acquiring a chart with the aerosol type profile. Then aerosol extinction of 532nm per season was selected for obtaining a chart with the seasonality of aerosols occurrence.

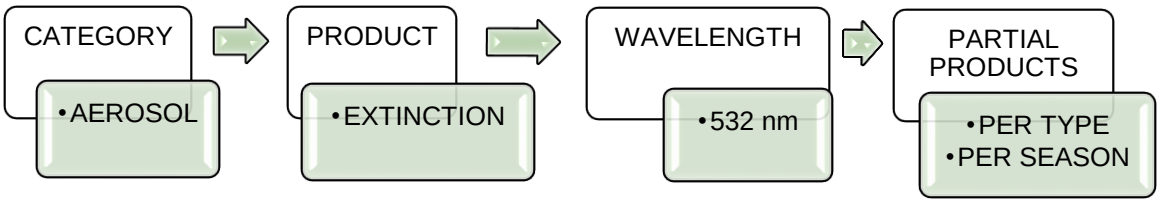

Chart 2 The procedure followed in the product selector panel in LIVAS database

3. Finally, all data were copied into Microsoft excel in order to create tables with basic statistics and relevant plots for all points of interest. A customly developed Excel/Basic application (Series–Calc/ kindly provided by Dr. E. Gerasopoulos) was used to calculate the statistics and sort time series accordingly to extract annual cycles etc.

The aforementioned analyses part was conducted exclusively at the National Observatory of Athens (NOA) in a personal portable computer, insomuch the applications used are serviceable and do not require specialized equipment in respect of downloading and processing data.

4. RESULTS

4.1. AEROSOL DATA PRESENTATION OVER THE SELECTED ARCHAIOLOGICAL SITES

In the following table, the coordinates of each archaeological station under study accompanied by the spatial area box selected via Giovanni program for monitoring AODs levels, are presented. The defined spatial boxes have the same width for all sites (± 0.1 degrees).

Table 8 Collective table with the characteristics and the defined bounding boxes of the studied archaeological sites

Code	***Coordinates***	***Bounding box***			
1MR	*N 40.88º E 25.52º*	**W (-)25.42**	**S (-)40.78**	**E (+)25.62**	**N (+)40.98**
2AV	*N 40.91º E 24.96º*	**W (-)24.86**	**S (-)40.81**	**E (+)25.06**	**N (+)41.01**
3FL	*N 41.01º E 24.28º*	**W (-)24.18**	**S (-)40.91**	**E (+)24.38**	**N (+)41.11**
4WT	*N 40.62º E 22.95º*	**W (-)22.85**	**S (-)40.52**	**E (+)23.05**	**N (+)40.72**
5VR	*N 40.48º E 22.31º*	**W (-)22.21**	**S (-)40.38**	**E (+)22.41**	**N (+)40.58**
6LS	*N 39.64º E 22.41º*	**W (-)22.31**	**S (-)39.54**	**E (+)22.51**	**N (+)39.74**
7DD	*N 39.54º E 20.78º*	**W (-)20.68**	**S (-)39.44**	**E (+)20.88**	**N (+)39.64**
8NC	*N 39.22º E 20.73º*	**W (-)20.63**	**S (-)39.12**	**E (+)20.83**	**N (+)39.32**
9MS	*N 39.19º E 26.30º*	**W (-)26.20**	**S (-)39.09**	**E (+)26.40**	**N (+)39.29**
10PL	*N 38.95º E 24.51º*	**W (-)24.41**	**S (-)38.85**	**E (+)24.61**	**N (+)39.05**
11DE	*N 38.48º E 22.49º*	**W (-)22.39**	**S (-)38.38**	**E (+)22.59**	**N (+)38.58**
12AC	*N 37.97º E 23.72º*	**W (-)23.62**	**S (-)37.87**	**E (+)23.82**	**N (+)38.07**
13MC	*N 37.73º E 22.76º*	**W (-)22.66**	**S (-)37.63**	**E (+)22.86**	**N (+)37.83**
14OL	*N 37.64º E 21.62º*	**W (-)21.52**	**S (-)37.54**	**E (+)21.72**	**N (+)37.74**
15IR	*N 37.66º E 26.88º*	**W (-)26.78**	**S (-)37.56**	**E (+)26.98**	**N (+)37.76**
16ME	*N 37.17º E 21.92º*	**W (-)21.82**	**S (-)37.07**	**E (+)22.02**	**N (+)37.27**
17DL	*N 37.40º E 25.26º*	**W (-)25.16**	**S (-)37.30**	**E (+)25.36**	**N (+)37.50**
18ST	*N 36.35º E 25.39º*	**W (-)25.29**	**S (-)36.25**	**E (+)25.49**	**N (+)36.45**
19RH	*N 36.44º E 28.22º*	**W (-)28.12**	**S (-)36.34**	**E (+)28.32**	**N (+)36.54**
20FS	*N 35.49º E 23.65º*	**W (-)23.55**	**S (-)35.39**	**E (+)23.75**	**N (+)35.59**
21KN	*N 35.29º E 25.16º*	**W (-)25.06**	**S (-)35.19**	**E (+)25.26**	**N (+)35.39**

1MR Maronia

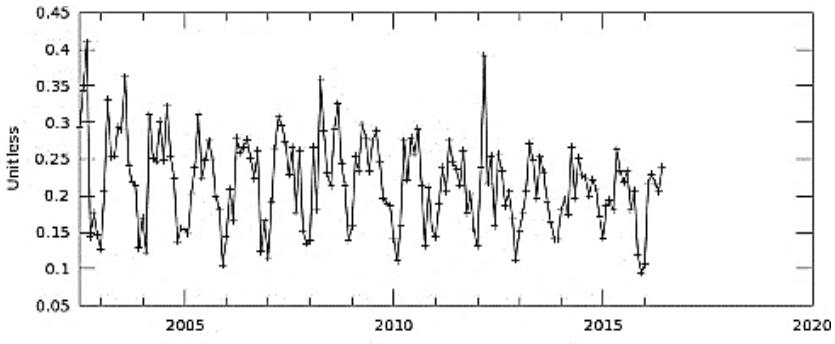

Diagram 1 Monthly AOD (0.55 μm) measurements for the time span 2002 – 2016 over Maronia (MODIS – Aqua Dark Target)

Table 9 Basic statistics

Lat	**40.88**
Long	25.52
Avg	0.218
Stdev	0.060
Min	0.095
Max	0.410
Median	0.219

The monthly average value of AOD at 0.55μm for the whole period, over the area of Maronia, is 0.218 ±0.06 with maximum and minimum 0.41 and 0.095 respectively. The median value is 0.219 (table 1).

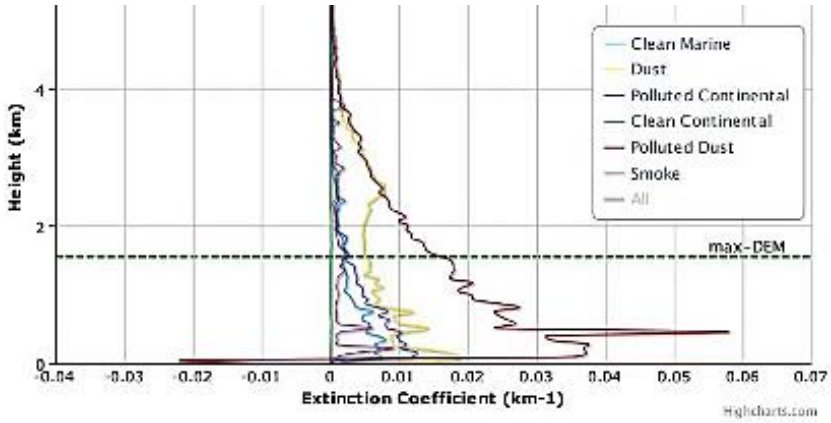

Chart 3 Vertical column of aerosol type observations (aerosol extinction at 532 nm per type for cell with centroid: Lat= 40.5º, Lon= 25.5º) over Maronia (LIVAS database)

Table 10 Aerosol subtype occurrence and AOD statistics

CM	**16.2066**	**AOD at 532 nm**	
D	28.8239	Mean	0.105
PC	7.8712		
CC	0.3599	Median	0.041
PD	42.9281		
S	2.9216	StDev	0.268

The vertical profile of aerosol types shows that the dominant types in this site are polluted dust and dust, and, aerosol presence starts below 4 km with a noted increase below 2 km.

2AV Avdira

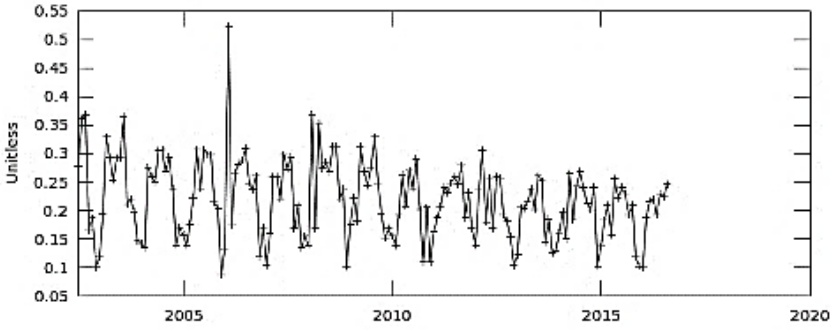

Diagram 2 Monthly AOD (0.55 μm) measurements for the time span 2002 – 2016 over Avdira (MODIS – Aqua Dark Target)

Table 11 Basic statistics

Lat	**40.91**
Long	24.96
Avg	0.219
Stdev	0.068
Min	0.087
Max	0.524
Median	0.219

The monthly average value of AOD at 0.55 for the whole period, over the area of Avdira, is 0.219 ±0.068 with maximum and minimum 0.524 and 0.087 respectively. The median value is 0.219.

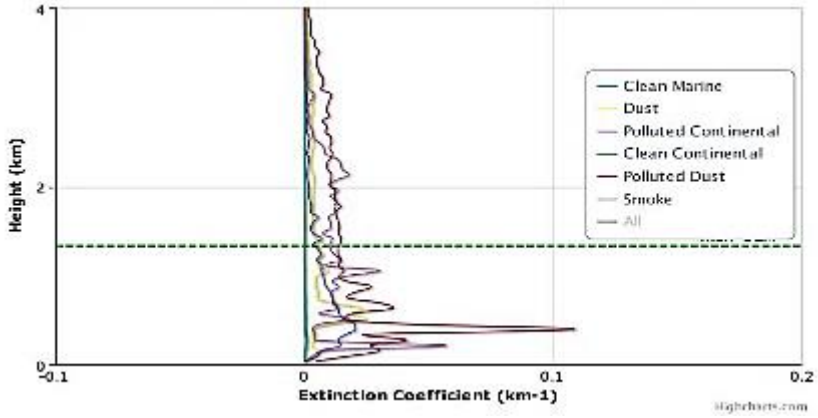

Chart 4 Vertical column of aerosol type observations (aerosol extinction at 532 nm per type for cell with centroid: Lat= 41.5º, Lon= 25.5º) over Avdira (LIVAS database)

Table 12 Aerosol subtype occurrence and AOD statistics

CM	**0,6733**	**AOD at 532 nm**	
D	22.9928	Mean	0.125
PC	8,0287		
CC	2.447	Median	0.0165
PD	47.4553		
S	17.3532	StDev	0.33

A balance in aerosol types is found with maximum concentrations up to 1.5 km from the surface. Polluted dust predominates and shows a peak at approximately 500 meters from the surface.

3FL Filippoi

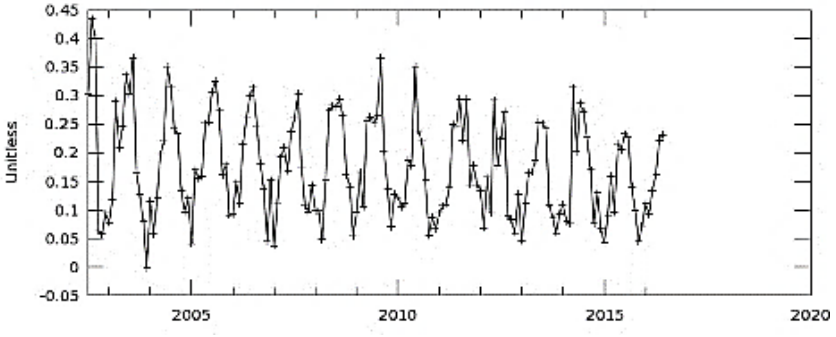

Diagram 3 Monthly AOD (0.55 μm) measurements for the time span 2002 – 2016 over Filippoi (MODIS – Aqua Dark Target)

Table 13 Basic statistics

Lat	**41.01**
Long	24.28
Avg	0.174
Stdev	0.088
Min	0.038
Max	0.434
Median	0.161

The monthly average value of AOD at 0.55 for the whole period, over the area of Filippoi, is 0.174 ±0.088 with maximum and minimum 0.434 and 0.038 respectively. The median value is 0.161.

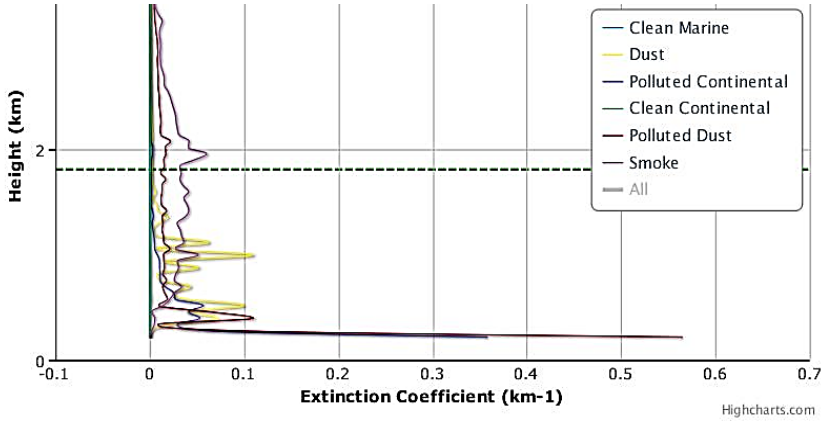

Chart 5 Vertical column of aerosol type observations (aerosol extinction at 532 nm per type for cell with centroid: Lat= 41.5º, Lon= 24.5º) over Filippoi (LIVAS database)

Table 14 Aerosol subtype occurrence and AOD statistics

CM	**0.4377**	**AOD at 532 nm**	
D	16.9038	Mean	0.265
PC	2.7982		
CC	11.1406	Median	0.131
PD	33.1093		
S	34.9904	StDev	0.55

Dust seems to be present at around 0.3 - 1 kilometer, while high concentrations of polluted dust and smoke occur in less than 200 meters from the surface.

4WT White Tower

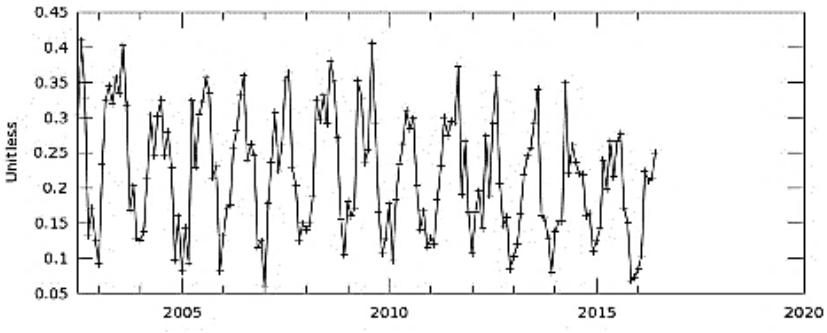

Diagram 4 Monthly AOD (0.55 μm) measurements for the time span 2002 – 2016 over the White Tower (MODIS – Aqua Dark Target

Table 15 Basic statistics

Lat	**40,62**
Long	22,95
Avg	0,219
Stdev	0,086
Min	0,06
Max	0,41
Median	0,218

The monthly average value of AOD at 0.55 for the whole period, over the White Tower, is 0.219 ±0.086 with maximum and minimum 0.41 and 0.06 respectively. The median value is 0.218.

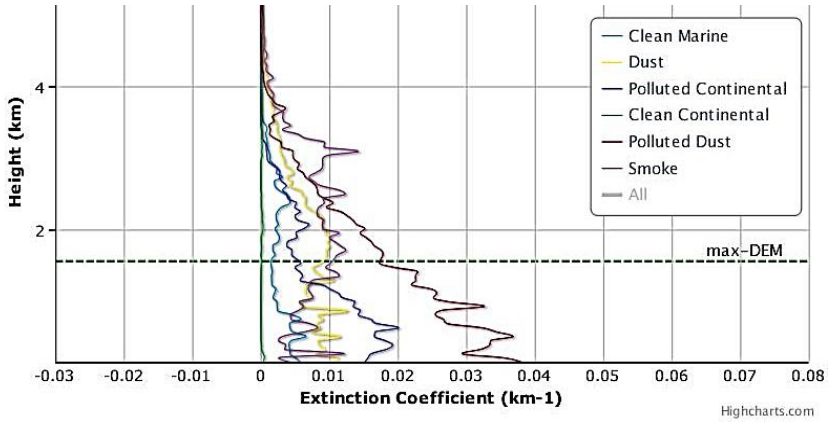

Chart 6 Vertical column of aerosol type observations (aerosol extinction at 532 nm per type for cell with centroid: Lat= 40.5^{o}, Lon= 22.5$^{o)}$ over the White Tower (LIVAS database)

Table 16 Aerosol subtype occurrence and AOD statistics

CM	**12.2426**	**AOD at 532 nm**	
D	22.226	Mean	0.151
PC	9.0192		
CC	1.2817	Median	0.06
PD	40.8636		
S	12.6368	StDev	0.357

As an urban and coastal site, the vertical profile shows significant fluctuation of all types of aerosols. Polluted dust is the dominant type near the surface followed by dust and polluted continental aerosol. Moving above 2 km the role of smoke also becomes important.

5VR Vergina

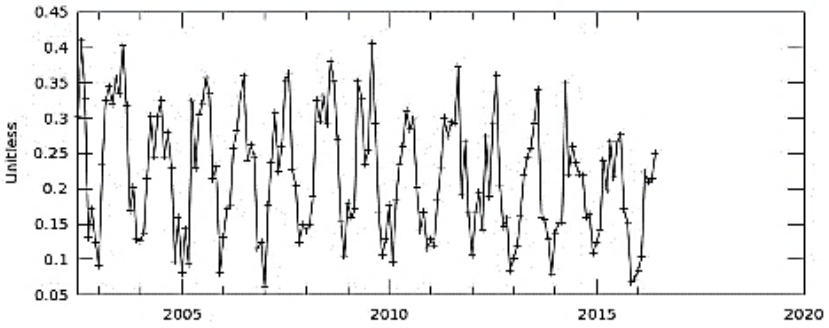

Diagram 5 Monthly AOD (0.55 μm) measurements for the time span 2002 – 2016 over Vergina (MODIS – Aqua Dark Target)

Table 17 Basic statistics

Lat	**40.48**
Long	22.31
Avg	0.219
Stdev	0.086
Min	0.06
Max	0.41
Median	0.218

The monthly average value of AOD at 0.55 for the whole period, over Vergina, is 0.219 ±0.086 with maximum and minimum 0.41 and 0.06 respectively. The median value is 0.218.

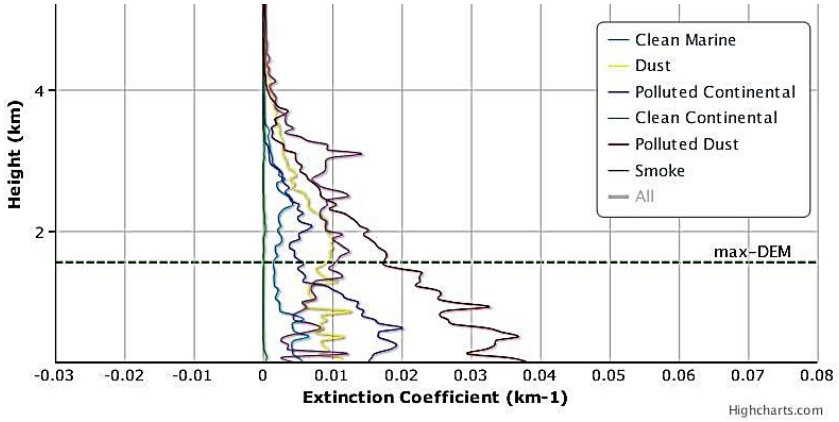

Chart 7 Vertical column of aerosol type observations (aerosol extinction at 532 nm per type for cell with centroid: Lat= 40.5º, Lon= 22.5º) over the White Tower (LIVAS database)

Table 18 Aerosol subtype occurrence and AOD statistics

CM	**12.2426**	**AOD at 532 nm**	
D	22.226	Mean	0.151
PC	9.0192		
CC	1.2817	Median	0.06
PD	40.8636		
S	12.6368	StDev	0.357

Fluctuations of all types of aerosols, are observed below 3,5 km, with the predominant type being polluted dust increasing near the surface. The second more dominant type near the surface is polluted continental.

6LS Larissa (Anc. Theatre)

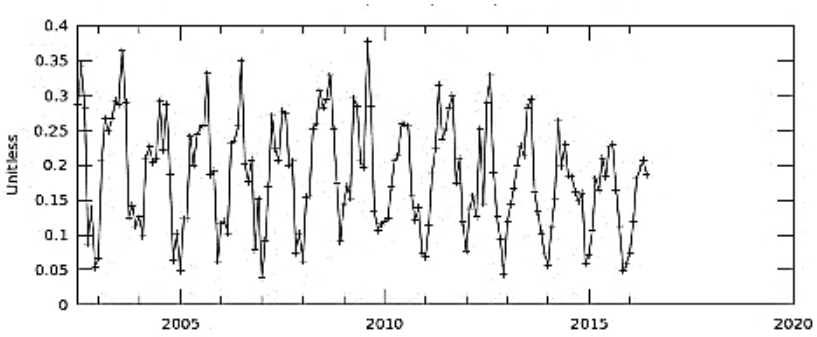

Diagram 6 Monthly AOD (0.55 μm) measurements for the time span 2002 – 2016 over the Ancient Theatre of Larissa (MODIS – Aqua Dark Target)

Table 19 Basic statistics

Lat	**39.64**
Long	22.41
Avg	0.185
Stdev	0.079
Min	0.039
Max	0.378
Median	0.186

The monthly average value of AOD at 0.55 for the whole period, over the Ancient Theatre of Larissa, is 0.185 ±0.079 with maximum and minimum 0.378 and 0.039 respectively. The median value is 0.186.

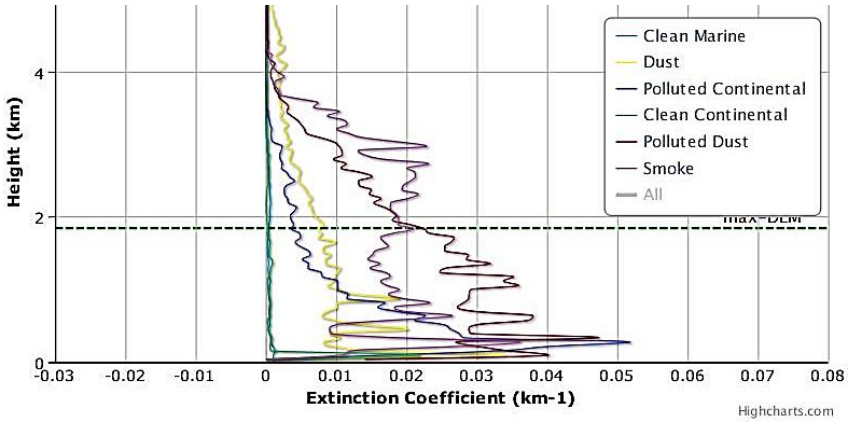

Chart 8 Vertical column of aerosol type observations (aerosol extinction at 532 nm per type for cell with centroid: Lat= 49.5^{o}, Lon= 22.5$^{o)}$ over the Ancient Theatre of Larissa (LIVAS database)

Table 20 Aerosol subtype occurrence and AOD statistics

CM	**2.6428**	**AOD at 532 nm**	
D	29.1937	Mean	0.201
PC	7.1276		
CC	2.4685	Median	0.081
PD	36.288		
S	21.5649	StDev	0.468

Once more, polluted dust is the dominant aerosol type gradually decreasing up to 3.8 km, while an almost constant profile is observed for smoke, from the surface and up to 3 km.

7DD Dodoni

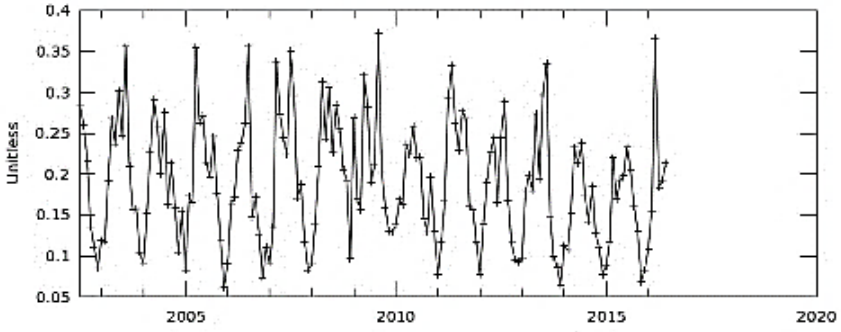

Diagram 7 Monthly AOD (0.55 μm) measurements for the time span 2002 – 2016 over Dodoni (MODIS – Aqua Dark Target)

Table 21 Basic statistics

Lat	**39.54**
Long	20.78
Avg	0.189
Stdev	0.074
Min	0.062
Max	0.372
Median	0.182

The monthly average value of AOD at 0.55 for the whole period, over Dodoni, is 0.189 ±0.074 with maximum and minimum 0.372 and 0.062 respectively. The median value is 0.182.

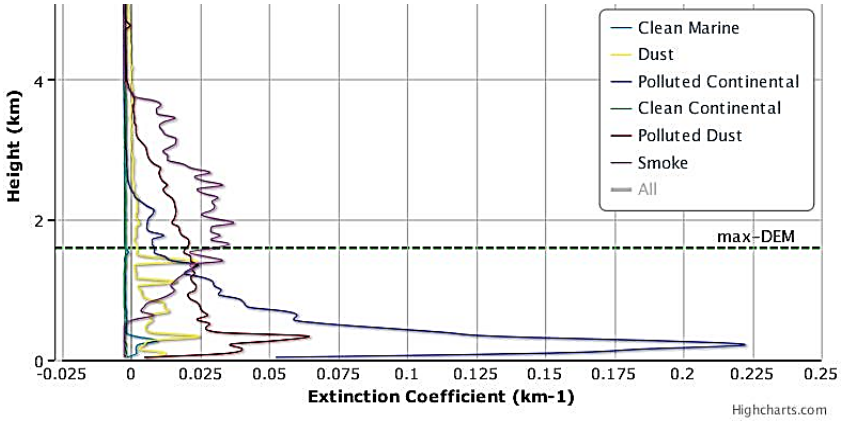

Chart 9 Vertical column of aerosol type observations (aerosol extinction at 532 nm per type for cell with centroid: Lat= 39.5^{o}, Lon= 20.5$^{o)}$ 532 nm) over Dodoni (LIVAS database)

Table 22 Aerosol subtype occurrence and AOD statistics

CM	**1.3053**	**AOD at 532 nm**	
D	23.7941	Mean	0.29
PC	13.6231		
CC	3.5714	Median	0.13044
PD	34.5349		
S	22.4556	StDev	0.54

Polluted continental increases significantly under 2 km, surpassing the other aerosol types, followed by polluted dust. A persistent, elevated layer of smoke is also found between 1.7-2.4 km.

8NC Nicopolis

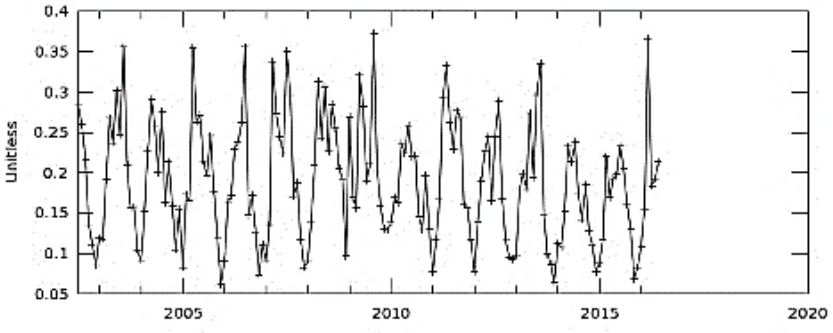

Diagram 8 Monthly AOD (0.55 μm) measurements for the time span 2002 – 2016 over Nicopolis (MODIS – Aqua Dark Target)

Table 23 Basic statistics

Lat	**39.22**
Long	20.73
Avg	0.189
Stdev	0.074
Min	0.062
Max	0.372
Median	0.182

The monthly average value of AOD at 0.55 for the whole period, over Nicopolis, is 0.189 ±0.074 with maximum and minimum 0.372 and 0.062 respectively. The median value is 0.182.

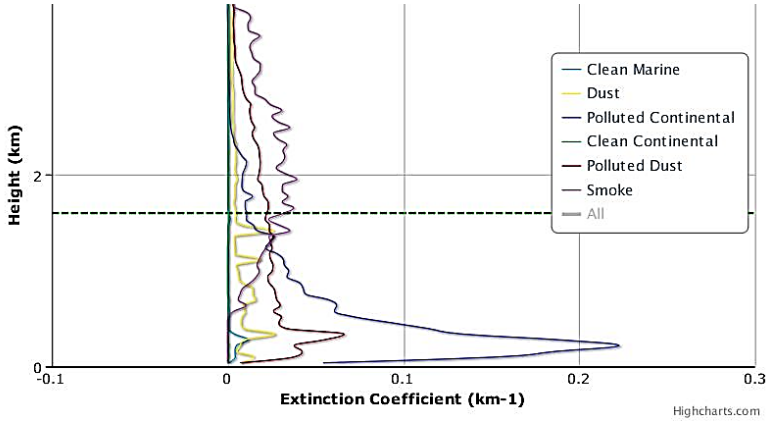

Chart 10 Vertical column of aerosol type observations (aerosol extinction at 532 nm per type for cell with centroid: Lat= 39.5º, Lon= 20.5º) 532 nm) over Nicopolis (LIVAS database)

Table 24 Aerosol subtype occurrence and AOD statistics

CM	**1.3053**	**AOD at 532 nm**	
D	23.7941	Mean	0.29
PC	13.6231		
CC	3.5714	Median	0.13044
PD	34.5349		
S	22.4556	StDev	0.54

Similarly to Dodoni, below 2 km the polluted continental profile shows an increase which becomes higher approximately near 500 m. An elevated layer of smoke is also present.

9MS Sanctuary of Messa

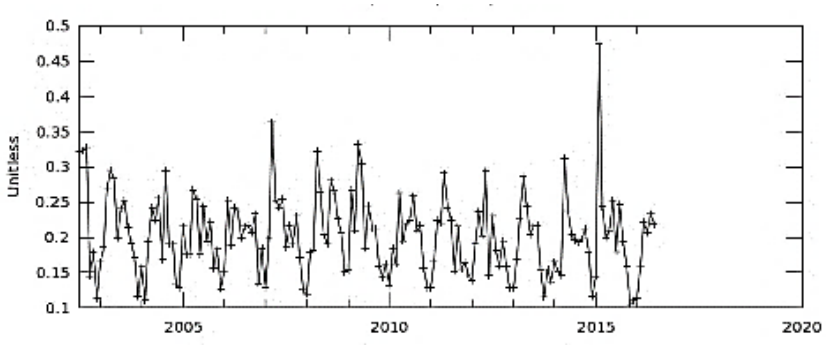

Diagram 9 Monthly AOD (0.55 μm) measurements for the time span 2002 – 2016 over the sanctuary of Messa (MODIS – Aqua Dark Target)

Table 25 Basic statistics

Lat	**39.19**
Long	26.3
Avg	0.203
Stdev	0.057
Min	0.105
Max	0.475
Median	0.198

The monthly average value of AOD at 0.55 for the whole period, over the site of Messa, is 0.203 ±0.057 with maximum and minimum 0.475 and 0.105 respectively. The median value is 0.198.

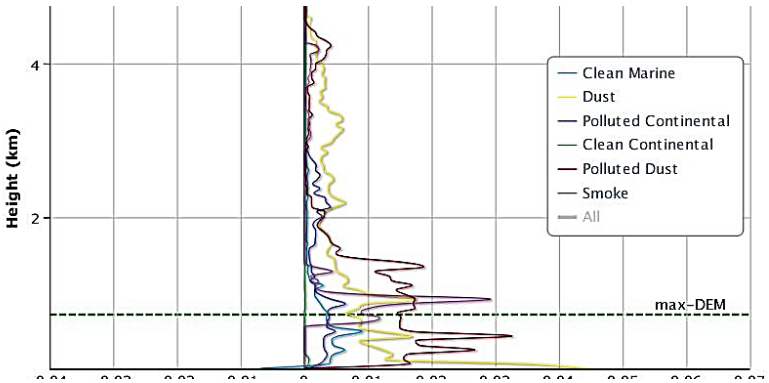

Chart 11 Vertical column of aerosol type observations (aerosol extinction at 532 nm per type for cell with centroid: Lat= 39.5º, Lon= 26.5º) 532 nm) over the sanctuary of Messa (LIVAS database)

Table 26 Aerosol subtype occurrence and AOD statistics

CM	**16.2168**	**AOD at 532 nm**	
D	40.6858	Mean	0.075
PC	6.969		
CC	0.354	Median	0.027
PD	33.0531		
S	2.323	StDev	0.227

Dust and polluted dust present the greatest fluctuations, particularly below 2 km, with concentrations of dust being superior near the surface.

10PL Palamari (Skyros)

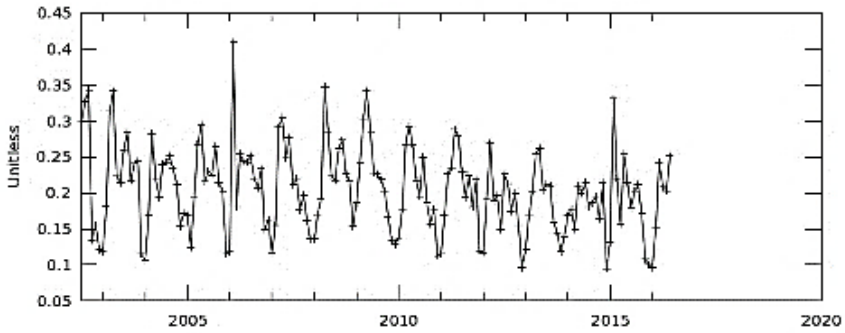

Diagram 59 Monthly AOD (0.55 μm) measurements for the time span 2002 – 2016 over Palamari (MODIS – Aqua Dark Target)

Table 27 Basic statistics

Lat	**38.95**
Long	24.51
Avg	0.206
Stdev	0.060
Min	0.094
Max	0.409
Median	0.208

The monthly average value of AOD at 0.55 for the whole period, over Palamari, is 0.206 ±0.060 with maximum and minimum 0.409 and 0.094 respectively. The median value is 0.208.

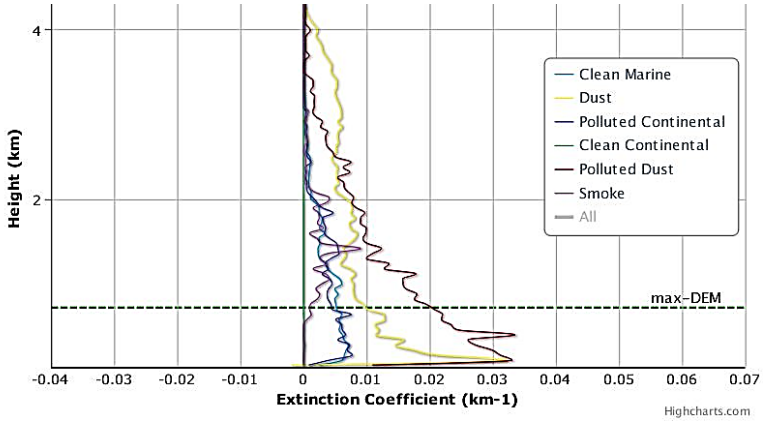

Chart 12 Vertical column of aerosol type observations (aerosol extinction at 532 nm per type for cell centroid: Lat= 38.5º, Lon= 24.5º) over Palamari (LIVAS database)

Table 28 Aerosol subtype occurrence and AOD statistics

CM	**24.8705**	**AOD at 532 nm**	
D	31.9215	Mean	0.093
PC	7.142		
CC	0.0316	Median	0.03
PD	34.0768		
S	1.0559	StDev	0.21

The profile of aerosols shows that their fluctuations start from 4th kilometer and beneath with dust present between 2-4 km. From 500 meters and below both polluted dust and dust stand out. Significant presence show also, clean marine aerosols.

11DE Delphi

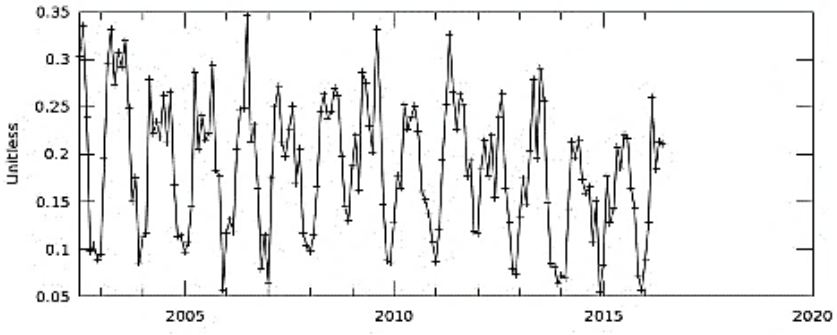

Diagram 11 Monthly AOD (0.55 μm) measurements for the time span 2002 – 2016 over Delphi (MODIS – Aqua Dark Target)

Table 29 Basic statistics

Lat	**38.48**
Long	22.49
Avg	0.186
Stdev	0.071
Min	0.055
Max	0.346
Median	0.186

The monthly average value of AOD at 0.55 for the whole period, over Delphi, is 0.186 ±0.071 with maximum and minimum 0.346 and 0.055 respectively. The median value is 0.186.

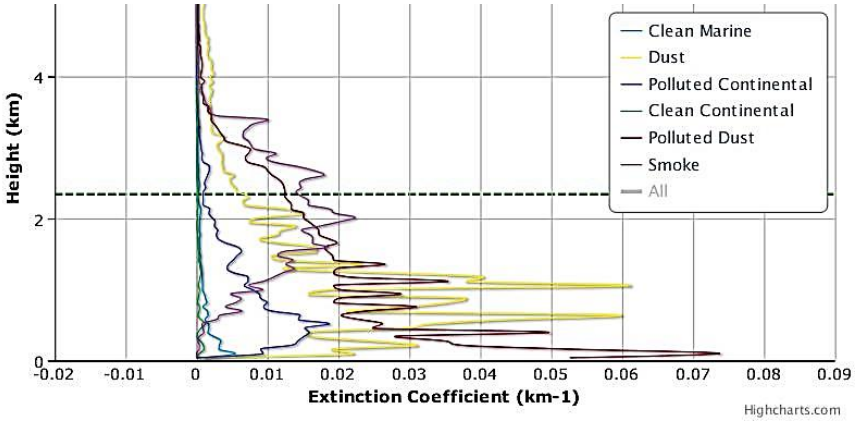

Chart 13 Vertical column of aerosol type observations (aerosol extinction at 532 nm per type for cell centroid: Lat= 38.5º, Lon= 22.5º) over Delphi (LIVAS database)

Table 30 Aerosol subtype occurrence and AOD statistics

CM	**2.2679**	**AOD at 532 nm**	
D	38.3703	Mean	0.181
PC	5.0543		
CC	3.1771	Median	0.077
PD	32.1303		
S	18.53	StDev	0.467

Intense fluctuations of dust and polluted dust are observed, mainly below the 2nd km., while it is rather interesting to see a solid layer of polluted continental aerosol from 1 km to 3.5 km.

12AC Acropolis

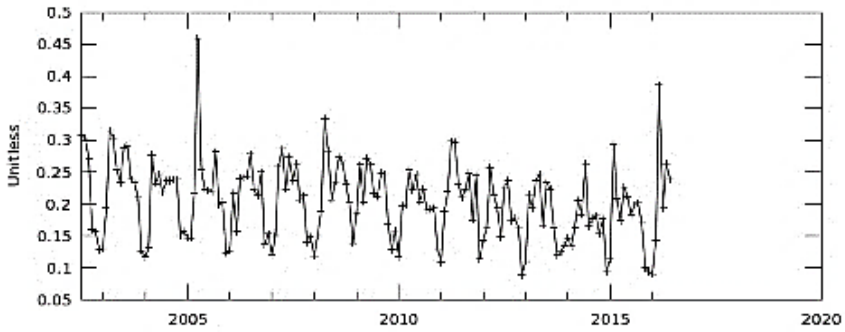

Diagram 12 Monthly AOD (0.55 μm) measurements for the time span 2002 – 2016 over Acropolis (MODIS – Aqua Dark Target)

Table 31 Basic statistics

Lat	**37.97**
Long	23.72
Avg	0.204
Stdev	0.059
Min	0.088
Max	0.46
Median	0.208

The monthly average value of AOD at 0.55 for the whole period, over Acropolis, is 0.204 ±0.059 with maximum and minimum 0.46 and 0.088 respectively. The median value is 0.208.

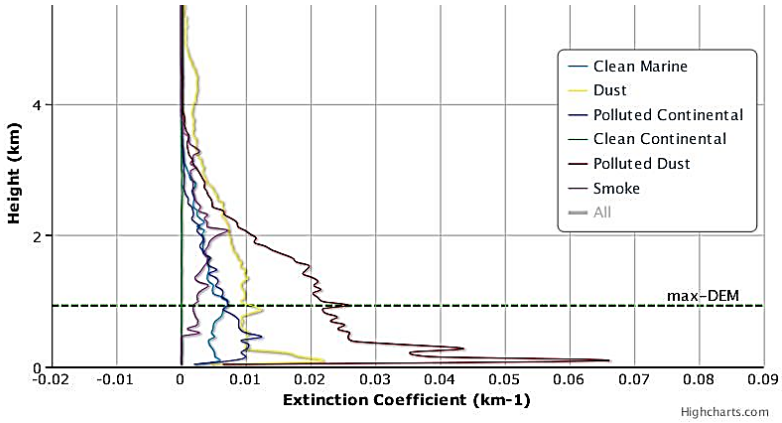

Chart 14 Vertical column of aerosol type observations (aerosol extinction at 532 nm per type for cell centroid: Lat= 37.5º, Lon= 23.5º) over Acropolis (LIVAS database)

Table 32 Aerosol subtype occurrence and AOD statistics

CM	**22.1287**	**AOD at 532 nm**	
D	23.8656	Mean	0.119
PC	8.6951		
CC	0.9824	Median	0.058
PD	39.5989		
S	4.1197	StDev	0.267

The presence of mainly polluted dust but also dust is evidenced with large concentrations from the 2nd km and below. Important is also the presence of clean marine aerosols that affect the region.

13MC Mycenae

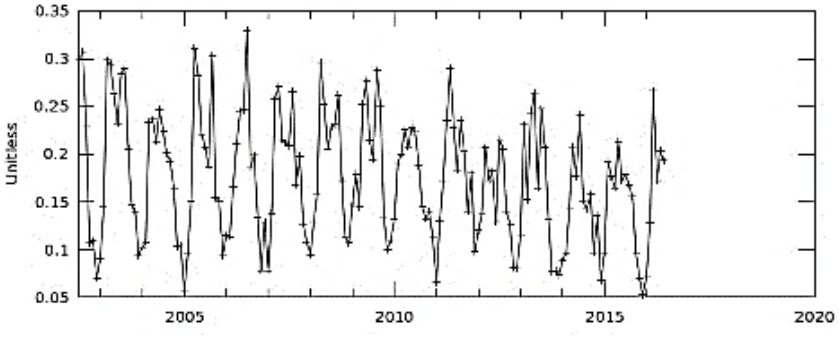

Diagram 13 Monthly AOD (0.55 μm) measurements for the time span 2002 – 2016 over Mycenae (MODIS – Aqua Dark Target)

Table 33 Basic statistics

Lat	**37.73**
Long	22.76
Avg	0.179
Stdev	0.055
Min	0.072
Max	0.333
Median	0.178

The monthly average value of AOD at 0.55 for the whole period, over Mycenae, is 0.179 ±0.055 with maximum and minimum 0.333 and 0.072 respectively. The median is 0.178.

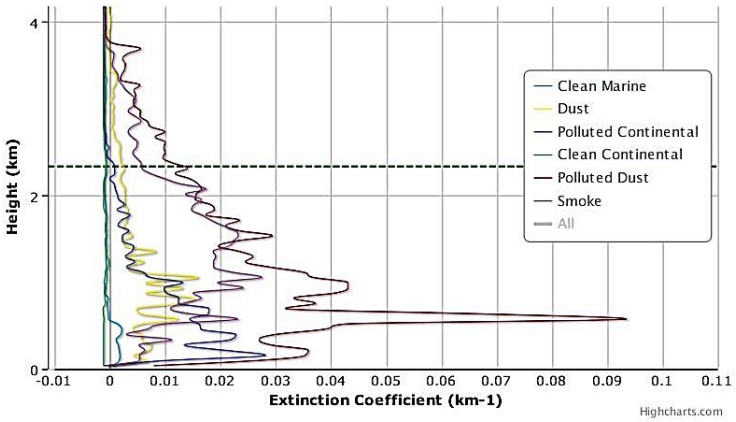

Chart 15 Vertical column of aerosol type observations (aerosol extinction at 532 nm per type for cell centroid: Lat= 37.5º, Lon= 22.5º) over Mycenae (LIVAS database)

Table 34 Aerosol subtype occurrence and AOD statistics

CM	**4.5219**	**AOD at 532 nm**	
D	23.4084	Mean	0.163
PC	6.4853		
CC	2.9154	Median	0.075
PD	43.3319		
S	18.215	StDev	0.321

Variations of all types of aerosols are observed from the 4th km and below. At the 2nd km it is obvious that polluted dust surpasses with a maximum at 500 m. Dust and smoke are also observed near the surface.

14OL Olympia

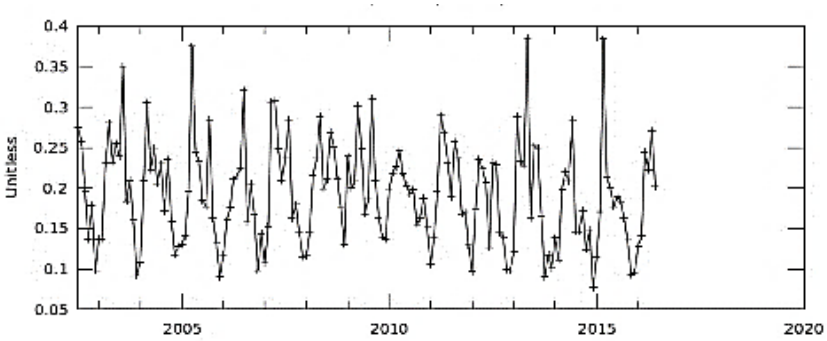

Diagram 14 Monthly AOD (0.55 μm) measurements for the time span 2002 – 2016 over Olympia (MODIS – Aqua Dark Target)

Table 35 Basic statistics

Lat	**37.64**
Long	21.62
Avg	0.192
Stdev	0.063
Min	0.077
Max	0.385
Median	0.191

The monthly average value of AOD at 0.55 for the whole period, over Olympia, is 0.192±0.063 with maximum and minimum 0.385 and 0.077 respectively. The median value is 0.191.

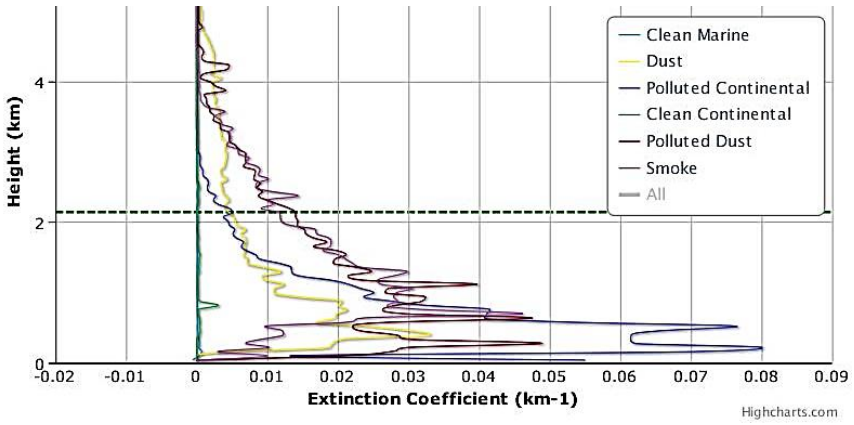

Chart 16 Vertical column of aerosol type observations (aerosol extinction at 532 nm per type for cell centroid: Lat= 37.5º, Lon= 21.5º) over Olympia (LIVAS database)

Table 36 Aerosol subtype occurrence and AOD statistics

CM	**0.6464**	**AOD at 532 nm**	
D	29.7532	Mean	0.21179
PC	10.629		
CC	2.5171	Median	0.08114
PD	36.1574		
S	19.5418	StDev	0.55057

At least three types of aerosol show considerable fluctuation from 5 km and below. From the 1st km down to the surface polluted dust stands out in terms of other aerosols. Follow the rest (dust, smoke and polluted continental) with smaller but still significant concentrations.

15IR Ireon (Samos)

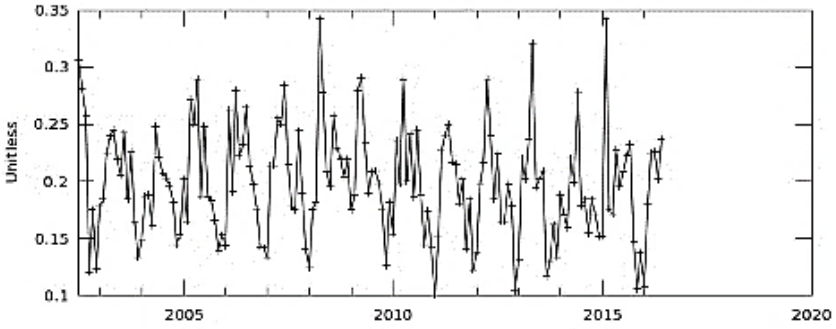

Diagram 15 Monthly AOD (0.55 μm) measurements for the time span 2002 – 2016 over Ireon (MODIS – Aqua Dark Target)

Table 37 Basic statistics

Lat	**37.66**
Long	26.88
Avg	0.199
Stdev	0.048
Min	0.100
Max	0.342
Median	0.196

The monthly average value of AOD at 0.55 for the whole period, over Ireon, is 0.199 ±0.048 with maximum and minimum 0.342 and 0.100 respectively. The median value is 0.196.

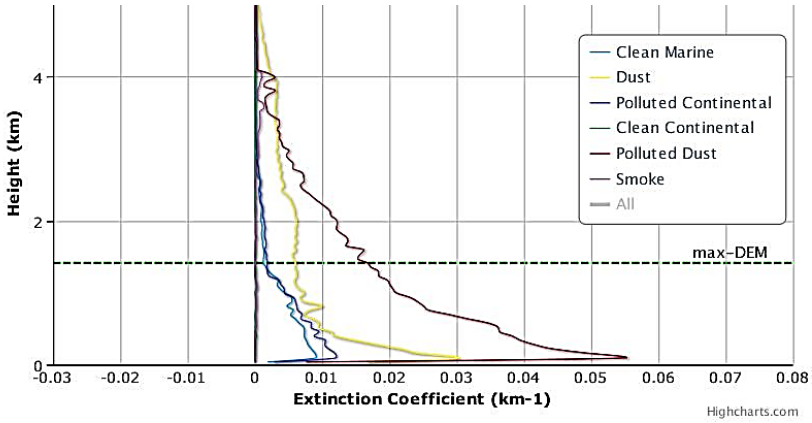

Chart 17 Vertical column of aerosol type observations (aerosol extinction at 532 nm per type for cell centroid: Lat= 37.5°, Lon= 26.5°) over Ireon (LIVAS database)

Table 38 Aerosol subtype occurrence and AOD statistics

CM	**12.4324**	**AOD at 532 nm**	
D	27.5848	Mean	0.110
PC	7.0894		
CC	1.1282	Median	0.045
PD	48.4398		
S	2.5345	StDev	0.276

The presence of aerosols starts from the 4th km and below and becomes greater after the 2nd km. The main aerosol affecting the area is polluted dust. Dust, clean marine aerosols and polluted continental are also present.

16ME Ancient Messene

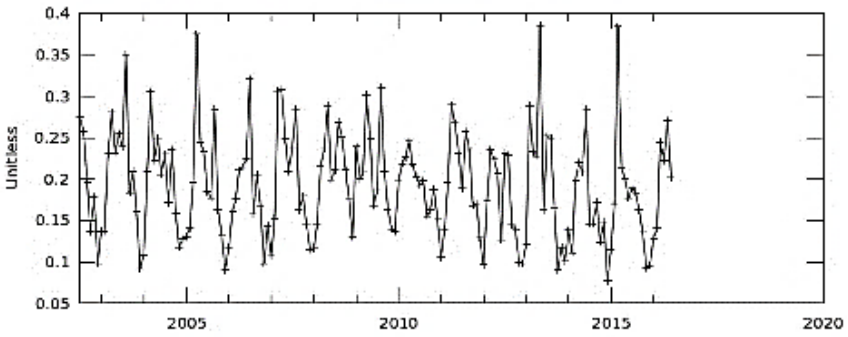

Diagram 16 Monthly AOD (0.55 μm) measurements for the time span 2002 – 2016 over Anc. Messene (MODIS – Aqua Dark Target)

Table 39 Basic statistics

Lat	**37.17**
Long	21.92
Avg	0.193
Stdev	0.063
Min	0.077
Max	0.385
Median	0.191

The monthly average value of AOD at 0.55 for the whole period, over Ancient Messene, is 0.193 ±0.063 with maximum and minimum 0.385 and 0.077 respectively. The median value is 0.191.

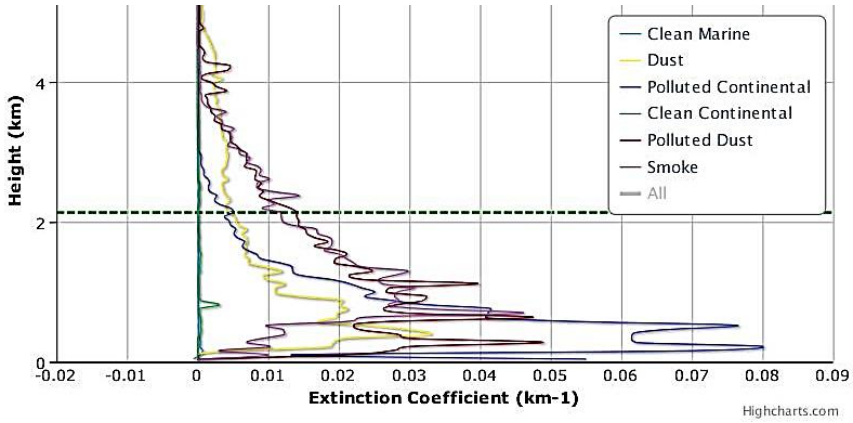

Chart 18 Vertical column of aerosol type observations (aerosol extinction at 532 nm per type for cell centroid: Lat= 37.5º, Lon= 21.5º) over Anc. Messene (LIVAS database)

Table 40 Aerosol subtype occurrence and AOD statistics

CM	**0.6464**	**AOD at 532 nm**	
D	29.7532	Mean	0.211
PC	10.629		
CC	2.5171	Median	0.081
PD	36.1574		
S	19.5418	StDev	0.55

The variations of aerosols start around the 4th km. After the 2nd km the fluctuations increase. The main aerosols affecting the area near the surface is polluted dust and dust. Smoke and polluted continental aerosols are also present.

17DL Delos

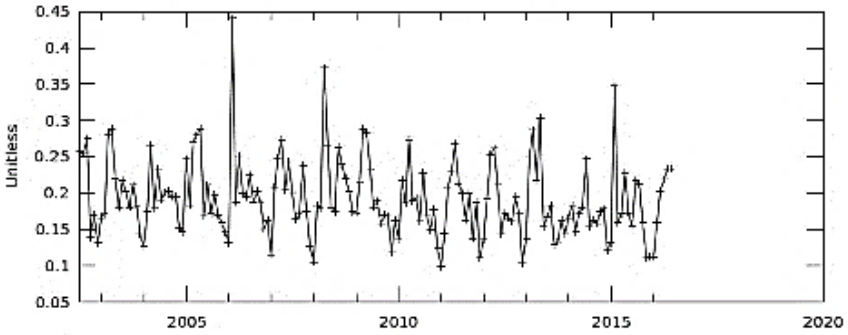

Diagram 17 Monthly AOD (0.55 μm) measurements for the time span 2002 – 2016 over Delos (MODIS – Aqua Dark Target)

Table 41 Basic statistics

Lat	**37.40**
Long	25.26
Avg	0.193
Stdev	0.053
Min	0.099
Max	0.440
Median	0.183

The monthly average value of AOD at 0.55 for the whole period, over Delos, is 0.193 ±0.053 with maximum and minimum 0.440 and 0.099 respectively. The median value is 0.183.

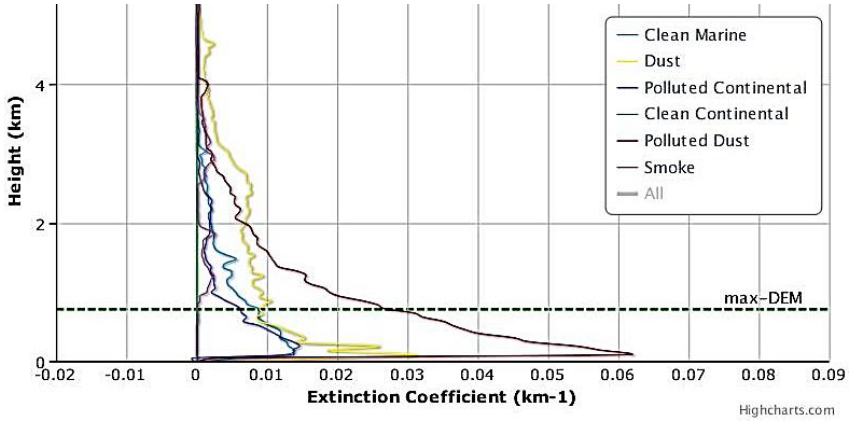

Chart 19 Vertical column of aerosol type observations (aerosol extinction at 532 nm per type for cell centroid: Lat= 37.5º, Lon= 25.5º) over Delos (LIVAS database)

Table 42 Aerosol subtype occurrence and AOD statistics

CM	**24.3206**	**AOD at 532 nm**	
D	29.3483	Mean	0.114
PC	5.7172		
CC	0	Median	0.044
PD	35.3797		
S	4.2159	StDev	0.269

The presence of aerosols starts approximately at 4 km. From 800m down to the surface polluted dust and dust stand out in terms of other aerosols. Dust shows an almost stable vertical distribution up to 3 km. Clean marine aerosols show also significant concentrations in this area.

18ST Santorini (Ancient Thira)

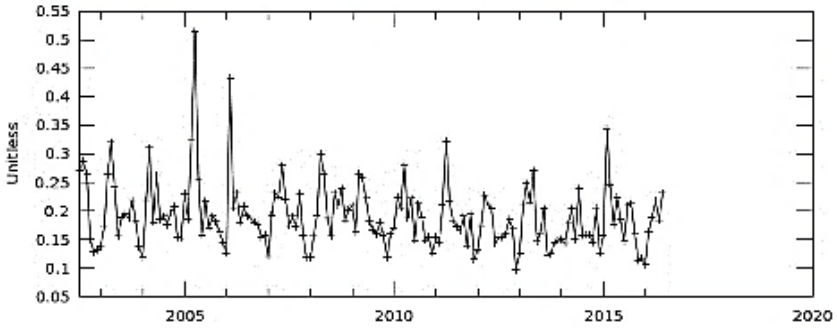

Diagram 18 Monthly AOD (0.55 μm) measurements for the time span 2002 – 2016 over Ancient Thira (MODIS – Aqua Dark Target)

Table 43 Basic statistics

Lat	**36.35**
Long	25.39
Avg	0.191
Stdev	0.057
Min	0.097
Max	0.515
Median	0.184

The monthly average value of AOD at 0.55 for the whole period, over Anc. Thira, is 0.191 ±0.057 with maximum and minimum 0.515 and 0.097 respectively. The median value is 0.184.

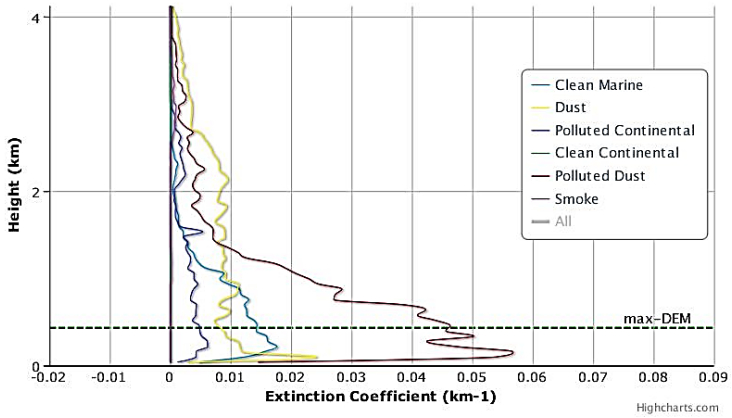

Chart 20 Vertical column of aerosol type observations (aerosol extinction at 532 nm per type for cell centroid: Lat= 36.5º, Lon= 25.5º) over Ancient Thira (LIVAS database)

Table 44 Aerosol subtype occurrence and AOD statistics

CM	**27.9767**	**AOD at 532 nm**	
D	28.0599	Mean	0.104
PC	6.7299		
CC	0	Median	0.039
PD	36.3176		
S	0.4127	StDev	0.266

Once more dust shows an almost stable vertical distribution up to 3 km. Below 1 km polluted dust dominates, while clean marine as expected for an island imposes a significant contribution as well.

19RH Rhodes

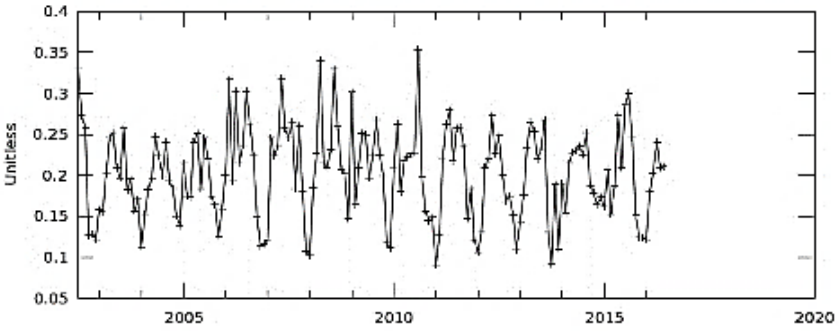

Diagram 19 Monthly AOD (0.55 μm) measurements for the time span 2002 – 2016 over Rhodes (MODIS – Aqua Dark Target)

Table 45 Basic statistics

Lat	**36.44**
Long	28.22
Avg	0.202
Stdev	0.055
Min	0.09
Max	0.353
Median	0.207

The monthly average value of AOD at 0.55 for the whole period, over the Medieval city of Rhodes, is 0.202 ±0.055 with maximum and minimum 0.353 and 0.09 respectively. The median value is 0.207.

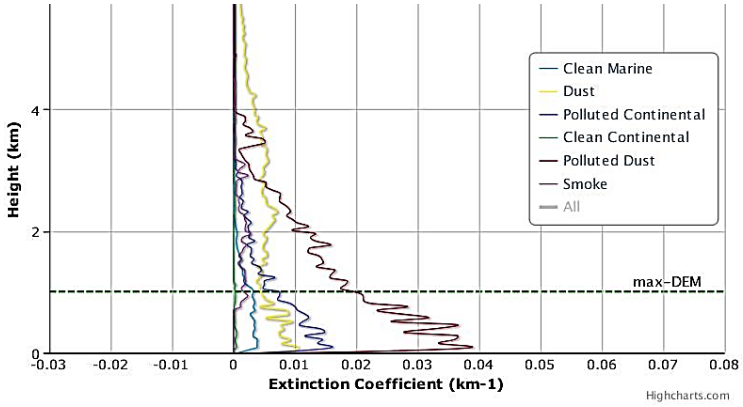

Chart 21 Vertical column of aerosol type observations (aerosol extinction at 532 nm per type for cell centroid: Lat= 36.5º, Lon= 28.5º) over Rhodes (LIVAS database)

Table 46 Aerosol subtype occurrence and AOD statistics

CM	**8.369**	**AOD at 532 nm**	
D	32.9123	Mean	0.10434
PC	10.1794		
CC	1.0817	Median	0.0251
PD	44.4455		
S	1.8364	StDev	0.26533

Dust is present throughout the whole column and up to almost 5 km. Below 3 km polluted dust is the predominant aerosol type, followed by polluted continental

20FS Falassarna

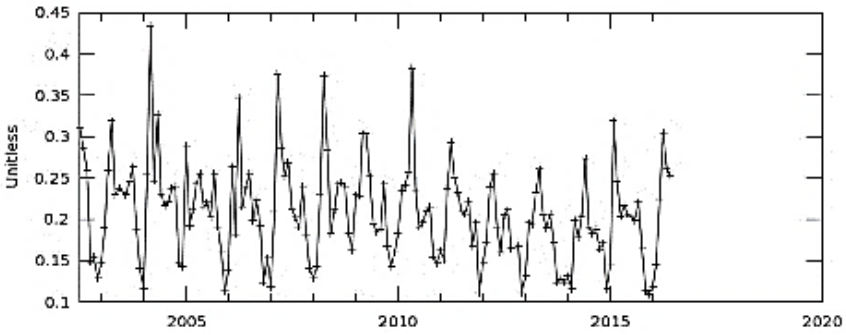

Diagram 20 Monthly AOD (0.55 μm) measurements for the time span 2002 – 2016 over Falassarna (MODIS – Aqua Dark Target)

Table 47 Basic statistics

Lat	**35.49**
Long	23.65
Avg	0.208
Stdev	0.059
Min	0.109
Max	0.434
Median	0.205

The monthly average value of AOD at 0.55 for the whole period, over Falassarna, is 0.208 ±0.059 with maximum and minimum 0.434 and 0.109 respectively. The median value is 0.205.

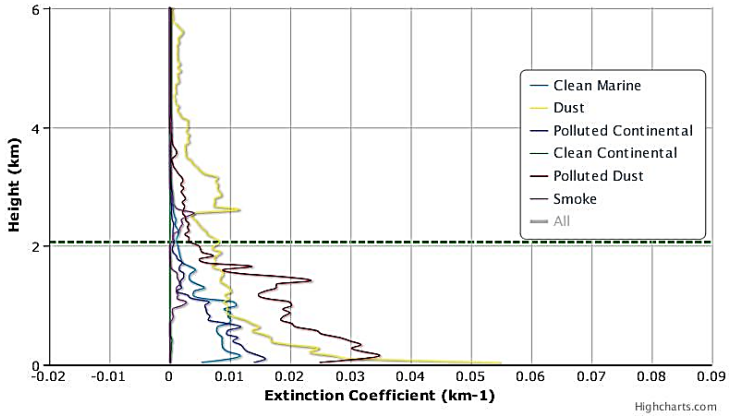

Chart 22 Vertical column of aerosol type observations (aerosol extinction at 532 nm per type for cell centroid: Lat= 35.5º, Lon= 23.5º) over Falassarna (LIVAS database)

Table 48 Aerosol subtype occurrence and AOD statistics

CM	**25.8894**	**AOD at 532 nm**	
D	31.7242	Mean	0.112
PC	7.3939		
CC	0.15	Median	0.035
PD	31.6009		
S	2.1217	StDev	0.319

The profile of dust shows that it is present also at 6 km. This site is situated in the west-southernmost Greece and the dominance of dust is highly expected. From the 2nd km and below, along with dust, polluted dust and clean marine aerosols also make their appearance, reaching the surface.

21KN Knossos

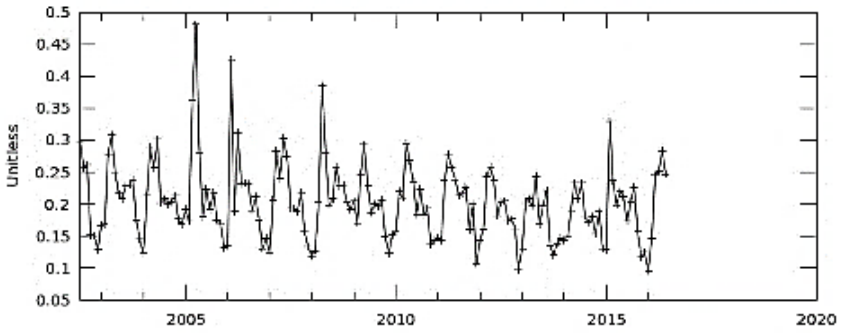

Diagram 21 Monthly AOD (0.55 μm) measurements for the time span 2002 – 2016 over Knossos (MODIS – Aqua Dark Target)

Table 49 Basic statistics

Lat	**35.29**
Long	25.16
Avg	0.204
Stdev	0.060
Min	0.095
Max	0.481
Median	0.201

The monthly average value of AOD at 0.55 for the whole period, over Knossos, is 0.204 ±0.060 with maximum and minimum 0.481 and 0.095 respectively. The median value is 0.201.

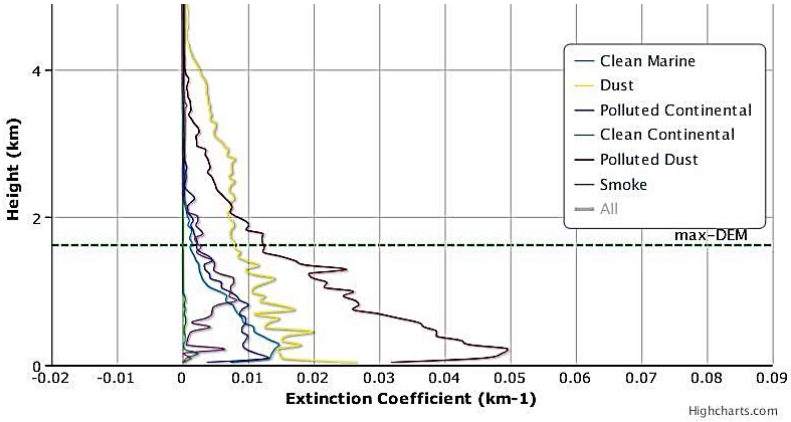

Chart 23 Vertical column of aerosol type observations (aerosol extinction at 532 nm per type for cell centroid: Lat= 35.5º, Lon= 25.5º) over Knossos (LIVAS database)

Table 50 Aerosol subtype occurrence and AOD statistics

CM	**15.675**	**AOD at 532 nm**	
D	36.2841	Mean	0.128
PC	6.6603		
CC	0.6411	Median	0.054
PD	37.7179		
S	2.6966	StDev	0.309

Another Cretan site, with dust and polluted dust being the dominant types of aerosol Clean marine aerosols are exhibited from the 2nd km and downwards.

4.2. SEASONAL PATTERNS

1MR Maronia

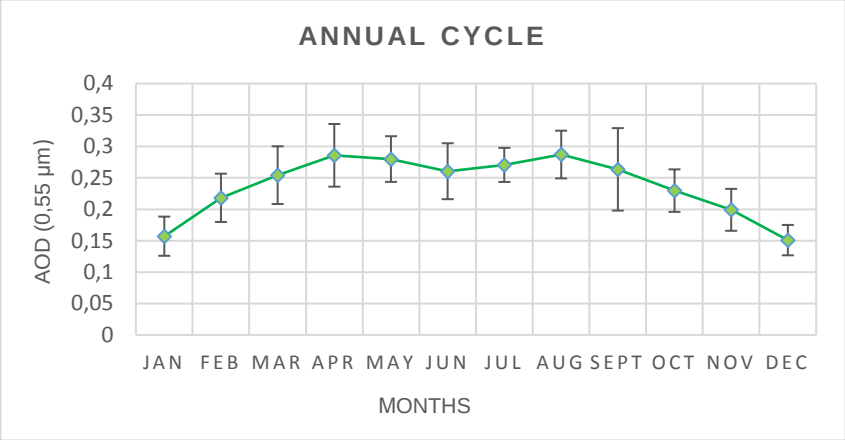

Graph 1 Annual cycle of AOD at 0.55 μm for Maronia (monthly average values for each month for the period 2002-2016 and the standard deviation bars)

The seasonal variability for the area of Maronia shows a bimodal distribution. Maximum AODs are encountered in summer with a peak in August and a monthly average value of 0.287 followed by a secondary peak in April. From November to February the minimum AODs are found (0.199 – 0.218). The period between March and September shows a plateau around the maximum value.

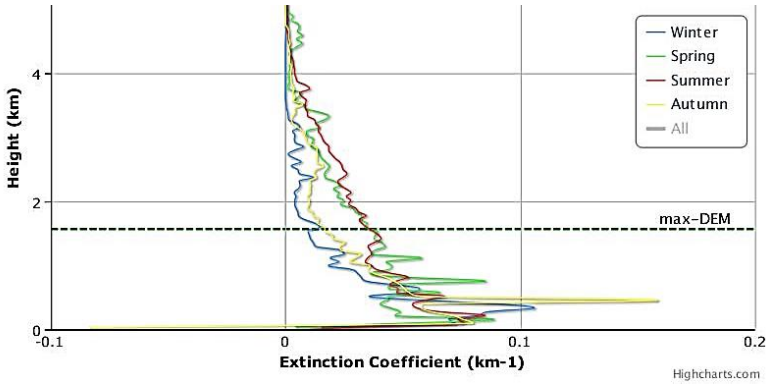

Chart 24 Vertical column of aerosol seasonal observations (aerosol extinction at 532 nm per season for cell centroid: Lat= 40.5º, Lon= 25.5º) over Maronia (LIVAS database)

An appreciable increase after the 2nd km is noticeable, indicative of the average aerosol mixing layer (MLH). It is observed that on the surface the pollution influence is mainly in spring and autumn.

.

2AV Avdira

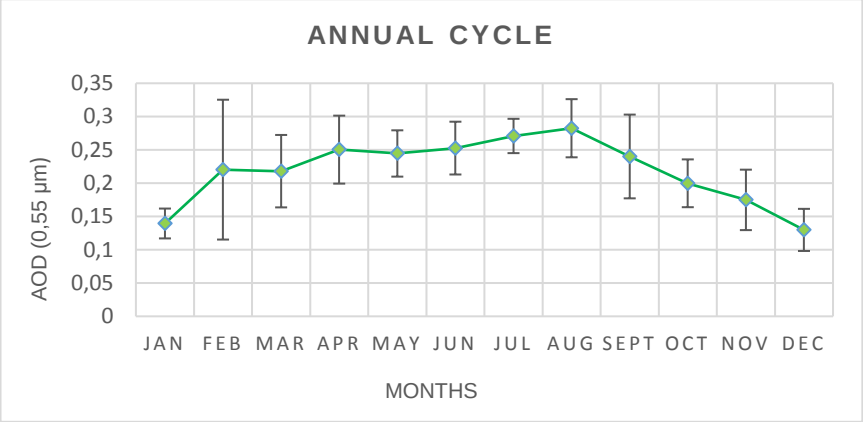

Graph 2 Annual cycle of AOD at 0.55 μm for Avdira (monthly average values for each month for the period 2002-2016 and the standard deviation bars)

The seasonal variability for the area of Avdira shows maximum AODs in summer, with a peak in August and a monthly average value of 0.282. Minimum AODs are found from October to January (0.199 – 0.140).

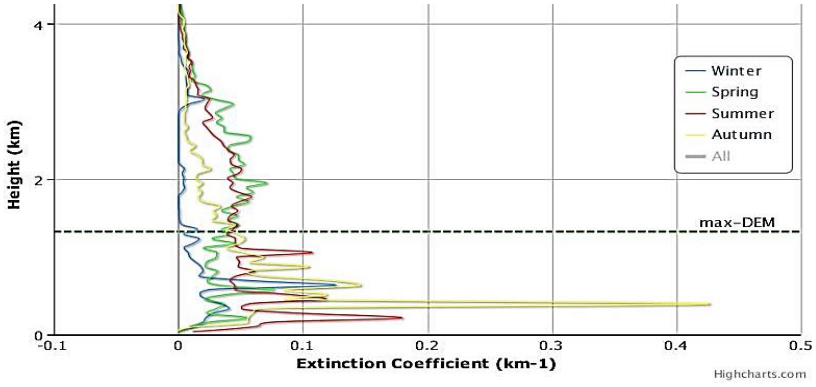

Chart 25 Vertical column of aerosol seasonal observations (aerosol extinction at 532 nm per season for cell centroid: Lat= 41.5º, Lon= 25,5º) over Avdira (LIVAS database)

A considerable increase at about 1500m is seen. Although, autumn presents high concentrations at 500 m, pollution seems to influence the surface mostly in summer concentrations at the 500 m.

3FL Filippoi

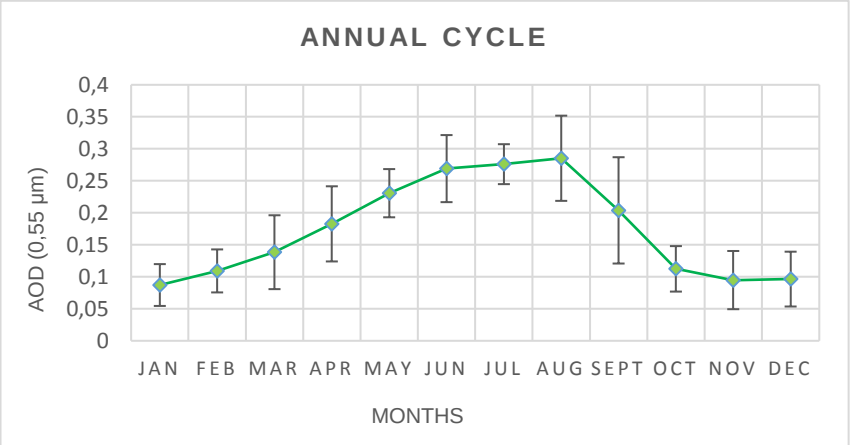

Graph 3 Annual cycle of AOD at 0.55 μm for Filippoi (monthly average values for each month for the period 2002-2016 and the standard deviation bars)

The seasonal variability for the area of Filippoi shows a summer maximum with AOD peaking in August and a monthly average value of 0.285. From October to February the minimum AODs (0.112 – 0.109) are found.

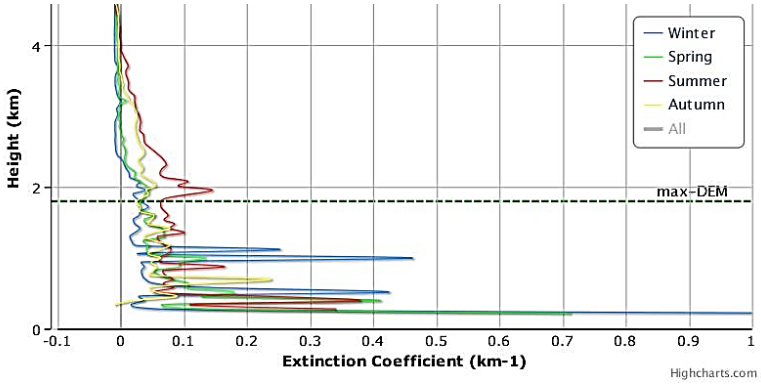

Chart 26 Vertical column of aerosol seasonal observations (aerosol extinction at 532 nm per season for cell centroid: Lat= 41.5º, Lon= 24.5º) over Filippoi (LIVAS database)

Pollution seems to be balanced throughout the different seasons, with spiky behavior.

.

4WT White Tower

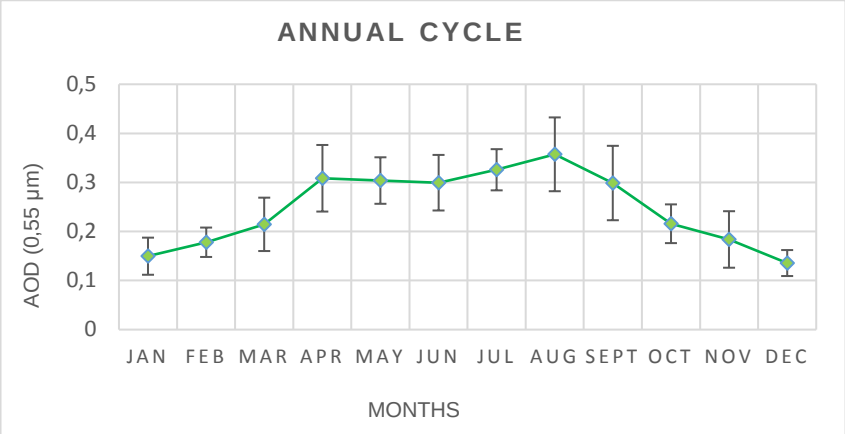

Graph 4 Annual cycle of AOD at 0.55 μm for the White Tower (monthly average values for each month for the period 2002-2016 and the standard deviation bars)

On a seasonal basis, maximum AODs are encountered in summer with a peak in August and a monthly average value of 0.357. From November to February the minimum AODs (0.183 – 0.178) are found. From April to July a plateau is observed.

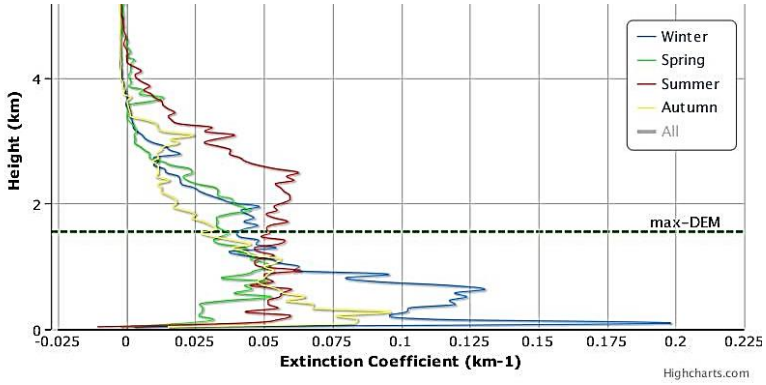

Chart 27 Vertical column of aerosol seasonal observations (aerosol extinction at 532 nm per season for cell centroid: Lat= 40.5º, Lon= 22.5º) over the White Tower (LIVAS database)

This urban site shows intense seasonal variability of the height that aerosols is confined (MHL). This height starts from around 800m in winter to up to 2.8 km in summer, and in the latter case the homogeneous concentration with height is striking. It is during winter when most of the pollution is evidenced near the surface.

5VR Vergina

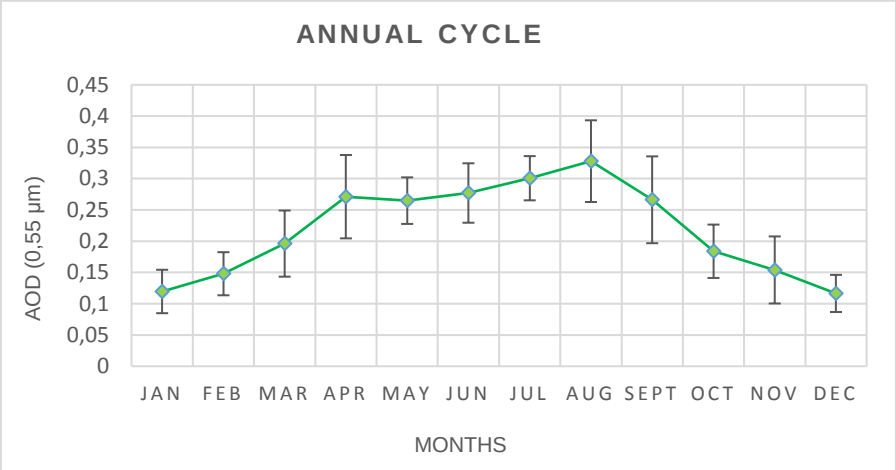

Graph 5 Annual cycle of AOD at 0.55 μm for Vergina (monthly average values for each month for the period 2002-2016 and the standard deviation bars)

A summer maximum is observed for the area of Vergina with a peak in August and a monthly average value 0.327. From November to February the minimum AODs (0.154 – 0.147) are found. From April to July a plateau is also observed.

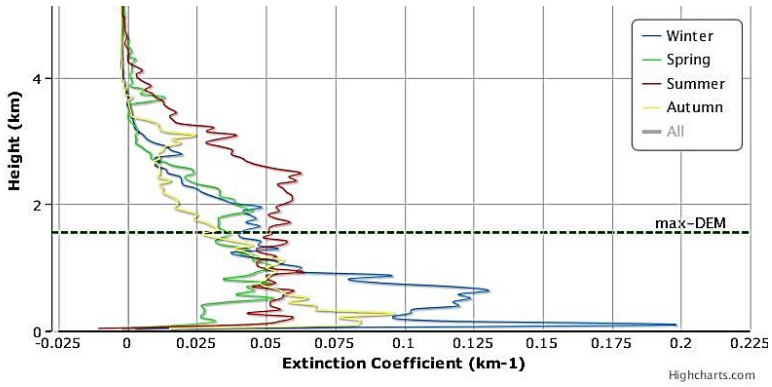

Chart 28 Vertical column of aerosol seasonal observations (aerosol extinction at 532 nm per season for cell centroid: Lat= 40.5º, Lon= 22.5º) over Vergina (LIVAS database)

Pollution action initiates around the 3rd km in summer and with a stable motion reaches the surface. Important presence of pollution is observed in winter months at 100m from the surface. Autumn and spring also show high levels of pollution on the surface.

6LS Ancient Theater of Larissa

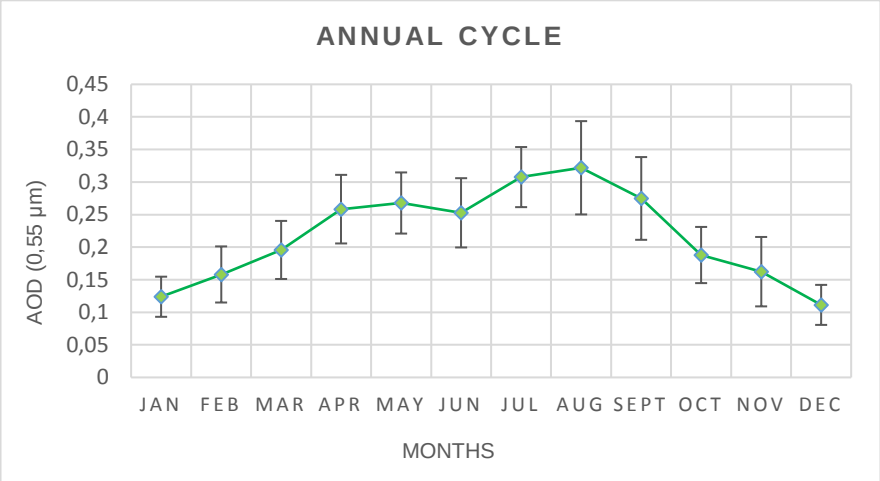

Graph 6 Annual cycle of AOD at 0.55 μm for the Ancient Theater of Larissa (monthly average values for each month for the period 2002-2016 and the standard deviation bars)

A summer maximum is observed for the Ancient Theater of Larissa with a peak in August and a monthly average value 0.321. From November to February the minimum AODs (0.162 – 0.158) are found. A hump in spring is also seen.

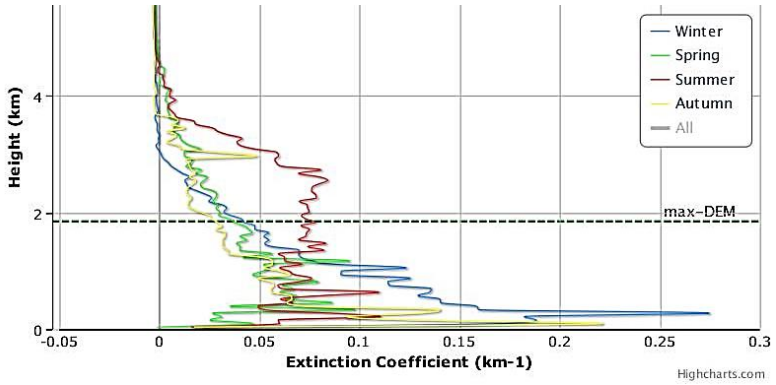

Chart 129 Vertical column of aerosol seasonal observations (aerosol extinction at 532 nm per season for cell centroid: Lat= 49.5º, Lon= 22.5º) over the Ancient Theater of Larissa (LIVAS database)

The vertical distribution per season in this site resembles our finding for White Tower. The MLH starts from around 1 km in winter to up to 2.5 km in summer, and in the latter case the homogeneous concentration with height is also present. During winter, most of the pollution is evidenced near the surface.

7DD Dodoni

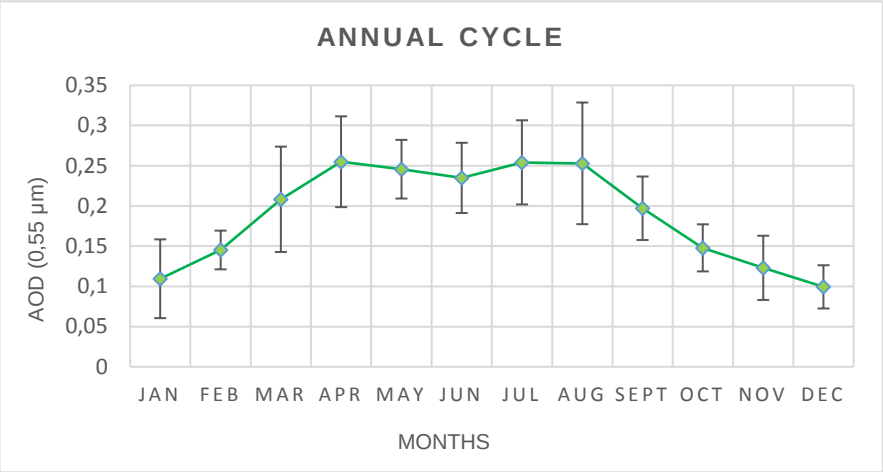

Graph 7 Annual cycle of AOD at 0.55 μm for Dodoni (monthly average values for each month for the period 2002-2016 and the standard deviation bars)

The seasonal variability for the area of Dodoni demonstrates an almost flat plateau in spring and summer, with peak values in the order of 0.255. From October to February the minimum AODs (0.197 – 0.109) are found.

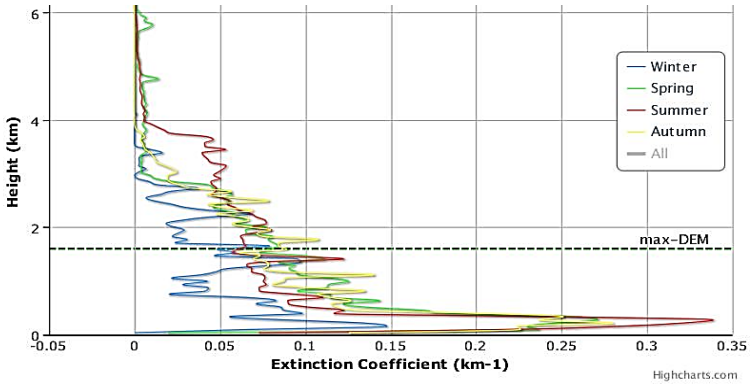

Chart 30 Vertical column of aerosol seasonal observations (aerosol extinction at 532 nm per season for cell centroid: Lat= 39.5º, Lon= 20.5º) over Dodoni (LIVAS database)

In the transition seasons (spring and autumn) pollution goes up to almost 3 km, in summer even close to 4 km while in winter, there is no typical profile.

8NC Nicopolis

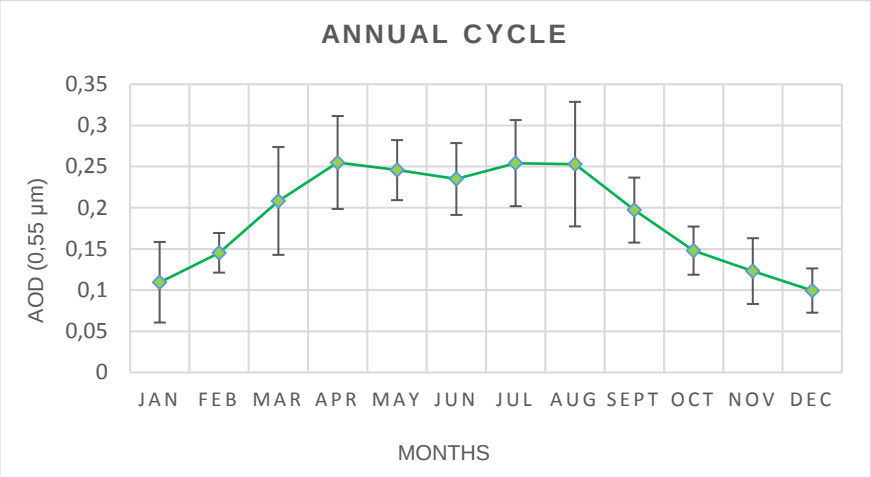

Graph 8 Annual cycle of AOD at 0.55 μm for Nicopolis (monthly average values for each month for the period 2002-2016 and the standard deviation bars)

Similarly to Dodoni, the seasonal variability for the area of Nicopolis demonstrates an almost flat plateau in spring and summer, with peak values in the order of 0.255, and a minimum in the range 0.1-0.15 during the cold months.

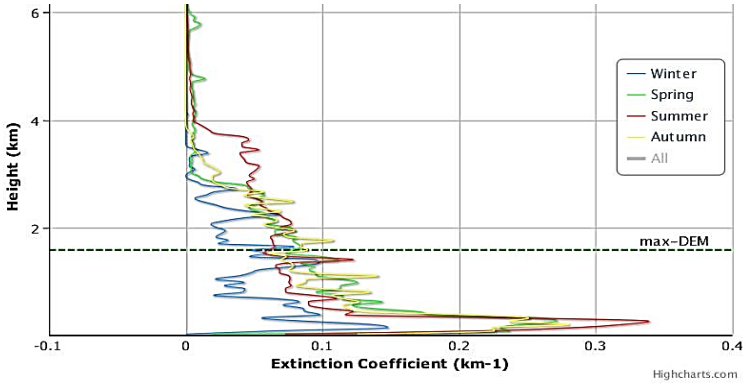

Chart 1301 Vertical column of aerosol seasonal observations (aerosol extinction at 532 nm per season for cell centroid: Lat= 39.5º, Lon= 20.5º) over Nicopolis (LIVAS database)

In the transition seasons (spring and autumn) pollution goes up to almost 3 km, in summer even close to 4 km while in winter, there is no typical profile.

9MS Sanctuary of Messa

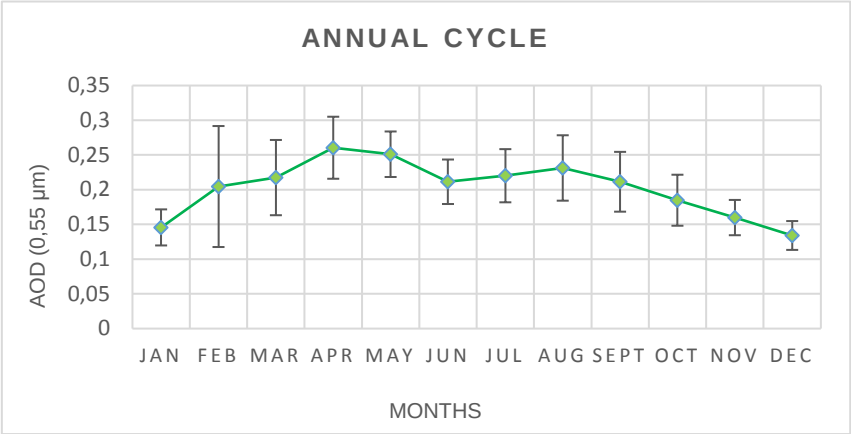

Graph 9 Annual cycle of AOD at 0.55 μm for the sanctuary of Messa (monthly average values for each month for the period 2002-2016 and the standard deviation bars)

Seasonality around Messa shows a spring maximum with a peak in April with monthly average value of 0.260. A secondary hump is shown in summer peaking in summer While from November to January the minimum AODs values (0.134 and 0.145) are encountered.

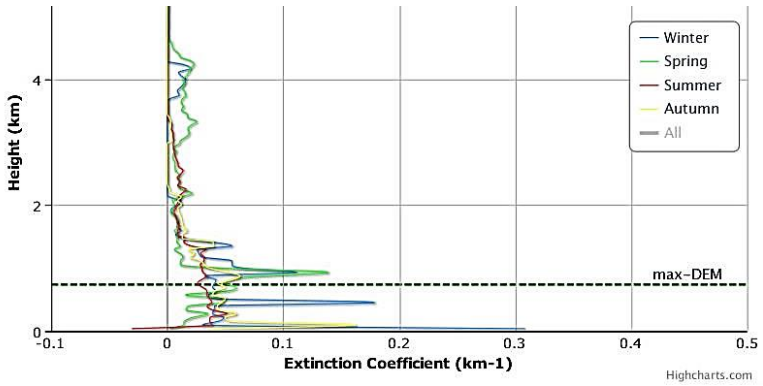

Chart 32 Vertical column of aerosol seasonal observations (aerosol extinction at 532 nm per season for cell centroid: Lat= 39.5º, Lon= 26.5º) over the sanctuary of Messa (LIVAS database)

An MLH in the order of 1.2-1.5 km is shown while it is interesting to observe an elevated layer of pollution between 3 and 4.5 km during winter.

10PL Palamari

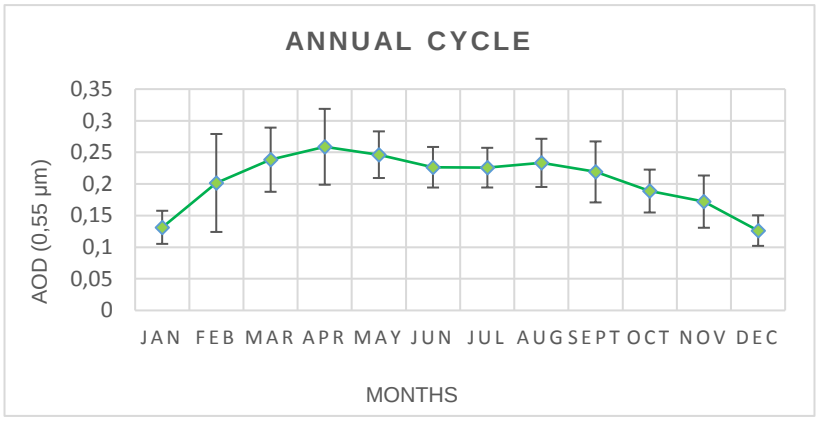

Graph 10 Annual cycle of AOD at 0.55 μm for Palamari (monthly average values for each month for the period 2002-2016 and the standard deviation bars)

The seasonal variability for the area of Palamari is characterized by a spring maximum with a peak in April and a monthly average value of 0.258. In summer a plateau is observed, while minimum AODs are found in winter (0.172 – 0.131).

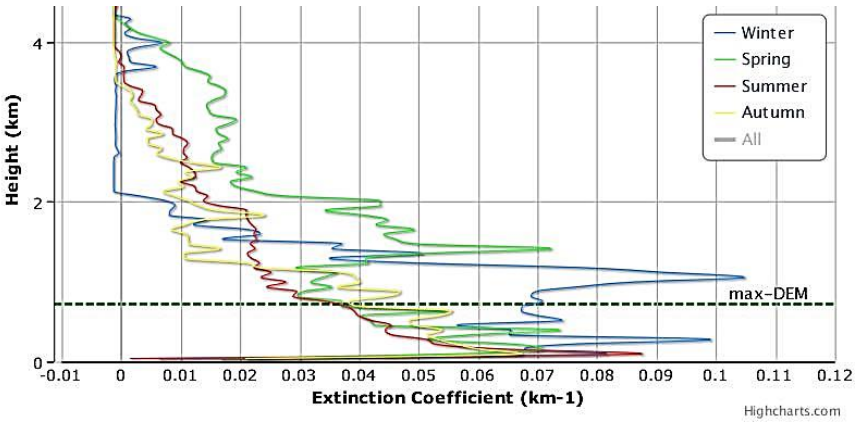

Chart 33 Vertical column of aerosol seasonal observations (aerosol extinction at 532 nm per season for cell centroid: Lat= 38.5^{o}, Lon= 24.5^{o}) over Palamari (LIVAS database)

Pollution in the area is always present giving a maximum in spring which shows high levels of pollution from the 4th km. Summer and autumn have significant amounts of pollution, as well.

11DE Delphi

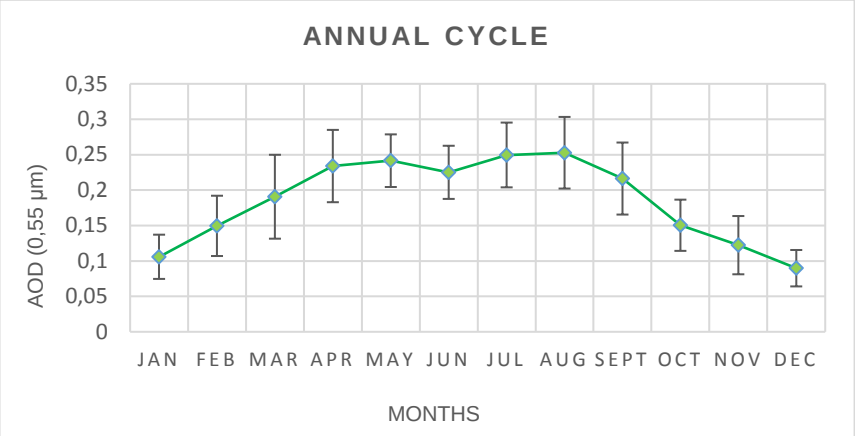

Graph 11 Annual cycle of AOD at 0.55 μm for Delphi (monthly average values for each month for the period 2002-2016 and the standard deviation bars)

In the area of Delphi, seasonality shows a bimodal distribution with maximum AODs in spring with a peak in May and in summer with a peak in August and with monthly average values of 0.241 and 0.252 respectively. Minimum AODs are found from November to January (0.122 – 0.106).

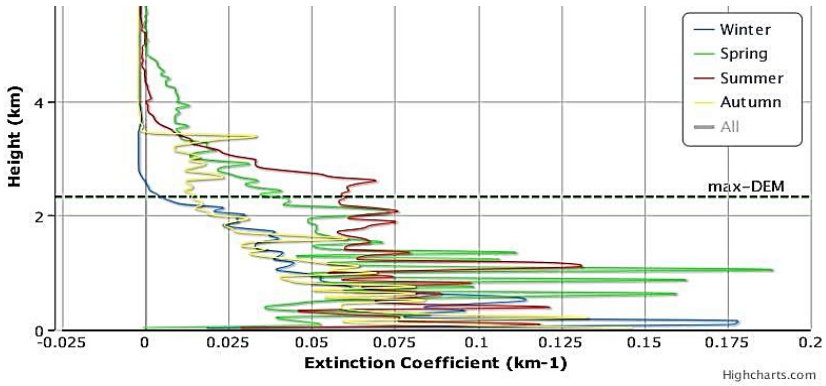

Chart 34 Vertical column of aerosol seasonal observations (aerosol extinction at 532 nm per season for cell centroid: Lat= 38.5º, Lon= 22.5º) over Delphi (LIVAS database)

Pollution is present during the whole year with most of it in spring and summer. The variations in the spring start slightly below the 5th kilometer and increases significantly shortly before the 2nd km. In summer start at the 4th km and greatly increase from the 3rd and after acting up the surface. Less pollution rates, but with significant action encounter in winter and autumn as well.

12AC Acropolis

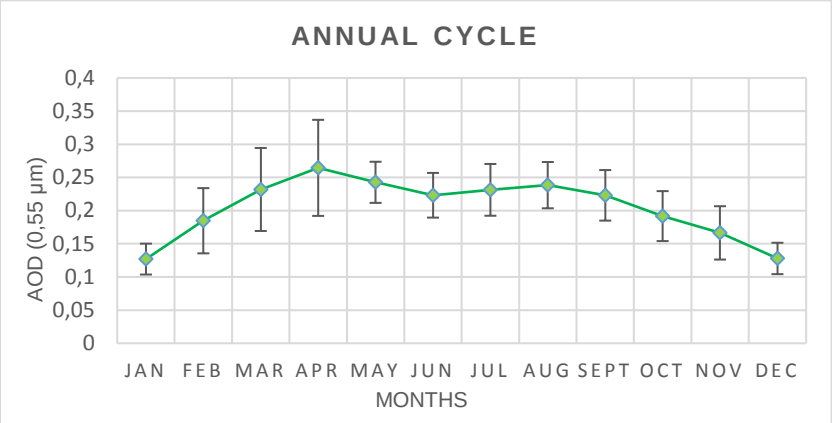

Graph 12 Annual cycle of AOD at 0.55 μm for the Acropolis (monthly average values for each month for the period 2002-2016 and the standard deviation bars)

For the area of Acropolis, there is a spring maximum with a peak in April (0.264). From May to August a plateau is observed. The minimum averaged values are from November to January (0.166 – 0.126).

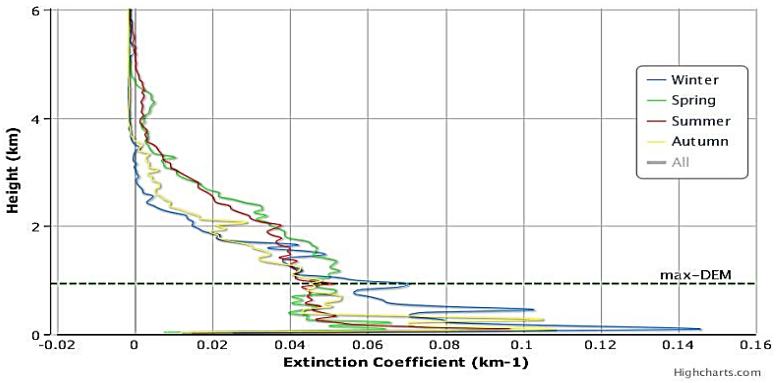

Chart 35 Vertical column of aerosol seasonal observations (aerosol extinction at 532 nm per season for cell centroid: Lat= 37.5º, Lon= 23.5º) over the Acropolis (LIVAS database)

The urban site of the Acropolis demonstrates considerable levels of pollution of the height that aerosols is confined (MHL). This height starts from around the 3rd km with spring presenting the higher intensity. In a general basis, pollution influences the area during the whole year.

13MC Mycenae

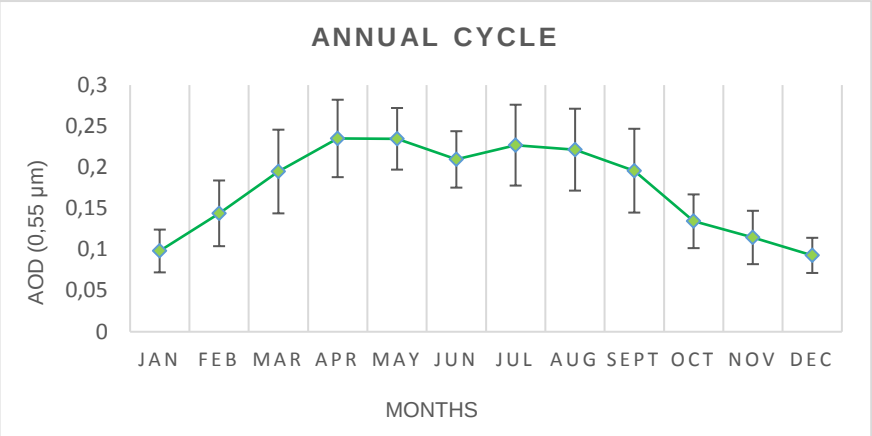

Graph 13 Annual cycle of AOD at 0.55 μm for the Mycenae (monthly average values for each month for the period 2002-2016 and the standard deviation bars)

The seasonal variability for the area of Mycenae shows a bimodal distribution with a spring maximum in April and a monthly average value of 0.235 and summer maximum in July with an average value of 0,226. Minimum AODs are found from October to January (0.134 – 0.098).

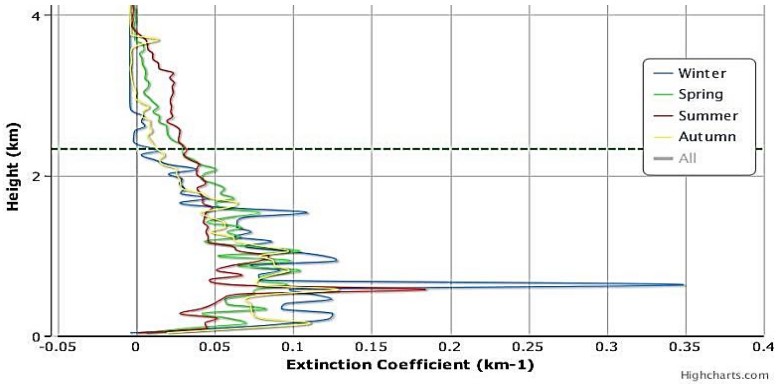

Chart 36 Vertical column of aerosol seasonal observations (aerosol extinction at 532 nm per season for cell centroid: Lat= 37.5º, Lon= 22.5º) over Mycenae (LIVAS database)

Pollution action initiates around the 4rd km in summer and with a stable motion reaches the surface. Important presence of pollution is observed in winter months with intense action around 800m from the surface. Autumn and spring also show high levels of pollution from

the 4th km. The average aerosol mixing layer (MLH) is obvious at the height of the 2nd km.

14OL Olympia

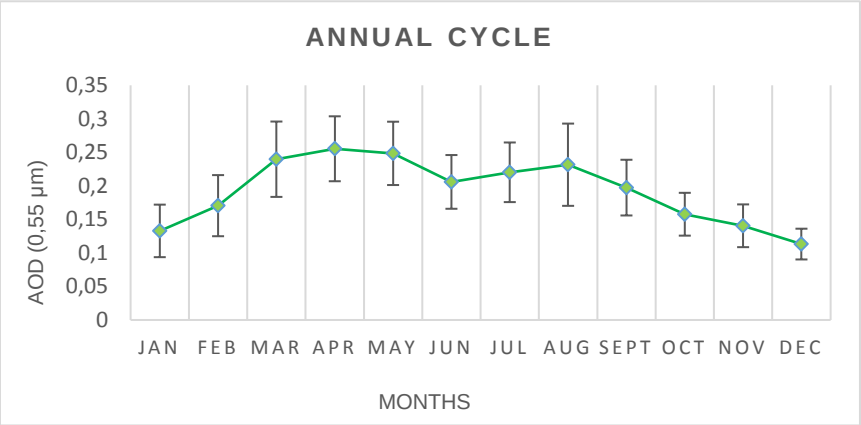

Graph 14 Annual cycle of AOD at 0.55 μm for Olympia (monthly average values for each month for the period 2002-2016 and the standard deviation bars)

The seasonal variability for the area of Olympia is characterized by a spring maximum with a peak in April and a monthly average value of 0.255. Minimum AODs are found from October to January (0.157 – 0.132).

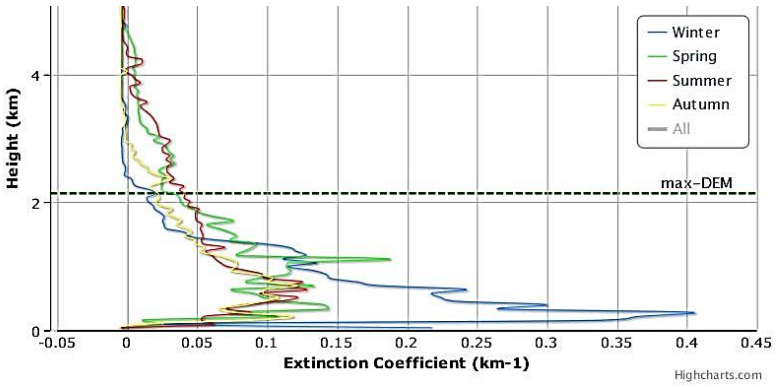

Chart 37 Vertical column of aerosol seasonal observations (aerosol extinction at 532 nm per season for cell centroid: Lat= 37.5º, Lon= 21.5º) over Olympia (LIVAS database)

Pollution rates are obvious almost from the 4th km with summer and spring seasons presenting higher content of aerosols. Under the boundary layer, along with summer and spring, winter gives significant amounts of pollution.

15IR Ireon

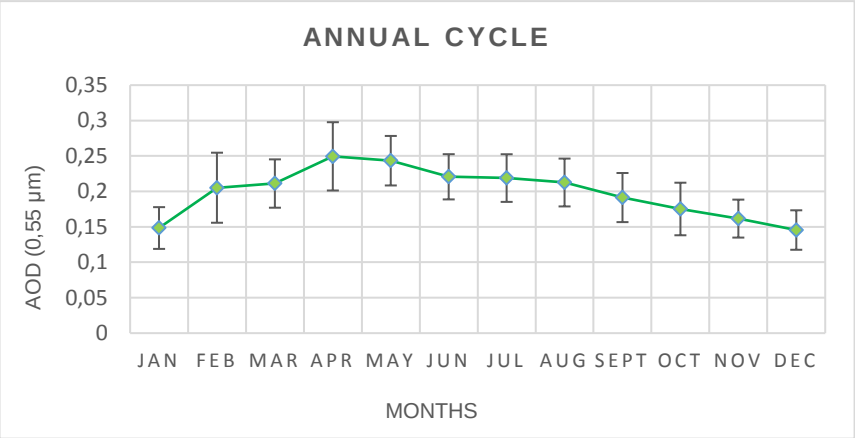

Graph 15 Annual cycle of AOD at 0.55 μm for Ireon (monthly average values for each month for the period 2002-2016 and the standard deviation bars)

Concerning seasonality in the area of Ireon, a stable state is observed with gradual fall of the values from July to December (minimum AODs at 0.145). Maximum AODs are in spring with a peak in April (0.249).

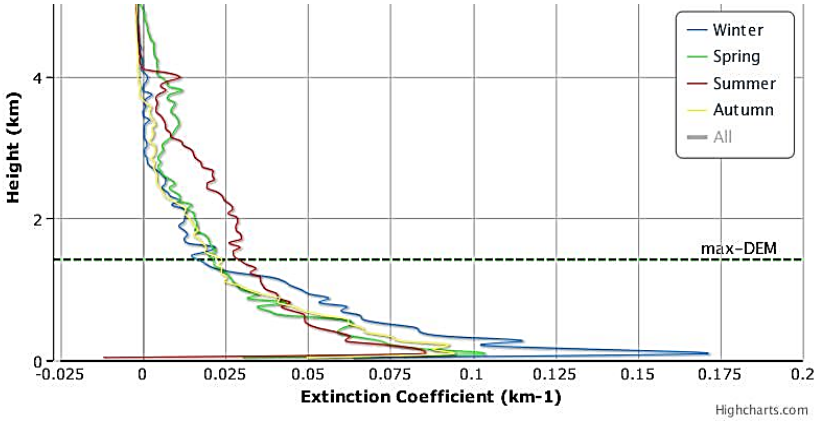

Chart 38 Vertical column of aerosol seasonal observations (aerosol extinction at 532 nm per season for cell centroid: Lat= 37.5º, Lon= 26.5º) over Ireon (LIVAS database)

The seasonal profiles give a constant presence of pollution with higher levels in summer and spring between the 4th km and the boundary level. Under the 1500 m, winter months have a significant participation in pollution rates.

16ME Ancient Messene

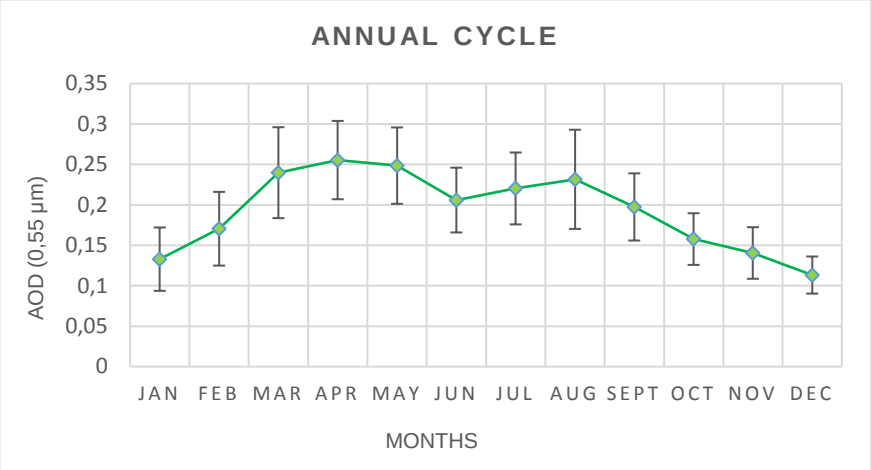

Graph 16 Annual cycle of AOD at 0.55 μm for Ancient Messene (monthly average values for each month for the period 2002-2016 and the standard deviation bars)

The seasonal pattern for the area of Ancient Messene is characterized by a bimodal distribution with a spring maximum in April with average value at 0.255 and a summer maximum with a peak in August (0.231). The minimum values are observed in December and January at 0.113 and 0.132 respectively.

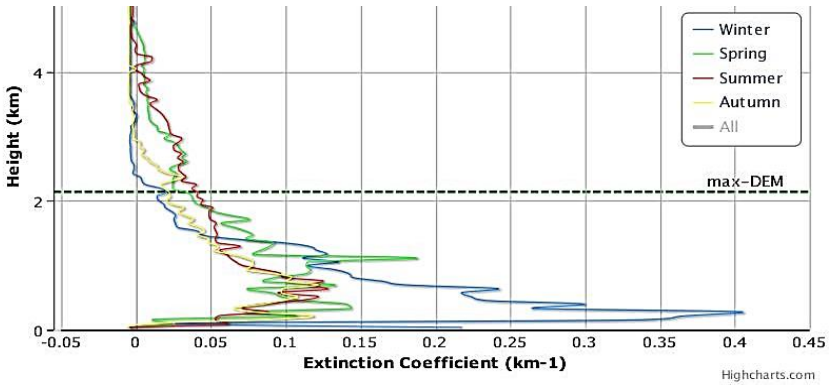

Chart 39 Vertical column of aerosol seasonal observations (aerosol extinction at 532 nm per season for cell centroid: Lat= 37.5^{o}, Lon= 21.5^{o}) over Ancient Messene (LIVAS database)

Under the 4th km aerosol action is noticeable with all seasons apart from winter being present. Under the 2nd km, there is an outbreak with spring, summer and winter giving important quantities of pollution concentrations.

17DL Delos

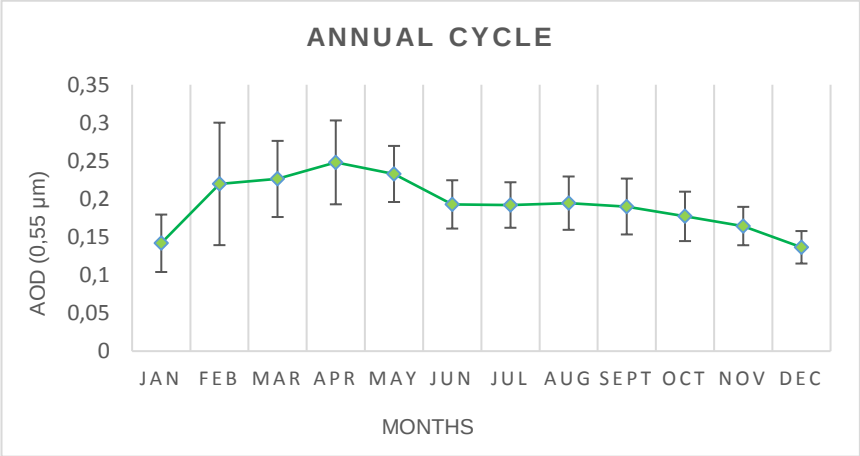

Graph 17 Annual cycle of AOD at 0.55 μm for Delos (monthly average values for each month for the period 2002-2016 and the standard deviation bars)

Based on seasonality, in Delos, a spring maximum is observed with a peak in April (0.248). From June to October AODs show an almost flat plateau. The minimum values are noticed in December (0.136) and January (0.141).

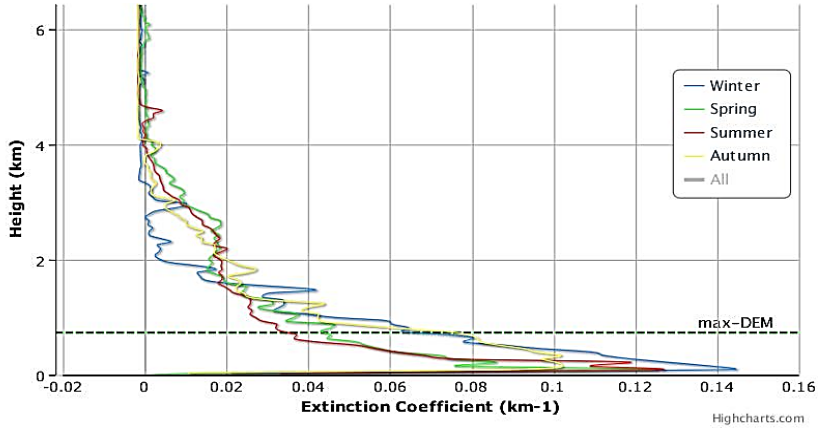

Chart 40 Vertical column of aerosol seasonal observations (aerosol extinction at 532 nm per season for cell centroid: Lat= 37.5º, Lon= 25.5º) over Delos (LIVAS database)

The intense fluctuations begin at the 4th km with spring season giving the higher levels of pollution till the 2nd km. Along with spring months, summer and autumn also present pollution, mainly below the 2nd km.

18ST Santorini (Anc. Thera)

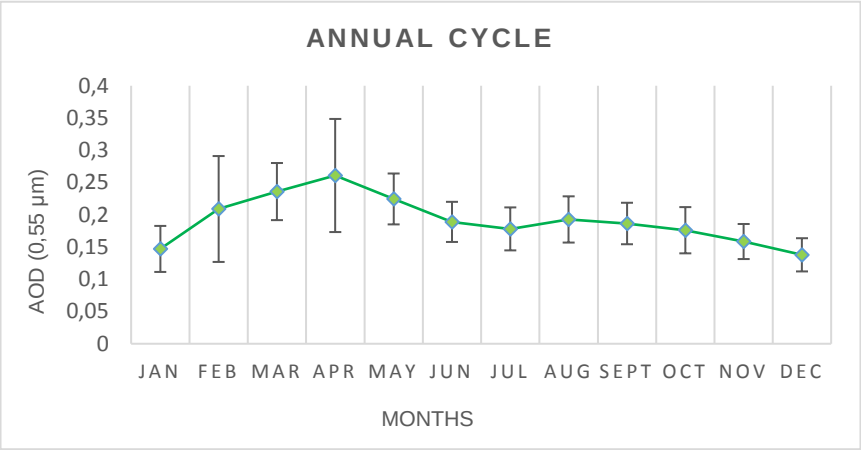

Graph 18 Annual cycle of AOD at 0.55 μm for Ancient Thira (monthly average values for each month for the period 2002-2016 and the standard deviation bars)

A spring maximum is noticed for the area of Anc. Thira, with a peak in April with average value at 0.260. From June to December a plateau is also observed. The minimum value is seen in December and January (0.137 and 0.147).

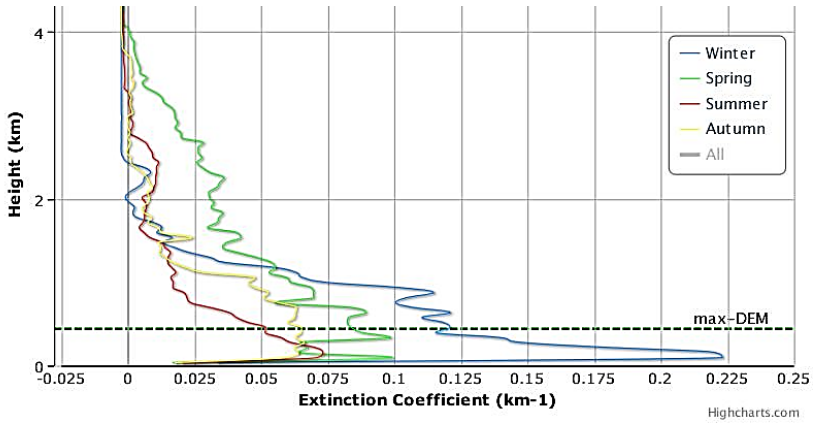

Chart 41 Vertical column of aerosol seasonal observations (aerosol extinction at 532 nm per season for cell centroid: Lat= 36.5º, Lon= 25.5º) over Ancient Thira (LIVAS database)

The fluctuations of pollution starts from the 4th km and below. A significant increase after the 2nd km is apparent. Pollution appears to influence the surface mostly in spring and winter. During the summer months, there is no particular action of aerosols.

19RH Rhodes

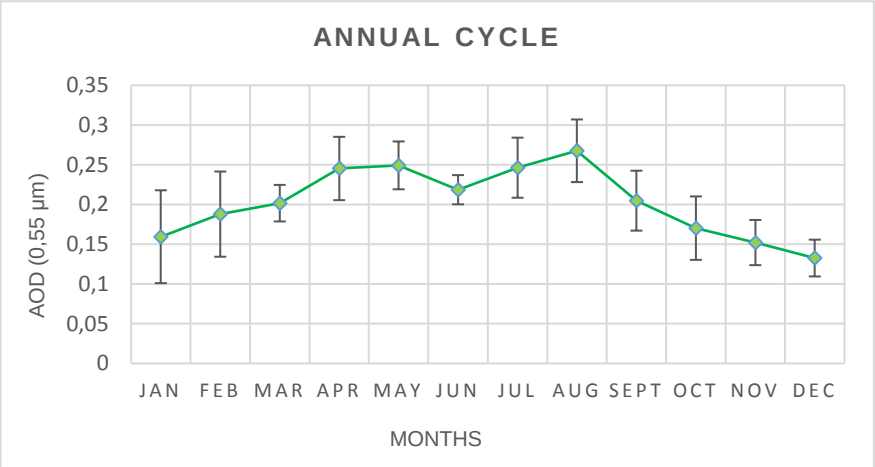

Graph 19 Annual cycle of AOD at 0.55 μm for Rhodes (monthly average values for each month for the period 2002-2016 and the standard deviation bars)

In Rhodes, the seasonal variability demonstrates a bimodal distribution with a spring maximum in May (0.249) and a summer maximum in August (0.267). Minimum AODs are observed during winter (December with an average value at 0.132).

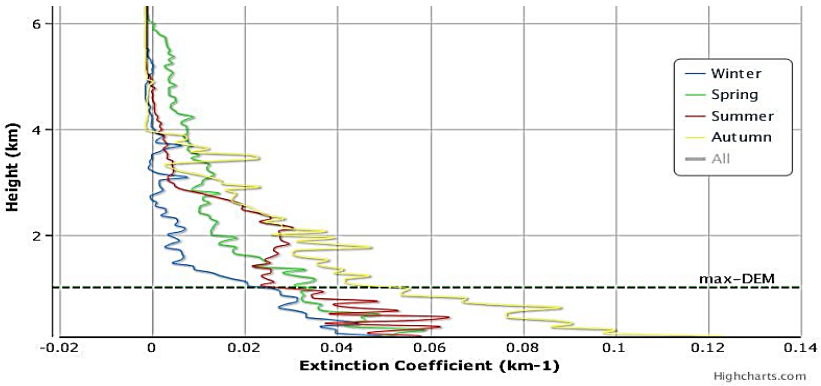

Chart 42 Vertical column of aerosol seasonal observations (aerosol extinction at 532 nm per season for cell centroid: Lat= 36.5º, Lon= 28.5º) over Rhodes (LIVAS database)

The action of aerosols is present already from the 6th km and below. Although a considerable growth in summer at the 4th km is obvious, autumn seems to influence in a greater way the surface. During the winter months, there is no particular action of pollution while the rest of the year the concentrations are in high levels. Summer and spring variations, along with autumn, under the

boundary level (aerosol mixing layer), are sharp and seem to influence the surface in an intense mode.

20FS Falassarna

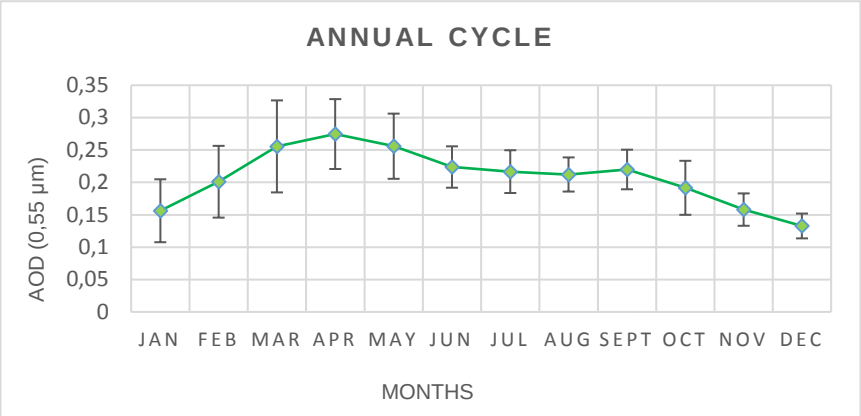

Graph 20 Annual cycle of AOD at 0.55 μm for Falassarna (monthly average values for each month for the period 2002-2016 and the standard deviation bars)

Maximum AODs in Falassarna are come across in spring with a peak in April and a monthly average value of 0.274. In December and January are found the minimum AODs (0.132 and 0.156). The period among May and September shows a plateau around the average value.

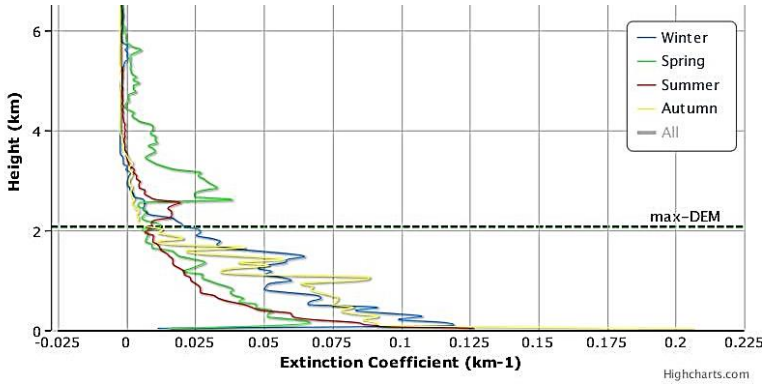

Chart 43 Vertical column of aerosol seasonal observations (aerosol extinction at 532 nm per season for cell centroid: Lat= 35.5º, Lon= 23.5º) over Falassarna (LIVAS database)

Below the 6th km most of the pollution is identified in the spring while shortly before the 2nd km. significant pollution rates during all seasons are observed(MHL).

21KN Knossos

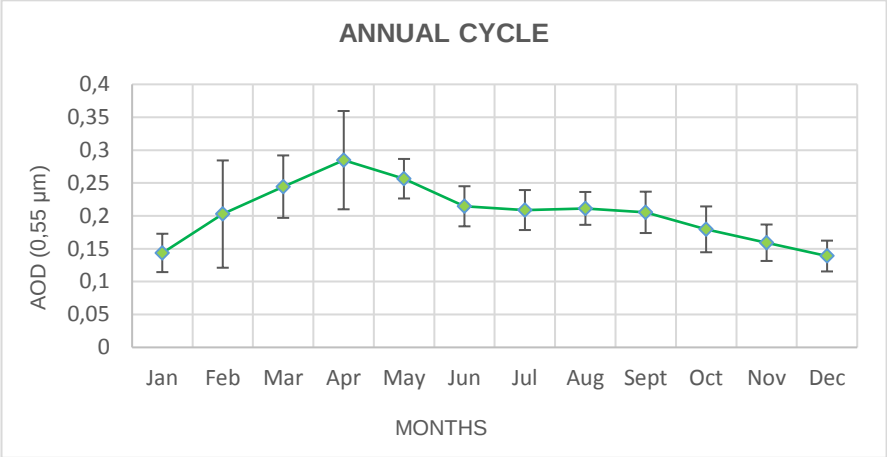

Graph 21 Annual cycle of AOD at 0.55 μm for Knossos (monthly average values for each month for the period 2002-2016 and the standard deviation bars)

A spring maximum is observed for the area of Knossos with a peak in April and a monthly average value 0.284. From October to January are found the minimum AODs (0.179 – 0.138). For the rest of the period a flat plateau is also observed.

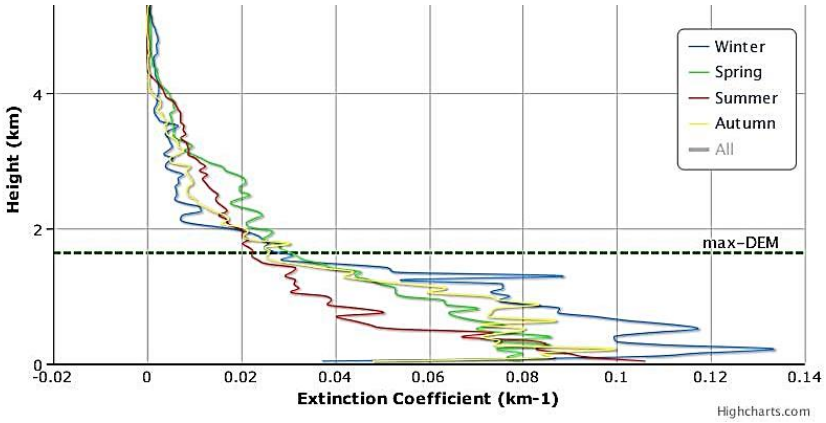

Chart 44 Vertical column of aerosol seasonal observations (aerosol extinction at 532 nm per season for cell centroid: Lat= 35.5º, Lon= 25.5º) over Knossos (LIVAS database)

The pollution starts from the 4th km and below for all seasons with spring rate being to some extent higher. An appreciable increase after the boundary layer is visible. It is observed that on the surface the pollution influence have effect mainly in spring, summer and autumn.

4.3. GEOGRAPHICAL AND TEMPORAL TRENDS

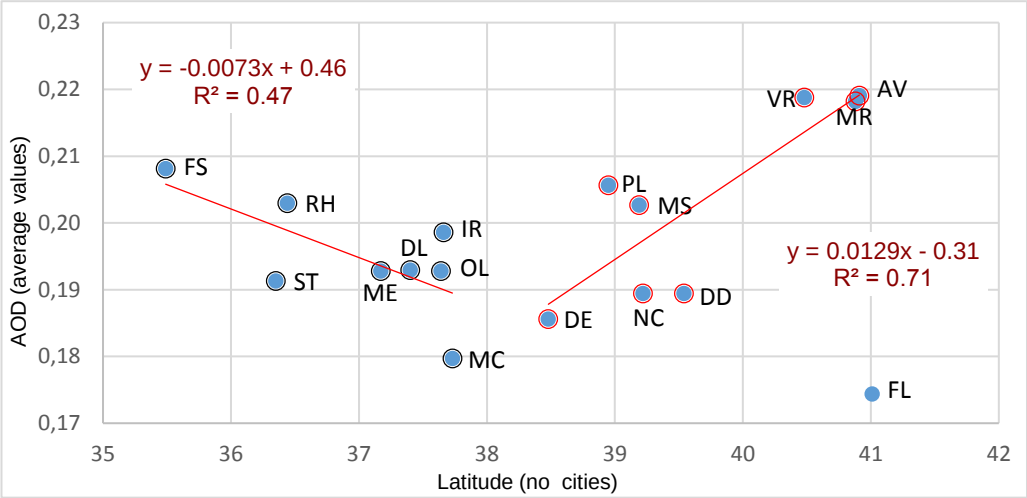

Graph 45 Geographical distribution (latitude degrees) of AODs monthly average values for the Period 2002 – 2016 of all sites (excluding cities). The red lines are the regression lines between the data points.

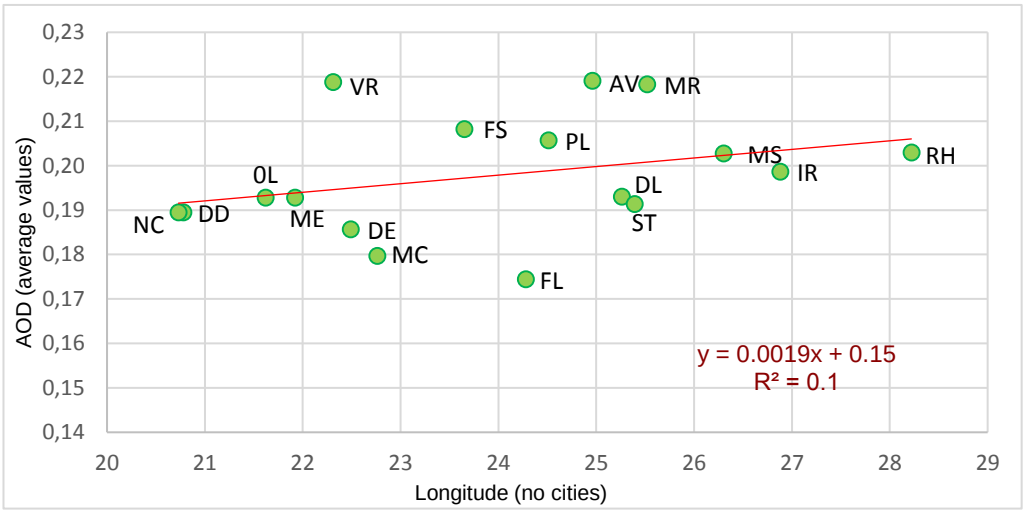

Graph 46 Geographical distribution (longitude degrees) of AODs monthly average values for the Period 2002 – 2016 of all sites (excluding cities). The red line is the regression line between the data points.

Based on the two graphs above, it is noticed that to the North and to the South there is greater exposure of the sites to aerosols compared to central regions in Greece. Moreover, the northern sites are somewhat more exposed compared to the southern ones. The

areas situated in the northern part of Greece, are influenced by the transported pollution from the industrial central and eastern Europe.

The southern part is frequently influenced by dust outbreaks from Saharan desert. Similarly, the western part presents less exposure το aerosols because of the Pindos mountain range, which operates as a blockage for meteorological systems from the west, leading to more rain and thus maintaining the atmosphere cleaner. On the other hand, the eastern part is slightly more exposed to aerosol as it is under the influence of Istanbul plume – but also from agricultural fire from the black Sea (Gerasopoulos, et al., 2010, Koukouli, et al., 2009).

During the last decade, an important decrease in AOD levels is observed in most of the sites, as seen in the following graphs. This is attributed to measures taken at the European level for controlling and mitigating aerosol emissions

1MR

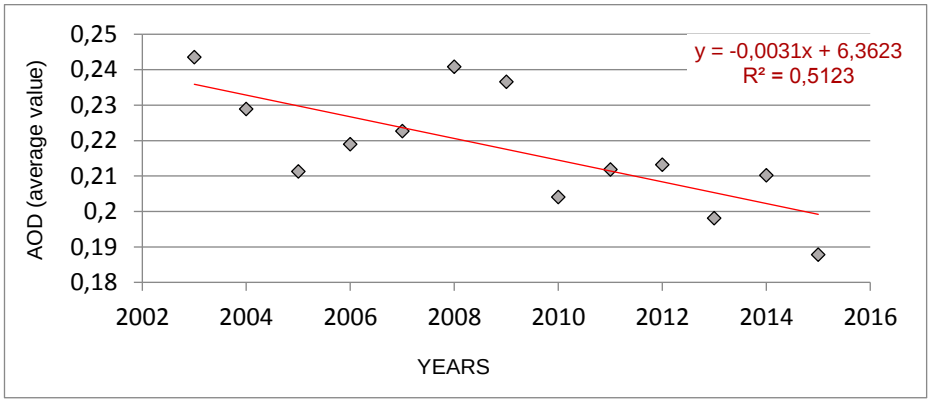

Graph 22 Negative trend of AODs for the last decade. The red line is the fitted line.

For the area of Maronia the decrease of AODs levels is -14%.

2AV

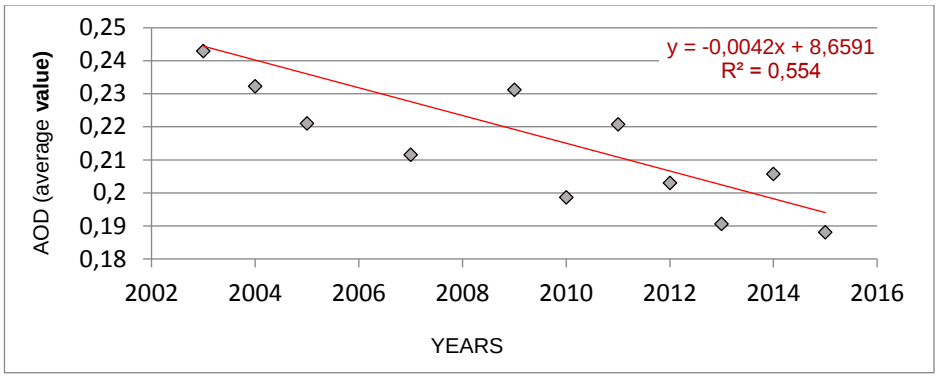

Graph 23 Negative trend of AODs for the last decade. The red line is the fitted line.

For the area of Avdira the decrease of AODs levels is -19%.

3FL

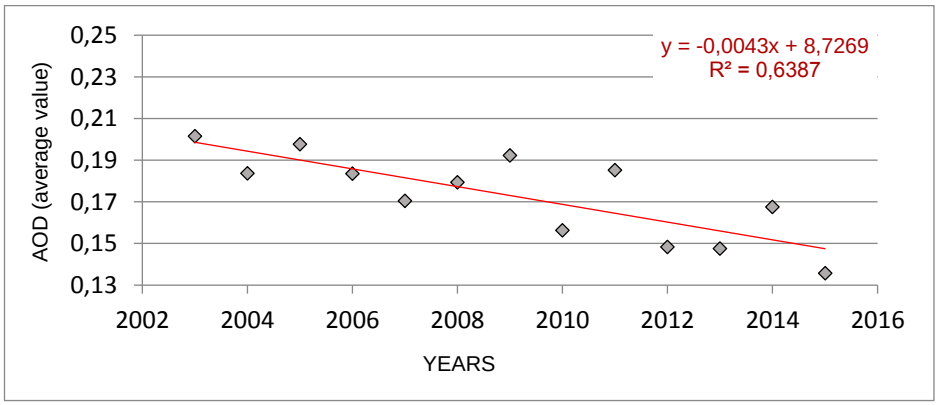

Graph 24 Negative trend of AODs for the last decade. The red line is the fitted line.

For the area of Filippoi the decrease of AODs levels is -25%.

4WT

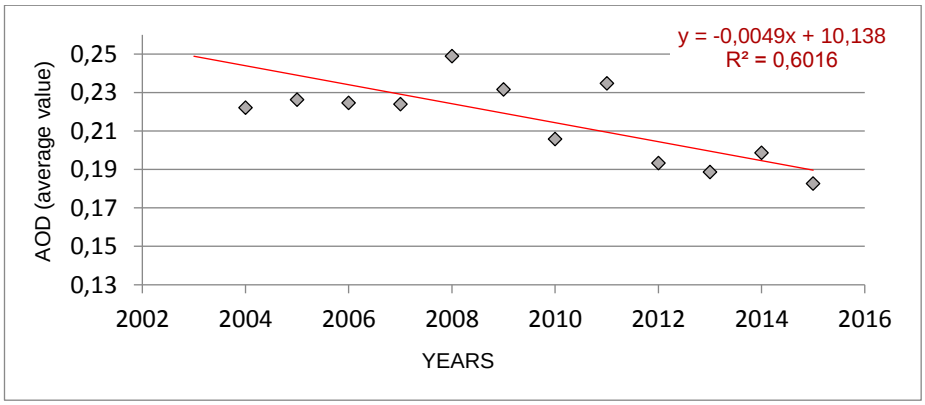

Graph 25 Negative trend of AODs for the last decade. The red line is the fitted line.

For the White Tower the decrease of AODs levels is -23%.

5VR

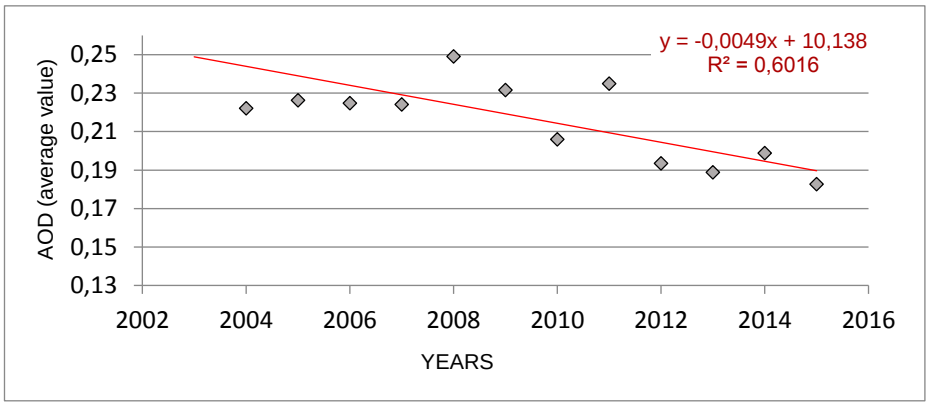

Graph 26 Negative trend of AODs for the last decade. The red line is the fitted line.

For the area of Vergina the decrease of AODs levels is -23%.

6LS

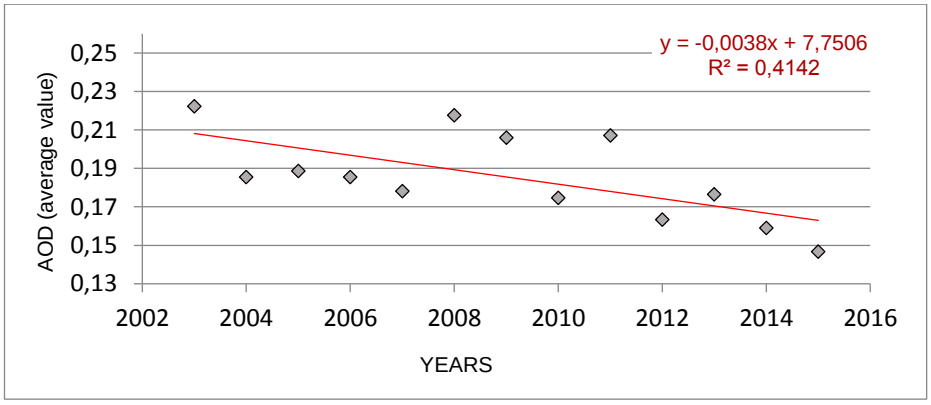

Graph 27 Negative trend of AODs for the last decade. The red line is the fitted line.

For the Ancient Theatre of Larissa, the decrease of AODs is -20%.

7DD

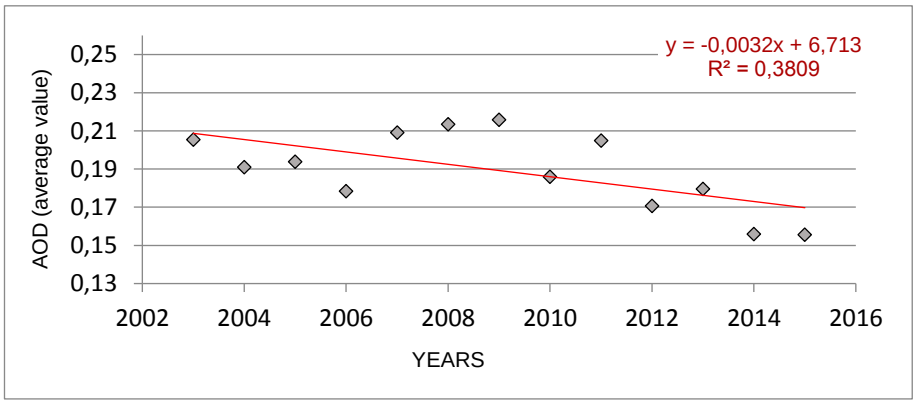

Graph 28 Negative trend of AODs for the last decade. The red line is the fitted line.

For the area of Dodoni the decrease of AODs levels is -17%.

8NC

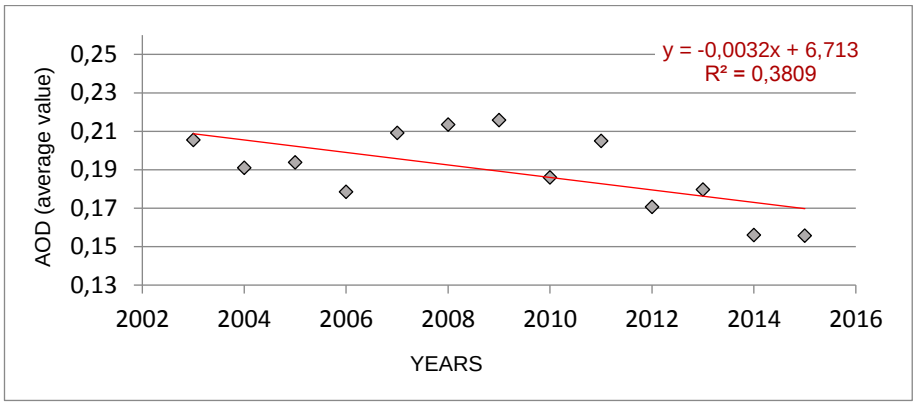

Graph 29 Negative trend of AODs for the last decade. The red line is the fitted line.

For the area of Nicopolis the decrease of AODs levels is -17%.

9MS

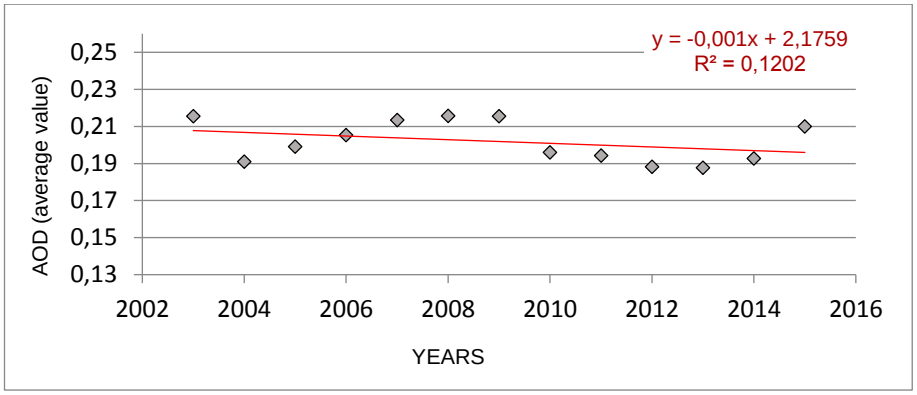

Graph 30 Negative trend of AODs for the last decade. The red line is the fitted line.

For the site of Messa the decrease of AODs levels is -5%.

10PL

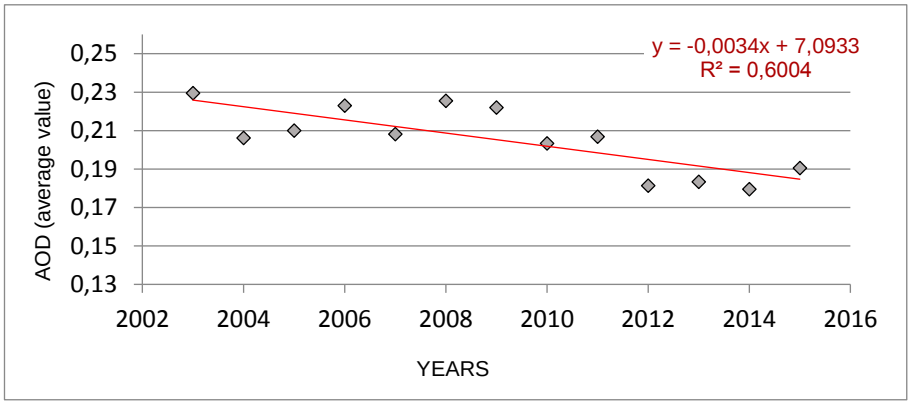

Graph 31 Negative trend of AODs for the last decade. The red line is the fitted line.

For the area of Palamari the decrease of AODs levels is -17%.

11DE

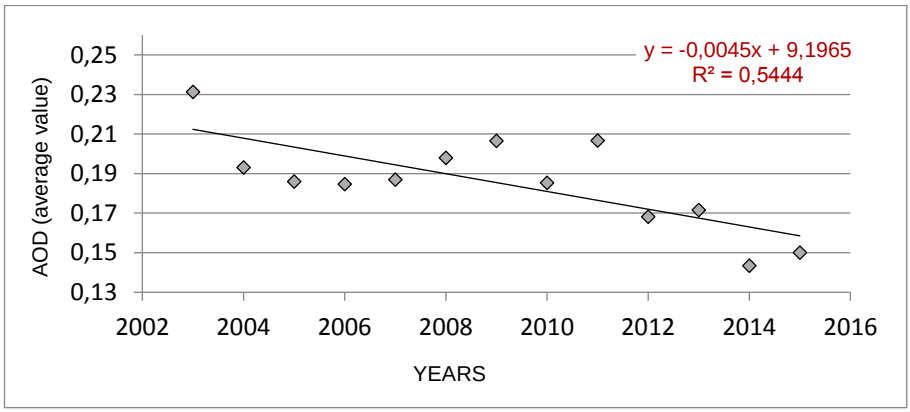

Graph 32 Negative trend of AODs for the last decade. The red line is the fitted line.

For the area of Delphi, the decrease of AODs levels is -24%.

12AC

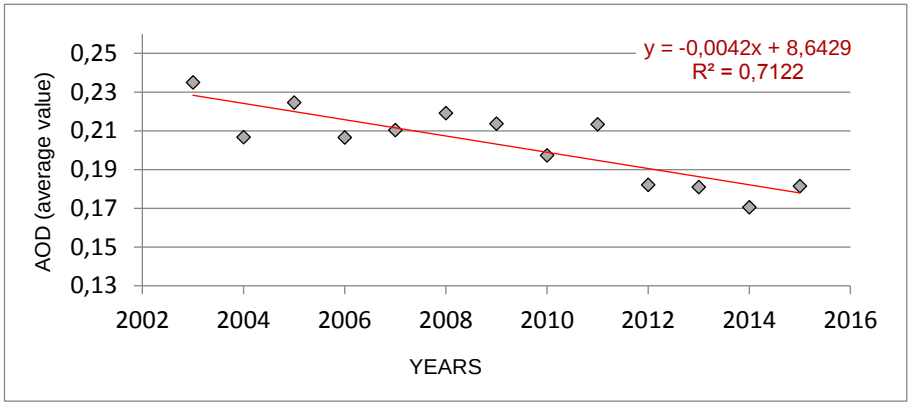

Graph 33 Negative trend of AODs for the last decade. The red line is the fitted line.

For the Acropolis, the decrease of AODs levels is -21%.

13MC

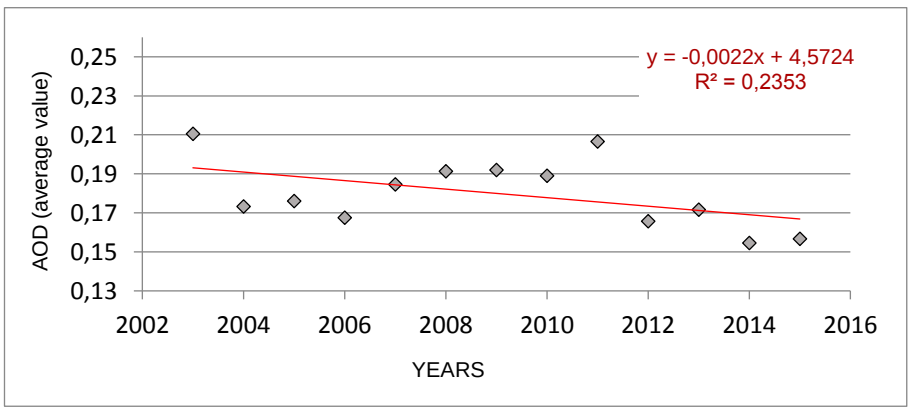

Graph 34 Negative trend of AODs for the last decade. The red line is the fitted line.

For the area of Mycenae, the decrease of AODs levels is -12%.

140L

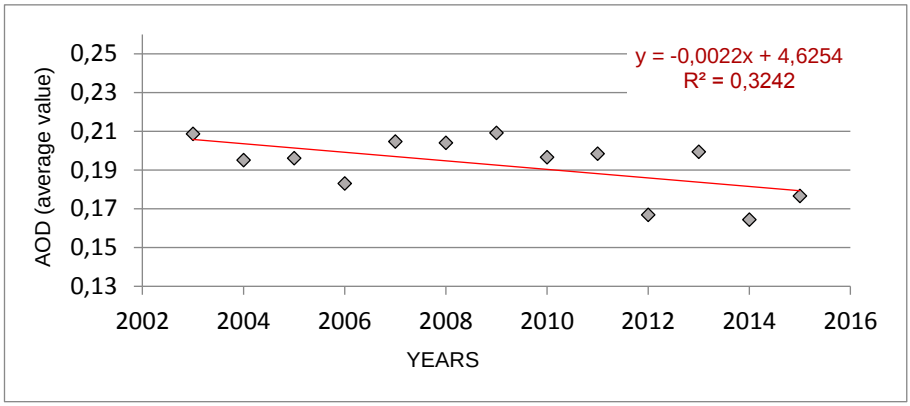

Graph 35 Negative trend of AODs for the last decade. The red line is the fitted line.

For the area of Olympia, the decrease of AODs levels is -11%.

15IR

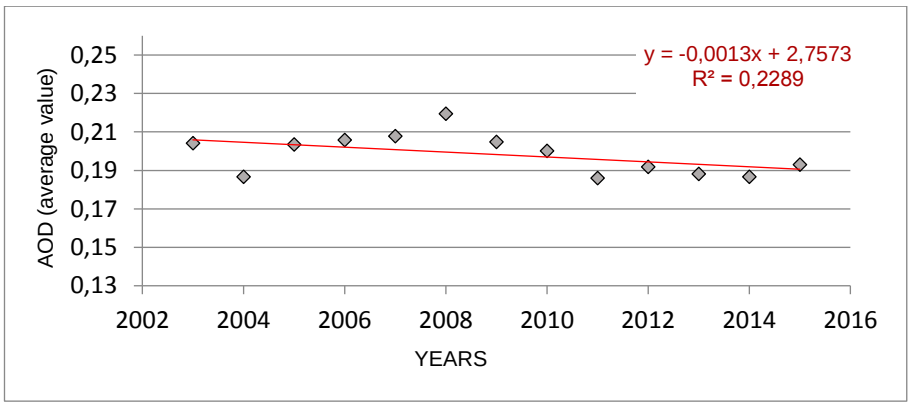

Graph 36 Negative trend of AODs for the last decade. The red line is the fitted line.

For the area of Ireon the decrease of AODs levels is -6%.

16ME

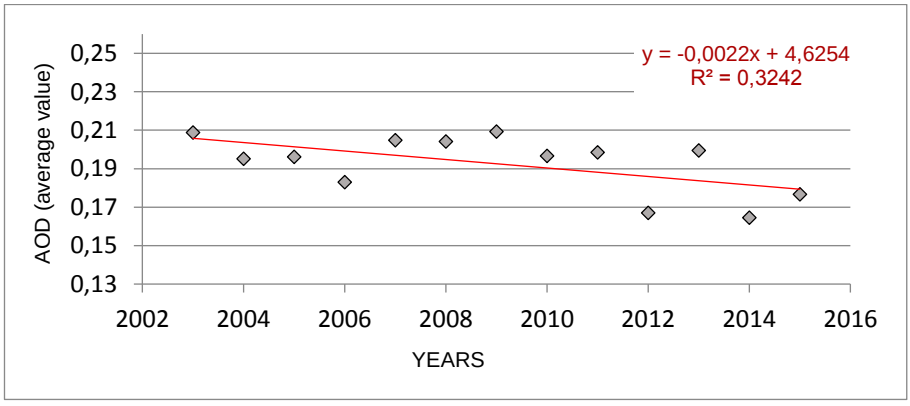

Graph 37 Negative trend of AODs for the last decade. The red line is the fitted line.

For the area of Ancient Messene, the decrease of AODs is -11%.

17DL

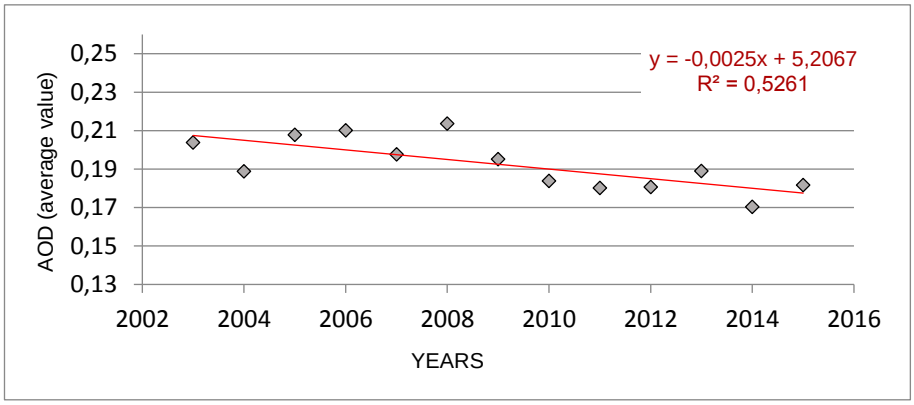

Graph 38 Negative trend of AODs for the last decade. The red line is the fitted line.

For the area of Delos, the decrease of AODs levels is -13%.

18ST

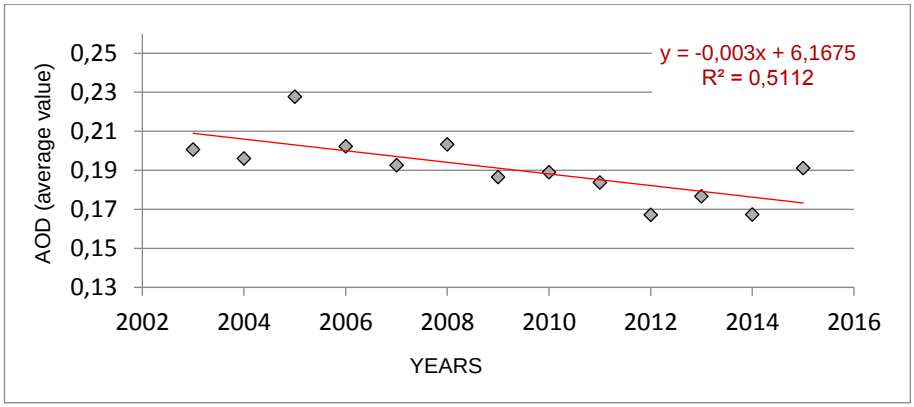

Graph 39 Negative trend of AODs for the last decade. The red line is the fitted line.

For the area of Anc. Thira, the decrease of AODs levels is -16%.

19RH

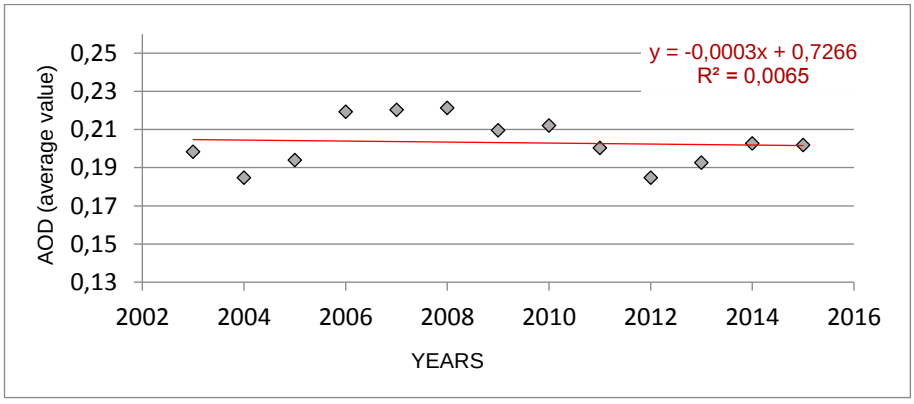

Graph 40 Negative trend of AODs for the last decade. The red line is the fitted line.

For the Medieval city of Rhodes, the decrease of AODs is -1%.

20FS

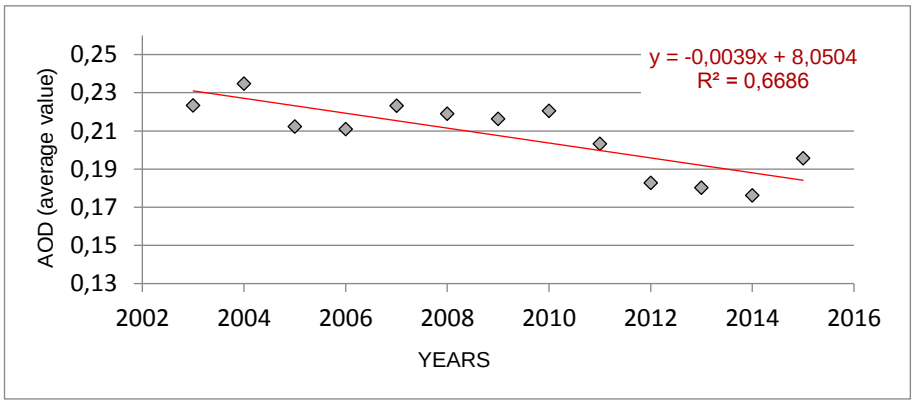

Graph 41 Negative trend of AODs for the last decade. The red line is the fitted line.

For the area of Falassarna the decrease of AODs levels is -19%.

21KN

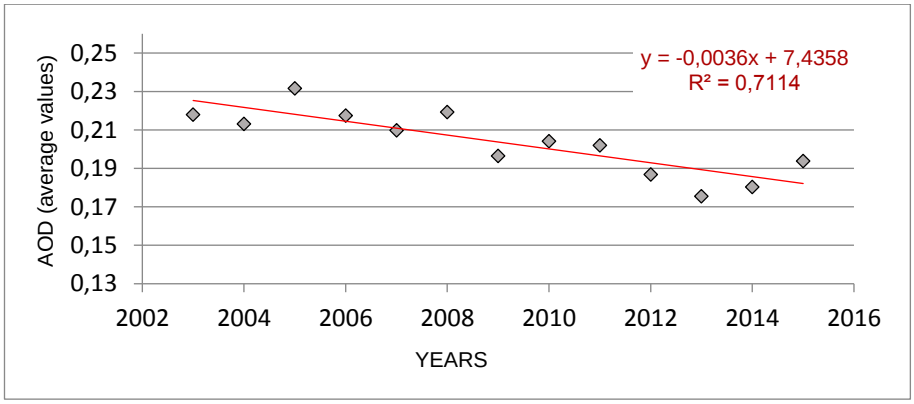

Graph 42 Negative trend of AODs for the last decade. The red line is the fitted line.

For the area of Knossos, the decrease of AODs levels is -18%.

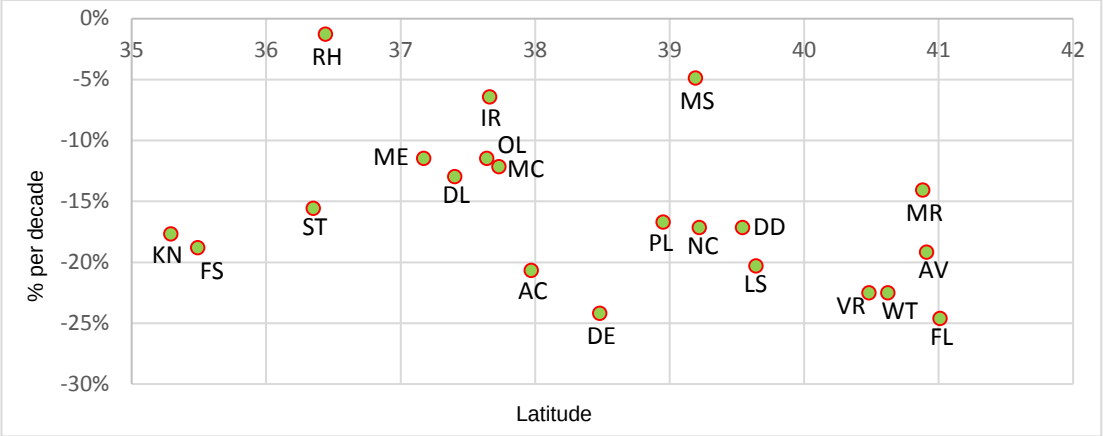

Graph 43 Negative trend of AODs monthly average values for the last 10 years (latitude degrees)

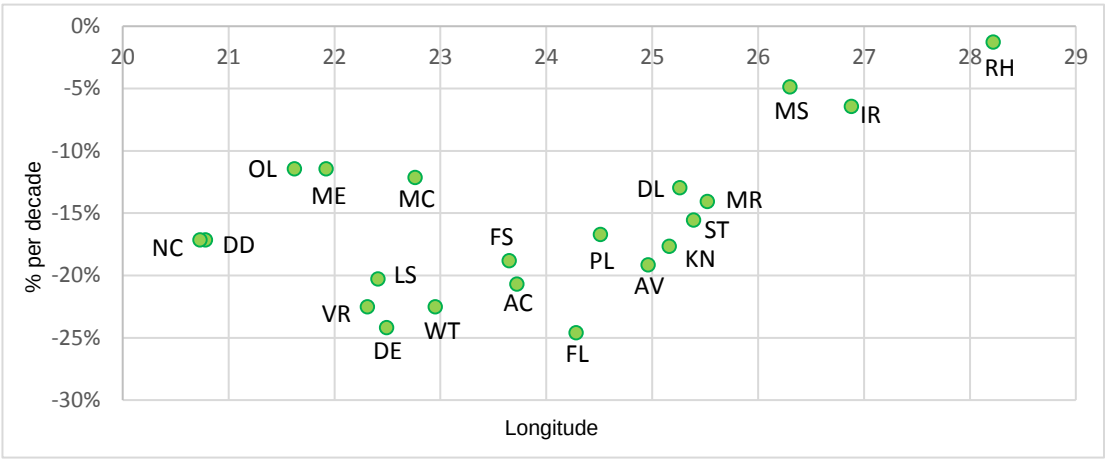

Graph 44 Negative trend of AODs monthly average values for the last 10 years (longitude degrees)

A negative trend of AODs is observed for the last decade over Greece in the range of -16%. The greatest decrease is found mostly in northern (Avdira -19%, Filippoi -25%), north-western (Vergina -23%), central (Delphi -24%) and in urban areas (White Tower -23%, Ancient Theater of Larissa -20%, Acropolis -21%, Knossos -18%).

5. CONCLUSIONS / DISCUSSION

Although aerosols impact on cultural heritage materials has not been widely studied, there are many studies that prove that air pollution and particularly aerosols contributes and accelerate the procedure of chemical weathering.

Specifically, the main deterioration pattern of stones, mainly in urban environments, which is the primary structural element of monuments, due to aerosol action, is the formation of crusts. On the other hand, aerosols such as dust particles have no direct impact on stone, but may have harmful mechanical effects through abrasion and soiling.

Remote sensing is undoubtedly a significant tool for systematic monitoring of air pollution over vast areas covering long time periods. Satellite remote sensing data can be used to study the exposure of cultural heritage materials on particulate pollution and hence to better understand the background for corrosion mechanisms and decide the most suitable conservation strategies.

The derived conclusions that follow are on the basis of the initial questions that were posed in the introductory part of this work.

The average values of AOD observations (table 51) show that the intensity of exposure to particulate pollution is somewhat greater in the North (Maronia 0.218 ±0.060, Avdira 0.219 ±0.068, White Tower 0.219 ±0.086, Vergina 0.219 ±0.086). The next pattern reveals slightly lower values and this is located at the south (Falassarna, 0.208±0.059, Knossos 0.204±0.060, Rhodes 0.203±0.056). Similar values are found in the central north Aegean Sea (Site of Messa 0.203 ±0.057, Palamari 0.206 ±0.060, Ireon 0.199). Finally, two more clusters of sites are formed in terms of AOD values. One from sites in Peloponnese and the part of the Aegean to the east of this area (Olympia, Messene, Delos, Santorini) with values in the range 0.191-0.193, and in central Greece (Dodoni, Larissa, Nicopolis, Delphi,

Mycenae) with values in the range 0.18-0.189. The difference of those less polluted areas from those which exhibit the highest levels is in the order of 15-20%.

Table 51 Collective general statistics of AOD observations for all the archaeological sites of interest (monthly average values for the time period 2002 – 2016)

	Lat	Long	Avg	Stdev	Min	Max	Median
1MR	40.88	25.52	0.218	0.060	0.095	0.410	0.219
2AV	40.91	24.96	0.219	0.068	0.087	0.524	0.219
3FL	41.01	24.28	0.174	0.088	0.038	0.434	0.161
4WT	40.62	22.95	0.219	0.086	0.060	0.410	0.218
5VR	40.48	22.31	0.219	0.086	0.060	0.410	0.218
6LS	39.64	22.41	0.185	0.079	0.039	0.378	0.186
7DD	39.54	20.78	0.189	0.074	0.062	0.372	0.182
8NC	39.22	20.73	0.189	0.074	0.062	0.372	0.182
9MS	39.19	26.3	0.203	0.057	0.105	0.475	0.198
10PL	38.95	24.51	0.206	0.060	0.094	0.409	0.208
11DE	38.48	22.49	0.186	0.071	0.055	0.346	0.186
12AC	37.97	23.72	0.204	0.060	0.088	0.46	0.208
13MC	37.73	22.76	0.180	0.056	0.072	0.333	0.178
14OL	37.64	21.62	0.193	0.063	0.077	0.385	0.191
15IR	37.66	26.88	0.199	0.048	0.100	0.342	0.196
16ME	37.17	21.92	0.193	0.063	0.077	0.385	0.191
17DL	37.4	25.26	0.193	0.053	0.099	0.44	0.183
18ST	36.35	25.39	0.191	0.057	0.097	0.515	0.184
19RH	36.44	28.22	0.203	0.056	0.09	0.353	0.207
20FS	35.49	23.65	0.208	0.059	0.109	0.434	0.205
21KN	35.29	25.16	0.204	0.060	0.095	0.481	0.201

Regarding the type of aerosol dominating in each site, in the northern regions, intense is the presence of polluted dust[16], followed by dust[17]. Heading to the west, elevated levels of smoke are observed. In central and south Greece, the main particulate pollutant is dust, though in the east there are large quantities of dust and clean marine[18] aerosols (seaside areas affected by air masses from the

[16] A mixture of smoke and dust subtypes (Brett, et al., 2015)
[17] Mineral desertic dust. The Sahara Desert is the major contributor to dust load in Europe (Mishra, et al., 2012)
[18] Marine aerosols have different natural sources that can be classified as primary, i.e. derived from the mechanical process of bubble bursting, and secondary,

Adriatic Sea and the Mediterranean). Finally, in the southern part of the country, most aerosol components are present, namely polluted dust, dust, smoke and polluted continental[19] along with clean marine.

The presence of aerosols shows a summer maximum at the northern areas and a spring maximum at the southern and western part. This is related to the seasonality of the emission sources that affect the two areas, which is anthropogenic pollution from the Balkans and East Europe at the north and Sahara dust at the south (Gerasopoulos, et al., 2010; Koukouli, et al., 2009). The incoming desert dust over the Eastern Mediterranean is observed principally in spring, and in some cases in winter.

The eastern side present a relatively stable rate the whole year. The annual AOD cycles present a main bimodal distribution (graph 1), with one mode in spring and one in summer. At the north, the summer maximum dominated over the spring one and this pattern is reversed moving to the south. There is one site (Filippoi) where a unimodal, summer maximum distribution is observed, at the same time encountering the lowest level of AOD in the Hellenic territory (it cannot currently be evaluated whether this is due to some local particularities or fail in the satellite representation of aerosol level in the area).

As already mentioned, the notable year-by-year variability of AOD levels and the spatial variability of the different types of aerosols are the results of fluctuating transport of desert dust, from the south (Sahara Desert in northern Africa), or other anthropogenic sources e.g. biomass burning aerosols, from the north (Athanassiou, et al., 2013).

A negative trend of aerosol optical depth is observed during the last ten years for all sites. The higher reduction is observed at the north (Filippoi, White Tower, Vergina) and the lowest at the east parts of Greece (Messon, Ireon, Rhodes). The reduction of anthropogenic

derived through ocean emission of precursor biogenic volatile organic compounds (Kiliyanpilakkil & Meskhidze, 2011)

[19] A mixture of smoke and clean continental aerosols (Brett, et al., 2015)

emissions and other urban scale counter measures adopted, probably explain the significant decline of AODs levels in urban centers (White Tower -23%, Ancient Theater of Larissa -20%, Acropolis -21%, Knossos -18%), which is in average higher than that of the other remote areas (table 52).

Table 52 Collective table of negative trends of AOD over the archaeological sites of interest for the last 10 years

	Lat	Long	Average	Slopex10	% per decade
1MR	40.88	25.52	0.218	-0.031	-14%
2AV	40.91	24.96	0.219	-0.042	-19%
3FL	41.01	24.28	0.173	-0.043	-25%
4WT	40.62	22.95	0.219	-0.049	-23%
5VR	40.48	22.31	0.219	-0.049	-23%
6LS	39.64	22.41	0.186	-0.038	-20%
7DD	39.54	20.78	0.189	-0.032	-17%
8NC	39.22	20.73	0.189	-0.032	-17%
9MS	39.19	26.3	0.202	-0.010	-5%
10PL	38.95	24.51	0.205	-0.034	-17%
11DE	38.48	22.49	0.185	-0.045	-24%
12AC	37.97	23.72	0.203	-0.042	-21%
13MC	37.73	22.76	0.18	-0.022	-12%
14OL	37.64	21.62	0.193	-0.022	-11%
15IR	37.66	26.88	0.198	-0.013	-6%
16ME	37.17	21.92	0.193	-0.022	-11%
17DL	37.4	25.26	0.192	-0.025	-13%
18ST	36.35	25.39	0.191	-0.030	-16%
19RH	36.44	28.22	0.203	-0.003	-1%
20FS	35.49	23.65	0.208	-0.039	-19%
21KN	35.29	25.16	0.204	-0.036	-18%

The total negative trend of aerosol optical depth is mostly attributed to decreasing masses of fine aerosol particles originated from anthropogenic sources. This general reduction in anthropogenic aerosol noted in many parts of the world is known as global brightening (Zerefos, et al., 2009), an effect opposite to the up to recently dominating global dimming. Moreover, the North Atlantic

Oscillation[20] patterns are considered to be the main phenomenon affecting the Mediterranean areas, leading to the conclusion that the decreasing AOD trend is probably related to the increasing precipitation. (Papadimas , et al., 2007). The coarse aerosol load also exhibits a decreasing trend, but in smaller scale than that of fine aerosols, fact that proves the general decrease in the region arises mostly from reduced anthropogenic emissions (Floutsi, et al., 2016).

[20] The North Atlantic Oscillation (NAO) is one of the most prominent modes of variability in the Northern Hemisphere. The NAO teleconnection is characterized by a meridional displacement of atmospheric mass over the North Atlantic area. Together with the El Niño (ENSO) phenomenon, the NAO is a major source of seasonal to interdecadal variability in the global atmosphere (Wanner, et al., 2001).

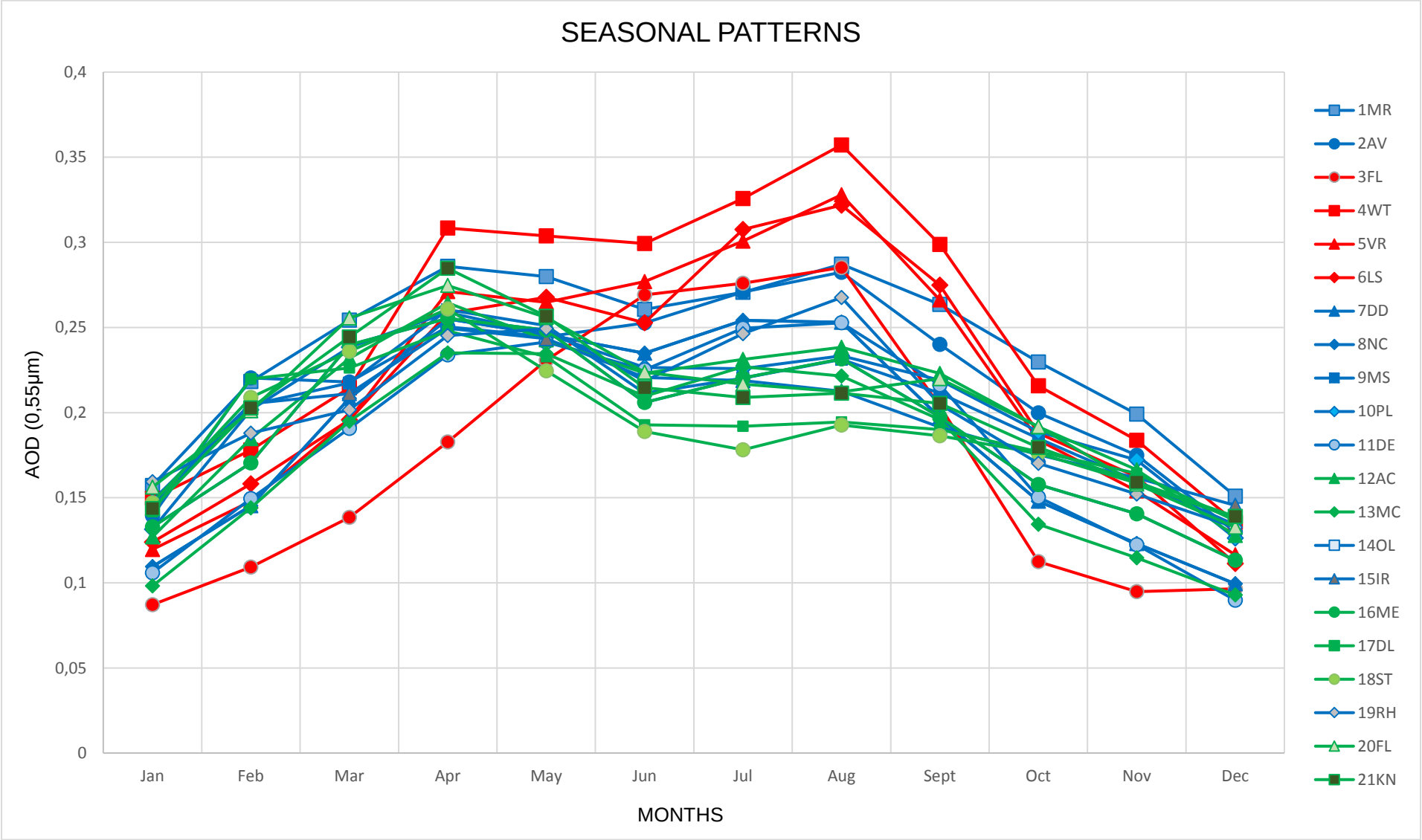

Graph 45 Total presentation of annual cycles of AOD at 0.55 μm (monthly average values for each month for the period 2002-2016)

The current thesis attempted to shed light on the potential contribution of remote sensing on understanding the ambient environment that affects cultural heritage values at risk. Although the contribution of remote sensing techniques for monitoring pollution levels and other relevant parameters in a methodical way, to be used for protecting cultural heritage sites, is undoubtful, there is still an error of 15 – 25% in the measurements, therefore the combination of satellite remote sensing with a system of ground samples set up in the areas of interest could possibly be more accurate, and seems an imperative (Li, et al., 2009). In addition, given the spatial and temporal variability of aerosols, in-situ measurements (observations) and ground based measurements (e.g. sun-photometers) should complement remote satellite observations (Agapiou, et al., 2013).

Continuous monitoring of particulate pollution over cultural heritage sites, can unambiguously support the selection of appropriate measures to improve air quality, and contribute to the field of preventive conservation of monuments in order to avoid further damage.

As a future work, identifying air pollution levels and trends in specific areas of importance for cultural heritage, will assist in exerting pressure for mitigating air pollution reasons. This is especially crucial in urban environments, and creating digital databases is needed so as to observe the long-term distribution of air pollutants over archaeological sites (Agapiou, et al., 2013).

Of great importance, could be the development of a model, which based on the current conditions (geomorphological features, climatological conditions, pollution levels), their projection for the next decades when feasible, or in the concept of a scenario based sensitivity analysis, at the points of interests, would enable the prediction of the effects of these factors on monuments (deterioration patterns). Such a tool would enforce decision making towards

efficient antipollution and preventive conservation measures, targeting at mitigating further formation of deterioration patterns.

BIBLIOGRAPHY

Athanassiou, G., Hatzianastassiou, N., Gkikas, A. & Papadimas, C., 2013. Estimating Aerosol Optical Depth Over the Broader Greek Area from MODIS Satellite. *Water, Air and Soil Pollution*, 22 June.

Lajas, D., Ingmann, . P., Wehr, T. & Ansmann, A., 2007. *AEROSOLS AND CLOUDS: IMPROVED KNOWLEDGE THROUGH SPACE BORNE LIDAR MEASUREMENTS.* s.l., AMS.

Viglaki-Sofianou, M., 2012. *YPPO.* [Online] Available at: http://odysseus.culture.gr/h/3/gh351.jsp?obj_id=2366 [Accessed December 2016].

Agapiou, A. et al., 2013. *Mapping air pollution using Earth Observation techniques for cultural heritage sites.* s.l., First International Conference on Remote Sensing and Geoinformation of the Environment.

Agapiou, A. et al., 2015. Cultural Heritage Management and Monitoring Using Remote Sensing Data and GIS: The Case Study of Paphos Area, Cyprus. *Computers, Environment and Urban Systems*, 4 September, pp. 230 - 239.

Agbota, H., Young, C. & Strlic, M., 2013. Pollution Monitoring at Heritage Sites in Developing and Emerging Economies. *Studies in Conservation*, pp. 129 - 144.

Amoroso, G. & Fassina, V., 1984. *Stone Decay and Conservation.* s.l.:Elsevier.

AMS, 2015. *Meteorology Glossary.* [Online] Available at: glossary.ametsoc.org

ATE Bank, 2008. Ancient Theater of Larissa. In: *The Unknown Treasures of Greece, Ancient Theaters.* s.l.:ATE Bank, pp. 122-126.

Borrelli, E., 1999. Salts, Laboratory Handbook. *Conservation of Architectural Heritage, Historic Structures and Materials*, pp. 3 - 23.

Boucher, O., 2015. Atmospheric Aerosols. In: *Atmospheric Aerosols: Properties and Climate.* s.l.:Springer, pp. 9 - 24.

Bredaki M., S. C. o. K., 2008. *Knossos 2000 - 2008, Conservation, Consolidation and Promotion of the Palace and the Archaeological Site,* Hiraklion: YPPO.

Brett, M., Andrew, E., Meyer, M. & Russel-Smith, J., 2015. Carbon Accounting and Savanna Fire Management. *CSIRO*.

Chatzidakis, P., 2012. *YPPO.* [Online] Available at: http://odysseus.culture.gr/h/3/gh351.jsp?obj_id=2371 [Accessed December 2016].

Chin, M., 2009. *Atmospheric Aerosol Properties and Climate Impact, Synthesis and Assessment Product 2.3.,* s.l.: U.S. Climate Change Program.

Comer, D. C. & Harrower, M. J., 2013. *Mapping Archaeological Landscapes from Space.* s.l.:Springer.

Cracknell, A. P. & Hayes, L., 2007. *Introduction to Remote Sensing.* 2nd Edition ed. s.l.:CRC Press.

Dakaris, S., 2012. *YPPO.* [Online] Available at: http://odysseus.culture.gr/h/3/gh351.jsp?obj_id=2365 [Accessed December 2016].

Di Turo, F. et al., 2016. Impacts of Air Pollution on Cultural Heritage Corrosion at the European Level: What Has Been Achieved and What Are the Future Scenarios.. *Environmental Pollution*, 19 July, pp. 1 - 9.

Doehne, E. & Price, C., 2010. *Stone Conservation: An Overview of Current Research.* 2nd ed. s.l.:The Getty Conservation Institute.

Efstathiou, M., 2012. *YPPO.* [Online] Available at: http://odysseus.culture.gr/h/3/gh351.jsp?obj_id=2454 [Accessed December 2016].

Farrell, G. & Cleugh, H., 2003. *The Impacts on Health of Air Quality in Australia,* s.l.: CSIRO.

Floutsi, A. et al., 2016. Climatology and trends of aerosol optical depth over the Mediterranean basin during the last 12years (2002-2014) based on Collection 006 MODIS-Aqua data.. *The Sciense of the Total Environment*, MAY.

Gerasopoulos, E. et al., 2010. Three-Year Ground Based Measurements of Aerosol Optical Depth Over the Eastern Mediterranean: the Urban Environment of Athens. *Atmospheric Chemistry and Physics*, 18 August, pp. 2145-2159.

Gregory Leptoukh, S. C. J. F. A. G. J. M. S. B., 2007. *EXPLORING NASA AND ESA ATMOSPHERIC DATA USING GIOVANNI, THE ONLINE VISUALIZATION AND ANALYSIS TOOL.* Montreux, ESA.

Hadjimitsis, D. G., Themistocleous, K., Alexakis, D. D. & Sarris, A., 2013. Remote Sensing for Archaeological Applications: Management, Documentation and Monitoring. In: *Remote Sensing of Environment: Integrated Approaches.* s.l.:InTech.

ICOMOS, 2010. *Illustrated Glossary of Stone Deterioration Patterns.* s.l.:ICOMOS.

Kallingi, K., 2012. *YPPO.* [Online] Available at: http://odysseus.culture.gr/h/3/gh351.jsp?obj_id=2359 [Accessed December 2016].

Karadima, C., 2012. *YPPO.* [Online] Available at: http://odysseus.culture.gr/h/3/gh351.jsp?obj_id=2557 [Accessed December 2016].

Kiliyanpilakkil, V. & Meskhidze, N., 2011. Deriving the Effect of Wind Speed on Clean Marine Aerosol Optical Properties Using the A-Train Satellites. *Atmospheric Chemistry and Physics*, pp. 11401-11413.

King, M. D., Kaufman, Y. J. & Menzel, P. W., 1992. Remote Sensing of Cloud, Aerosol, and Water Vapor Properties from the

Moderate Resolution Imaging Spectrometer (MODIS). *IEEE TRANSACTIONS ON GEOSCIENCE AND REMOTE SENSING*, January, pp. 2 -27.

Kottaridi, A., 2012. *YPPO.* [Online] Available at: http://odysseus.culture.gr/h/3/gh355.jsp?obj_id=2362 [Accessed December 2016].

Koukouli, M. E. et al., 2009. Signs of a Negative Trend in the MODIS Aerosol Optical Depth over the Southern Balkans. *Atmospheric Environment*, 11 November, pp. 1219-1228.

Kourtzellis, I. & Tsolaki, D., 2012. *YPPO.* [Online] Available at: http://odysseus.culture.gr/h/3/gh351.jsp?obj_id=2560 [Accessed December 2016].

Kulkani, P., Baron , P. & Willeke, K., 2011. *Aerosols Measurement: Principles, Techniques and Applications.* 3rd ed. s.l.:Wiley.

Labropoulos, V., 2003. *Environment of Monuments, Museums and Archaeological Sites.* Athens: s.n.

Lampropoulos, V., 2004. *Erosion and Conservation of Stone.* Athens: s.n.

Lasaponara, R. & Masini, N., 2012. *Satellite Remote Sensing: A New Tool for Archaeology.* s.l.:Springer.

Lillesand, T. M., Kiefer, R. W. & Chipman, J. W., 2008. *Remote Sensing and Image Interpretation.* 7th edition ed. s.l.:Wiley.

Li, Z. et al., 2009. Uncertainties in satellite remote sensing of aerosols and impact on monitoring its long-term trend: a review and perspective. *Annales Geophysicae*, 27 March, pp. 2755 - 2770.

Marley, N. & Gaffney, J., 2006. *Introduction to Urban Aerosols and Their Impacts.* Washington, ACS.

Mishra, S., Tripathi, S., Agarmal, S. & Arola, A., 2012. Optical Properties of Accumulation Mode, Polluted Mineral Dust: Effects of Particle Shape, Hematite Content and Semi-External Mixing With

Carbonaceous Species. *Atmospheric Chemistry and Physics*, 28 May.

Moncmanova, A., 2007. *Environmental Deterioration of Materials.* s.l.:WITpress.

Moropoulou, A. et al., 2001. Correlation Between Aerosols, Deposits and Weathering Crusts on Ancient Marbles. *Environmental Technology*, pp. 607-618.

Nalpantis, D., 2012. *YPPO.* [Online] Available at: http://odysseus.culture.gr/h/2/gh251.jsp?obj_id=859 [Accessed December 2016].

NASA, 2016. *MODIS.* [Online] Available at: https://modis.gsfc.nasa.gov

NBG, 2004. *Great Civilizations, Ancient Greece,* Athens: National Bank of Greece.

Nikolaidou-Patera, M., 2012. *YPPO.* [Online] Available at: http://odysseus.culture.gr/h/3/gh351.jsp?obj_id=2387 [Accessed December 2016].

Niniou-Kindeli, B., 2012. *YPPO.* [Online] Available at: http://odysseus.culture.gr/h/3/gh351.jsp?obj_id=2615 [Accessed December 2016].

NOA, 2013. *LIVAS.* [Online] Available at: http://lidar.space.noa.gr:8080/livas/index.html [Accessed 2016].

NOA, 2013. *LIVAS, User's Manual.* Athens: NOA.

NOOA, 2005. *Earth System Research Laboratory, Global Monitoring Division.* [Online] Available at: www.esrl.nooa.gov/gmd/grad/surfrad/aod/

Papadimas , C., Hatzianastassiou , N., Mihalopoulos, N. & Vardavas, I., 2007. Changes in aerosol optical properties over the

Mediterranean Basin on 6-year (200o - 2006) MODIS Data. *Geophysical Research Abstracts*.

Penner, J. E. et al., 2001. Aerosols, their Direct and Indirect Effects. In: *Climate Change 2001: The Scientific Basis. Contribution of Working Group I to the Third Assessment Report of the Intergovermental Panel of Climate Change.* Cambridge, UK and New York, USA: Cambridge University Press, pp. 289 - 348.

Petsas, F., 2004. *Delphi, Monuments and Museum,* Athens: Krini.

Productions, C., 2016. *Shooting in Greece.* [Online] Available at: http://guide.clproductions.gr/en/aboutgreece.php [Accessed October 2016].

Rees, W. G., 2013. *Physical Principles of Remote Sensing.* 3rd edition ed. s.l.:Cambridge Unibersity Press.

Roy, P. S., Dwivedi, R. S. & Vijayan, D. V., 2010. *Remote Sensing Applications.* s.l.:NRSC.

Saiz - Jimenez, C., 2004. *Air Pollution and Cultural Heritage.* s.l.:AAB.

Seinfeld, J. H. & Pandis, S. N., 2016. *Atmospheric Chemistry and Physics: From Air Pollution to Climate Change.* 3rd ed. s.l.:Wiley.

Skoulikidis, T., 2000. *Erosion and Maintenance of the Building Materials of Monuments.* s.l.:Crete University Press.

Skyros Municipality, 2016. *Skyros.gr.* [Online] Available at: http://www.skyros.gr/index.php/el/?option=com_content&view=article&id=7&Itemid=125
[Accessed December 2016].

Spathari, E., 2001. *Myceanae, Archaeological and Historical Guide.* Athens: Esperos.

Themelis, P., 2014. *Ancient Messene, History - Monuments - People.* s.l.:Militos.

Themistocleous , K. et al., 2012. Long Term Monitoring of Air Pollution on Monuments and Cultural Heritage Sites in Cyprus Using Satellite Remote Sensing. *International Journal of Heritage in the Digital Era*, March, pp. 145 - 167.

Vallero, D., 2008. *Fundamentals of Air Pollution.* 4th ed. s.l.:Elsevier, AP.

Venieri, I., 2012. *YPPO.* [Online] Available at: http://odysseus.culture.gr/h/3/gh351.jsp?obj_id=2384 [Accessed December 2016].

Vikatou, O., 2006. *Olympia, the Archaeological Site and the MUSEUM,* s.l.: Athinon.

Voiland, A., 2010. *NASA, Earth Observatory.* [Online] Available at: earthobservatory.nasa.gov/Features/Aerosols

Wanner, H. et al., 2001. North Atlantic Oscillation - Concepts and Studies. *Surveys in Geophysics*.

Watt, J., Tidblad, J., Kucera, V. & HamiltonRon, 2009. *The Effects of Air Pollution on Cultural Heritage.* s.l.:Springer.

Wiseman, J. & El - Baz, F., 2007. *Remote Sensing in Archaeology.* s.l.:Springer.

WorldAtlas, 2016. *WorldAtlas.* [Online] Available at: http://www.worldatlas.com/

YPPO, 2001. *Mediaval City of Rhodes, Restoration ,* Rhodes: YPPO.

YPPO, 2012. *YPPO.* [Online] Available at: http://odysseus.culture.gr/h/3/gh351.jsp?obj_id=2575 [Accessed December 2016].

YSMA, 2011. *Acropolis Restoration Service,* Athens: YSMA.

Zerefos, C. S. et al., 2009. Solar Dimming and Brightening over Thessaloniki, Greece, and Beijing, China. *Tellus*, pp. 657 - 665.

APPENDIX A

HISTORICAL BACKGROUND OF THE STUDIED ARCHAEOLOGICAL SITES

Maronia

Figure 20 Aspect of ancient Maronia

Maronia was founded by Chian colonists on the SW slopes of Ismaros, in the mid-7th century B.C. and was developed into a prosperous and densely inhabited city-state. The mythical founder (oikistes) of the city was Maron, priest of Apollo. During the Classical period the city had a strong fortification wall, 10 km. long, enclosing an area of 4 km^2, which extended from the coast up to the top of Ismaros (Karadima, 2012).

Avdira

Figure 21 Aspect of ancient Avdira

In a privileged position with two natural harbors on the coast of Thrace, Abdera are one of the most important ancient cities of the northern Aegean. They founded in the 7th century. B.C. by settlers Clazomenae, who came to the area with the settler Timesio. About a century later, the area was colonized for the second time by inhabitants of Teos also Greek city located south of Clazomenae. The archaeological site of Abdera includes the northern and southern wall, the citadel of the ancient city and its cemeteries, extending mainly in the NW, N and NE and dated to the Archaic, Classical and Hellenistic periods (Kallingi, 2012).

Philippi

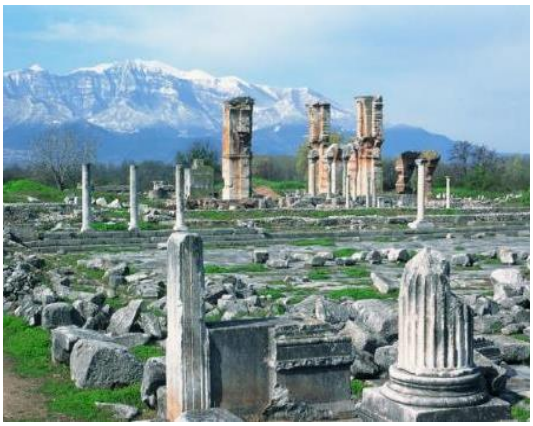

Figure 22 Aspect of Filippoi

The archaeological site of Philippi is located west of the modern town of Krinides. The most important monuments in the area are the city walls, the acropolis, the theatre, the forum, Basilica A, Basilica B, and the Octagon. Philippi, the most important archaeological site in Eastern Macedonia, lies at the boundary of the swamps that cover the southeast part of the plain of Drama. The site was formerly colonized by the people of Thasos, who knowing the area's plentiful supplies of precious metals, timber, and agricultural products, established the city of Krinides in 360 BC. Philip conquered, fortified, and renamed the city after himself (Nikolaidou-Patera, 2012).

White Tower

Figure 23 The White Tower

The White Tower, the landmark of Thessaloniki standing on the city's waterfront, was once the south-east tower of a large fortification. Its exact date is uncertain, but it was probably built in the 15th century after the conquest of Thessaloniki by the Turks, to replace a Byzantine tower. Throughout its long history, the tower's name and use changed several times. It was called the 'Fortress of Kalamaria' in the eighteenth century, and the 'Tower of the Genitsaroi' or 'Bloody Tower' in the nineteenth. In 1890, a prisoner whitewashed the tower's walls in exchange for his freedom, hence the name 'White Tower'. After the liberation of

Thessaloniki in 1912, the tower became public property (Nalpantis, 2012).

Vergina

Figure 24 Aspect of Vergina

The ancient city lying on the north slopes of the Pierian mountains is identified as Aigai, the capital of the kingdom of Lower Macedonia. The site was continuously inhabited from the Early Bronze Age while in the Early Iron Age it became an important center. The city touched its peak point of prosperity in the Archaic and Classical periods, when it was the most important urban center of the area, the seat of the Macedonian kings. Moreover, it was already famous in antiquity for the wealth of the royal tombs which were gathered in its wide necropolis. The most important monuments on the site are the royal tombs in the Great Tumulus, the cemetery of the tumuli, the Palace, the Theatre, the temple of Eukleia, the acropolis and the city walls (Kottaridi, 2012).

Ancient Theater of Larissa

Figure 31 The Ancient Theater of Larissa

The beautiful Hellenistic theater, lies on a cliff, in the ancient acropolis, in the center of Larissa, which in byzantine years was used as a fortress, consists a significant monument. It is constructed by Agias marble and was built in the beginning of the 3rd century B.C. During the first centuries, the theatre served a dual purpose: theatrical performances and hosting of the assemblies of the senior regional authority, called Koinon of the Thessalians. At

the end of the first century BC it was transformed into a roman arena and thus stayed in use until the late third century AD (ATE Bank, 2008).

Dodoni

Figure 26 Aspect of Dodoni

To the south of Ioannina, is located the second most important oracle of antiquity, this of Dodoni. It is not exactly known the principle of its' operation but is placed in prehistoric times. Flourished in 4th and 3rd century B.C. The sanctuary of Dodona, the religious centre for northwestern Greece, closely related to the cult of Zeus, father of the gods, lies in the narrow valley east of Tomaros. It's traditionally considered as the most ancient one in Greece and referred to by Homer in his epics (Dakaris, 2012).

Nicopolis

Figure 36 Aspect of Nicopolis

Nicopolis of Epirus, whose name contains the word victory, is built on the peninsula which separates the Amvrakikos gulf from the Ionian Sea. Marine and terrestrial roads led to Nicopolis and became an important commercial center. The city was established as a symbol of the great victory of Gaius Julius Caesar Octavianus and later Roman emperor August against Mark Antony and Cleopatra at Actium in 31 BC and flourished during the Roman period. Nicopolis belongs to the few ancient cities in the Greek area fortunate enough to escape the constant building and

reuse of the ancient building material. Thus, they kept in good condition many monuments. The Roman city gained strong defensive wall, with perimeter more than 5 km (YPPO, 2012).

Sanctuary of Messa

Figure 28 Aspect of the sanctuary of Messa

The sanctuary of Messa located in the homonymous valley, is 35 km. away from Mytilene. The sanctuary, center of pallesviaki worship and seat of the League of Lesbians, was within the limits of the territory of ancient Pyrrha. In ancient times, there was a rectangular building with devotional altars, relics are preserved in the foundation of the late Classical temple. The sanctuary was dedicated to Lesbian Trinity (Zeus, Hera and Dionysos). After the destruction of the late Roman era, the area acquired laboratory use, documented by the revelation furnaces. In Early Christian years, early Christian basilica cemeterial was founded (Kourtzellis & Tsolaki, 2012).

Palamari

During an excavation, an entire settlement in Palamari (northeast coastline of Skyros) was revealed. The settlement dates to the Copper Age (2500-1800 B.C) and is an impressive finding as it includes an organized city plan with roads and central pipes. The ruins of the walls show that it was a well-fortified settlement. Its fortification originated from Syria and Palestine and first appeared in the Aegean around 2300 B.C. Among

Figure 29 The archaeological site of Palamari

the findings there were brick terraces, fireplaces, ovens, floors, stone and bone tools, metal utensils etc. (Skyros Municipality, 2016).

Delphi

Figure 343 Aspect of Delphi

Delphi at an altitude of 500 – 700 m, confined in ancient Phocis became the most important of all the cities in the region because there was the sanctuary of Apollo. Delphi are located between the mountains Parnassus and Kirfis. Their activity dates to the 3rd millennium BC, thrives in the 8th century BC, when the first news about the worship of Apollo begun and continues until the Roman times (Petsas, 2004).

Acropolis

Figure 31 The Acropolis

The greatest and finest sanctuary of ancient Athens, dedicated to the goddess Athena, rules the center of the modern city from the rocky cliff known as the Acropolis. The unique masterpieces of ancient architecture, the Parthenon, Erechtheion, Propylaea, the Temple of Athena Nike etc. combine different orders and styles of Classical art in a most innovative manner influencing art and culture for many centuries. The Acropolis of the 5th century BC is the most precise reflection of the magnificence, power and wealth of Athens at its greatest peak, the golden age of Perikles. Pottery sherds of the Neolithic period and, from near the Erechtheion, of the Early and Middle Bronze Age, show that the hill was inhabited from a very early period (Venieri, 2012).

Mycenae

Figure 32 Aspect of Mycenae

Mycenae 'Rich in Gold', the kingdom of mythical Agamemnon, first sung by Homer in his epics, is the most important and richest palatial centre of the Late Bronze Age in Greece. Its name was given to one of the greatest civilizations of Greek prehistory, the Mycenaean civilization, while the myths related to its history have inspired poets and writers over many centuries, from the Homeric epics and the great tragedies of the Classical period to contemporary literary and artistic creation. Mycenae was built in the creek of the Argolic gulf and was first inhabited in 2500 BC, but reached its glory between 1600 and 1100 BC. It was a mighty fortress, leading the Aegean with both the trade and the force of arms. The palace shows a typical rectangular array. Out of it, but inside of the walls, is the religious center (Spathari, 2001).

Ancient Olympia

Figure 33 Aspect of Ancient Olympia

Near the western coast of the Peloponnese, in the valley of the river Alpheus, Olympia is located, a sanctuary dedicated to Zeus. The history of Olympia goes back to centuries, from prehistoric times to the early Christian period. It was established by Pelops from Phrygia and gave his name across the Peloponnese. From the archaic period, large buildings were built around the sanctuary to serve the needs of the pilgrims who come from every corner of Greece and the colonies of Italy and Ponte (Vikatou, 2006).

Ireon

Figure 34 Aspect of Ireon

The Ionic dipteral temple built during the tyranny of Polycrates (538-522 B.C.) is the most important of the sanctuaries dedicated to Hera. Only one column is still standing today, preserved up to half of its original height, while the foundations are preserved up to the base of the walls and the stylobate. Herodotus considered this temple as the largest in Greece. The temple had a total of 155 columns, belonging to four different sizes and types. Since no tiles were found, it is suggested that the roof was never completed. The Great Altar, very large even in its earlier phases, occupied always the same position. Seven successive phases have been distinguished, of which the earliest dates from the Late Bronze Age. The road leading from the city of Samos to the sanctuary, was an important feature of the landscape already in the beginning of the 6th century B.C. (Viglaki-Sofianou, 2012)

Ancient Messene

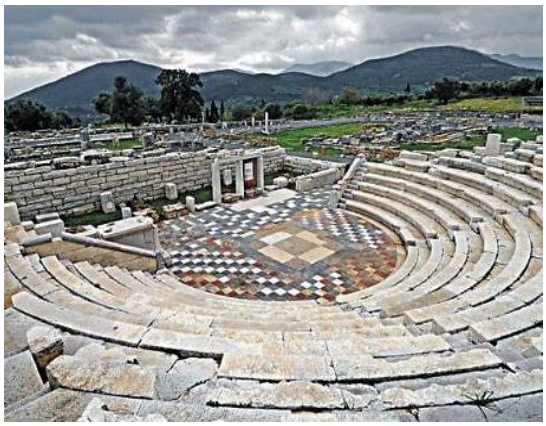

Figure 35 Aspect of Ancient Messene

Messene is a significant ancient city in terms of its size, form, and state of preservation, and still has much to offer. It possesses not only sanctuaries and public buildings, but also imposing fortifications, and houses and tombs. It enjoys, amongst other things, the advantage of never having been destroyed or covered by later settlements, and is located on an unspoiled inland site. Its natural setting combines the grandeur of the mountains of Delphi with the low-lying, riverine tranquillity of Olympia,

the dominating bare limestone mass of Ithome, the site of the ancient acropolis, with the low fertile valley around the ancient city (Themelis, 2014).

Delos

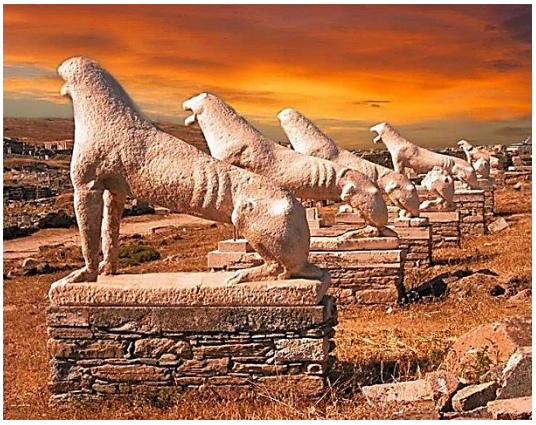

Figure 36 Aspect of Delos Island

It is estimated that, circa 90 B.C., about 30,000 people lived on this small island, which is no more than a dot on the map of the Mediterranean. The names inscribed on the tombstones in the ancient cemetery provide us with evidence that during the 2nd c. B.C., apart from the island's majority of Athenian and Roman residents, Delos was populated by folk from most Mediterranean cities: from the Peloponnese and Italy, from mainland regions, Central, Western Greece and Macedonia, Thrace, the Black Sea and Asia Minor, from the Aegean Islands, Cyprus, Crete, and faraway places including Troas, Mysia, Aiolis, Ionia, Lydia, Caria, Lycia, Bithynia, Paflagonia, Pontus, Cappadocia, Pisidia, Pamphilia, Cilicia, Syria, Media, Phoenicia, Palestine, Libya, Arabia and Egypt (Chatzidakis, 2012).

Ancient Thera (Santorini)

Figure 37 Aspect of Ancient Thera

Ancient Thera, the Classical city of the island is located on Mesa Vouno, 396 m. above sea level. It was founded in the 9th century B.C. by Dorian colonists whose leader was Theras, and continued to be inhabited until the early

Byzantine period. The preserved ruins belong to the Hellenistic and Roman phases of the city (Efstathiou, 2012).

Medieval City of Rhodes

Figure 60 Aspect of the Med. City of Rhodes

The ancient city of Rhodes was founded in 408 BC at the northern tip of the island and laid out on a regular grid per the principles of Hippodamus of Miletus. The ancient city was much reduced in size in Byzantine times, and was protected by fortifications from the 7th century. The early walls contained the area later known as the Collachio. The town conquered by the Knights of St. John in 1309. From this time until 1522 the town was the headquarters of the Order's island state, which also included most of the other Dodecanese islands and had to face the increasing pressure of Islam. In 1522, a landmark for the history of Rhodes, sultan Suleiman II the Magnificent managed to drive the Knights Hospitaller out of Rhodes. Rhodes remained under Ottoman occupation until 1912. They were driven away by the colonial expansion of Italy who held the Dodecanese islands until the surrender of Italy to the Allies in World War II. In 1948 Rhodes became formally part of Greece (YPPO, 2001).

Falassarna

Figure 38 Aspect of Ancient Falassarna

Falassarna is an ancient Greek harbor town on the northwest coast of Crete. The currently visible remains of the city were built around 333 BC, and include several imposing sandstone towers and bastions, with hundreds

of meters of fortification walls protecting the town, and a closed harbor. Notable finds in the harbor area include public roads, wells, warehouses, an altar, and baths. The acropolis is erected on a cape that rises 90 meters above the harbor and protrudes into the sea. The acropolis has many remains, including a temple dedicated to goddess Dictynna, fortification towers, cisterns, wells, and watchtower (Niniou-Kindeli, 2012).

Knossos

Figure 39 Aspect of Knossos

Knossos is the site of the most important and better known palace of Minoan civilization. It was the seat of the legendary king Minos. The Palace is also connected with thrilling legends, such as the myth of the Labyrinth with the Minotaur, and the story of Daidalos and Icaros. The site was continuously inhabited from the Neolithic period (7000-3000 B.C.) until Roman times. Intensive habitation occurred mostly in the Minoan period, when the so-called first (19th-17th centuries B.C.) and second palaces (16th-14th centuries B.C.) were built along with luxurious houses, a hospice and various other structures. After its partial destruction in 1450 B.C., Knossos was settled by Mycenaeans. The city flourished again during the Hellenistic period and in 67 B.C. it was captured by the Roman Quintus Caecilius Metelus Creticus (Bredaki M., 2008).

Arezina Sakka

Conservator of Antiquities and Works of Art